National Library of Canada
Acquisitions and Bibliographic Services Branch
395 Wellington Street
Ottawa, Ontario
K1A 0N4

Bibliothèque nationale du Canada
Direction des acquisitions et des services bibliographiques
395, rue Wellington
Ottawa (Ontario)
K1A 0N4

Your file Votre référence

Our file Notre référence

NOTICE

The quality of this microform is heavily dependent upon the quality of the original thesis submitted for microfilming. Every effort has been made to ensure the highest quality of reproduction possible.

If pages are missing, contact the university which granted the degree.

Some pages may have indistinct print especially if the original pages were typed with a poor typewriter ribbon or if the university sent us an inferior photocopy.

Reproduction in full or in part of this microform is governed by the Canadian Copyright Act, R.S.C. 1970, c. C-30, and subsequent amendments.

AVIS

La qualité de cette microforme dépend grandement de la qualité de la thèse soumise au microfilmage. Nous avons tout fait pour assurer une qualité supérieure de reproduction.

S'il manque des pages, veuillez communiquer avec l'université qui a conféré le grade.

La qualité d'impression de certaines pages peut laisser à désirer, surtout si les pages originales ont été dactylographiées à l'aide d'un ruban usé ou si l'université nous a fait parvenir une photocopie de qualité inférieure.

La reproduction, même partielle, de cette microforme est soumise à la Loi canadienne sur le droit d'auteur, SRC 1970, c. C-30, et ses amendements subséquents.

Canada

Curing of Thick Thermosetting Composites: Experiment, Simulation, and Scaling

Mehdi Hojjati

A Thesis

in

The Department

of

Mechanical Engineering

Presented in Partial Fulfillment of the Requirements
for the Degree of Doctor of Philosophy at
Concordia University
Montreal, Quebec, Canada

September 1994

ISBN 0-315-97580-6

Canada

ABSTRACT

Curing of Thick Thermosetting Composites:

Experiment, Simulation, and Scaling

Mehdi Hojjati, Ph.D.

Concordia University, 1994

Curing of thick thermosetting composites has been studied. The study consists of three parts: experiment, simulation, and scaling (modeling). One-dimensional through-the-thickness experiment using manufacturer recommended cure cycle was performed on a 330-layer laminate. Temperature overshoot and incomplete through-the-thickness consolidation were observed. Two-dimensional experiment was performed to reduce the temperature overshoot. Prebleeding method was used to obtain complete through-the-thickness consolidation.

A one-dimensional through-the-thickness and a two-dimensional simulations were developed. Heat conduction, kinetic, viscosity, and flow (squeezed sponge model) equations were solved as a coupled system of equations. Control-volume method combined with Alternating Direction Explicit (ADE) method were employed in the solution. Composite physical properties were considered as functions of fiber volume fraction. Experimental results for temperature history and compaction were compared with simulation results. Good agreement was obtained. The simulation was used to study the temperature history, composite compaction, and bleeder

effect during cure process. It was found that prebleeding technique is the most promising method for fabrication of thick composites.

Performing experiment requires the expensive prepreg materials and labor work. Using simulation is economical. However, simulation requires an accurate expression for kinetic equation which is not available for most resins. To solve those problems, scaling (modeling) has been introduced as an alternative to study the curing process.

Model laws for curing of thermosetting composites were established. The transient heat conduction coupled with kinetic equation and initial and boundary conditions were non-dimensionalized. Dimensionless parameters were extracted from those non-dimensional equations and accordingly model laws were constructed. It is shown how one can use model laws to design and fabricate a less expensive model composite structure for an expensive prototype one. The only feasible way to design a model is to use the same resin, but different fibers. For this case, it was shown that for same initial temperature in the material and same cure cycle for both model and prototype, the temperature and degree of cure at homologous points are the same. Also to transform the model experimental results to prototype for the same resin , it is not necessary to know the resin kinetic equation.

ACKNOWLEDGEMENT

The author would like to express his deep gratitude to Dr. Suong V. Hoa for his financial support and guidance during the course of this work.

Thanks to my parents, Mojtaba and Forough, for their love, support and encouragement during my studies.

Special thanks to my wife, Fariba, to my daughter, Nazanin, and to my son, Nivad, for their love, support, patience and understanding during the course of this work.

Contents

List of Figures xi

List of Tables xix

Nomenclature xx

1 Introduction 1

1.1 Literature Survey 7

1.2 Objectives 16

1.3 Thesis Overview 19

2 Mathematical Models 20

2.1 Heat Model 21

2.1.1 Initial and Boundary conditions 25

2.2 Kinetic Model 26

2.3 Viscosity Model 30

2.4 Flow Model 30

2.4.1 Initial and Boundary conditions 35

2.4.2 Equilibrium Equation 36

2.4.3 Coefficient of Volume Change 36

2.5 Summary 37

3 Numerical Solution **38**

3.1 Composite Physical Properties 39

3.1.1 Rule Of Mixture 44

3.1.2 Thermal Conductivity 44

3.1.3 Permeability 45

3.1.4 Fiber Bed Deformation 47

3.2 One-Dimensional Analysis 48

3.2.1 Heat Model 49

3.2.2 Discretization Procedure For Heat Model 51

3.2.3 Flow Model 56

3.2.4 Discretization Procedure For Flow Model 57

3.2.5 Closed-Form Solution For Flow Model 58

3.3 Two-Dimensional Analysis 61

3.3.1 Heat Model 61

3.3.2 Discretized Equation For Heat Model 61

3.3.3 Flow Model 69

3.3.4 Discretized Equation For Flow Model 70

3.4 Solution Techniques 71

3.5 Summary 74

4 Experimental Setup **75**

4.1 One-Dimensional Experiment 76

4.1.1 Experimental Tooling Set-up 76

4.1.2 Cure Cycle 78

4.1.3 Experimental Results 79

4.2 Two-Dimensional Experiment 81

4.2.1 Experimental Tooling Set-up 87

4.2.2 Experimental Results 88

4.3 Prebleeding Experiment 90

4.3.1 Experimental Tooling Setup 90

4.3.2 Cure Cycle 91

4.3.3 Experimental Results 91

4.3.4 Modified Fabrication Procedure 99

4.4 Summary 104

5 Experimental and Simulation Results **106**

5.1 One-dimensional Results 107

5.2 Two-dimensional Results 116

5.3 Prebleeding Results 116

5.4 Simulation Results 120

5.4.1 Consolidation effect 122
5.4.2 Composite thickness variation 125
5.4.3 Consolidation mechanism 128
5.4.4 Thickness effects 132
5.4.5 Pressure effect 138
5.4.6 Consolidation from top and bottom 138
5.4.7 Prebleeding 140
5.4.8 Bleeder effect 143
5.5 Summary 147

6 Model Laws **153**

6.1 Dimensional Governing Equation 158
6.2 Non-dimensional Governing Equations 159
6.3 Model Laws 161
6.4 Kinetic Equation 165
6.5 Convective Boundary condition 167
6.6 Model Design Procedure 168
6.7 Numerical Results 182
6.8 Summary 188

7 Conclusions and Contributions **190**

7.1 Conclusions 190
7.2 Contributions 193

7.3 Recommendations for future work 194

List of Figures

1.1 Typical two-step cure cycle for autoclave curing 3

1.2 Typical viscosity variation during the two-step cure cycle (Heating rates and hold times are identical) [6]. 4

2.1 Different systems of coordinates.$x_1x_2x_3$ is the laminate system of coordinates and xyz is the ply system of coordinates (principal directions). 22

2.2 Differential Scanning Calorimetry (DSC). 27

2.3 The piston and spring analogy for flow model [30]. 31

3.1 Comparison between the viscosities measured by Carpenter[56] and predicted viscosities. The inset shows the applied temperature profile (Dynamic heating). 42

3.2 Comparison between the viscosities measured by Carpenter[56] and predicted viscosities. The inset shows the applied temperature profile. 43

3.3 Transverse Permeability s_z vs Fiber Volume Fraction for AS4 Graphite Fibers. 46

3.4 One-dimensional through-the-thickness analysis: composite geometry and boundary conditions. 50

3.5 One-dimensional Through-the-Thickness analysis: computational domain. 52

3.6 Control Volumes for one-dimensional discretization. 53

3.7 Variation of resin pressure with time at the midpoint of the laminate . 59

3.8 Two-dimensional analysis: composite geometry and boundary conditions. 62

3.9 Two-dimensional analysis: computational domain. 64

3.10 Control-volumes for two-dimensional discretization. 65

3.11 Thermal and flow resistance 73

4.1 Experimental Tooling Setup (Bleed setup). 77

4.2 Measured temperature at different locations for one-dimensional experiment (330-layer laminate) 80

4.3 Location of different regions used to take photomicrograph (One-dimensional experiment and 330-layer laminate). 82

4.4 Cross-section photomicrograph (399X) at the top of laminate close to bleeder side (One-dimensional experiment and 330-layer laminate). 83

4.5 Cross-section photomicrograph (399X) at the middle of laminate (One-dimensional experiment and 330-layer laminate). 84

4.6 Cross-section photomicrograph (399X) at the bottom of laminate close to Aluminum plate (One-dimensional experiment and 330-layer laminate). 85

4.7 Cross-section photomicrograph (399X) at the top ten layers of laminate (One-dimensional experiment and 330-layer laminate). 86

4.8 Measured temperature at different locations for two-dimensional experiment (330-layer laminate) 89

4.9 No-bleed tooling setup 92

4.10 Measured temperature at the middle of 320-layer laminate- Prebleeding experiment. 93

4.11 Location of different regions used to take photomicrograph (prebleeding experiment and 320-layer laminate). 95

4.12 Cross-section photomicrograph (399X) at the top of laminate (prebleeding experiment and 320-layer laminate). 96

4.13 Cross-section photomicrograph (399X) at the bottom of laminate (prebleeding experiment and 320-layer laminate). 97

4.14 Void (399X) inside the laminate (prebleeding experiment and 320-layer laminate). 98

4.15 Cross-section photomicrograph (399X) at the top of laminate (Prebleeding experiment and 120-layer laminate). 101

4.16 Cross-section photomicrograph (399X) at the bottom of laminate (Prebleeding experiment and 120-layer laminate). 102

4.17 Resin rich area (399X) inside the laminate (prebleeding experiment and 120-layer laminate). 103

5.1 Tooling setup used for simulation (One-dimensional analysis and 330-layer laminate). 108

5.2 Comparison between measured and predicted temperature at top of laminate (One-dimensional analysis and 330-layer laminate). . . . 110

5.3 Comparison between measured and predicted temperature at middle of laminate (One-dimensional analysis and 330-layer laminate). . 111

5.4 Temperature distribution through-the-thickness (One-dimensional analysis and 330-layer laminate). 113

5.5 Laminate compaction evolution (One-dimensional analysis and 330-layer laminate). 114

5.6 Fiber volume fraction distribution through-the-thickness (One-dimensional analysis and 330-layer laminate). 115

5.7 Tooling setup used for simulation (Two-dimensional analysis and 330-layer laminate). 117

5.8 Comparison between measured and predicted temperature at top of laminate (Two-dimensional analysis and 330-layer laminate). . . . 118

5.9 Comparison between measured and predicted temperature at middle of laminate (Two-dimensional analysis and 330-layer laminate). . 119

5.10 Comparison between measured and predicted temperature at middle of laminate (Prebleeding experiment and 320-layer laminate). . . 121

5.11 Cure cycle 2-Recommended by manufacturer for thick composites [52]. 123

5.12 Cure cycle 3-Recommended for thick composites [49]. 124

5.13 Temperature profile at the center of the thick composite (5cm) using cure cycle 1. 126

5.14 Temperature profile at the center of the thick composite (5cm) using cure cycle 2. 127

5.15 Variation of laminate thickness during curing for different cure cycles. 129

5.16 Variation of viscosity at the middle of laminate (5cm) for different cure cycles. 130

5.17 Fiber volume fraction distribution through the thickness for 2.5cm thick laminate subjected to the cure cycle 2. 131

5.18 Temperature at the composite center for different thicknesses using cure cycle 1. 134

5.19 Final fiber volume fraction distribution for different thicknesses using cure cycle 1. 135

5.20 Temperature at the composite center for different thicknesses using cure cycle 2. 136

5.21 Final fiber volume fraction distribution for different thicknesses using cure cycle 2. 137

5.22 Pressure effect on final fiber volume fraction distribution through the thickness for 5cm thick composite. 139

5.23 Temperature at the composite center for consolidation from top and bottom for different thicknesses. 141

5.24 Final fiber volume fraction distribution for consolidation from top and bottom for different thicknesses. 142

5.25 Compaction cure cycle for prebleeding technique. 144

5.26 Simplified curing cycle for prebleeding technique. 145

5.27 Temperature profile at the center of composite made of prebled sub-laminates and subjected to the simplified curing cycle. 146

5.28 Predicted temperature at the middle of 5 cm thick laminate (Bleeder effect). 148

5.29 Predicted temperature at the top of 5 cm thick laminate (Bleeder effect). 149

5.30 Temperature distribution through-the-thickness of 5 cm thick laminate (Bleeder effect). 150

5.31 Compaction of 5 cm thick laminate (Bleeder effect). 151

6.1 Composite Geometry 157

6.2 Glass fiber volume fraction (model) versus Graphite fiber volume fraction (prototype) 174

6.3 Length scale factor (K_L) versus Graphite fiber volume fraction (prototype) 175

6.4 Thickness scale factor (K_N) versus Graphite fiber volume fraction (prototype) 176

6.5 Resin weight ratio 179

6.6 Fiber weight ratio 180

6.7 Convective heat transfer coefficient scale factor K_h versus graphite fiber volume fraction 181

6.8 Temperature variation at the center of composite (AS4/3501-6 with thickness 10cm and ν_f = .7 or Glass/3501-6 with thickness 4.67cm and ν_f = .544) 184

6.9 Degree of cure variation at the center of composite (AS4/3501-6 with thickness 10cm and ν_f = .7 or Glass/3501-6 with thickness 4.67cm and ν_f = .544) 185

6.10 Temperature distribution through-the-thickness (AS4/3501-6 with thickness 10cm and ν_f = .7 or Glass/3501-6 with thickness 4.67cm and ν_f = .544) 186

6.11 Degree of cure distribution through-the-thickness (AS4/3501-6 with thickness 10cm and ν_f = .7 or Glass/3501-6 with thickness 4.67cm and ν_f = .544) 187

List of Tables

2.1 Generalized boundary condition coefficients 26

3.1 Material properties of Hercules AS4/3501-6 [51,56]. 41

3.2 Material properties for flow model 60

4.1 Fiber volume fraction at different locations (one-dimensional experiments and 330-layer laminate). 87

4.2 Fiber volume fraction at different locations (Prebleeding experiments and 320-layer laminate). 100

4.3 Fiber volume fraction at different locations (Prebleeding experiments and 120-layer laminate). 104

5.1 Typical physical properties of polyester [68,69]. 107

6.1 Typical physical properties of glass fiber (model) 172

NOMENCLATURE

Main symbols are defined here. Others are defined locally.

A_i	pre-exponential factor
α	degree of cure
C_{ij}	direction cosine
c_p	composite specific heat
c_{pf}	fiber specific heat
c_{pr}	resin specific heat
E_i	activation energy
$\dot{g}$	heat generation source term
h	convective heat transfer coefficient
H_R	resin total heat of reaction
K_i	Kozeny constant
k_{ij}	thermal conductivity tensor component
k_f	fiber thermal conductivity
k_r	resin thermal conductivity
k_x, k_y, k_z	principal thermal conductivities
L	composite flat plate length
L_{cv+1}	number of elements along fiber direction
M	composite flat plate width
m_v	coefficient of volume change

μ	viscosity
μ_∞	viscosity constant
N	composite flat plate thickness
N_{cv+1}	number of element through the thickness
ν_o	initial fiber volume fraction
ν_f	fiber volume fraction
P	resin pressure
P_a	autoclave pressure
P_{bc}	bag pressure
P_f	pressure borne by fiber
q_i^f	resin flow rate
q_i^t	heat flux
R	universal gas constant
r_f	fiber radius
ρ	composite density
ρ_f	fiber density
ρ_r	resin density
s_{ij}	permeability tensor component
s_x, s_y, s_z	principal permeabilities
t	time
T	temperature

T_o	initial temperature
T_a	autoclave temperature
θ	fiber orientation
U	activation energy for viscosity
u_i	pseudo-temperature or pressure solution
v_i	pseudo-temperature or pressure solution
x_i	laminate system of coordinates
x, y, z	principal directions

Chapter 1

Introduction

Composite components constructed from continuous fiber reinforced thermosetting resin matrix prepreg materials are manufactured by arranging the uncured fiber resin mixture into the desired shape and then curing the material. The pertinent processing parameters in curing are time, temperature, and pressure. The curing process is accomplished by exposing the material to elevated temperatures and pressures for a predetermined length of time. The elevated temperatures applied during the cure provide the heat required for initiating and maintaining the chemical reactions in the resin which cause the desired changes in the molecular structure. The applied pressure provides the force needed to squeeze excess resin out of the material, to consolidate individual plies, and to compress vapor bubbles. The elevated temperature and pressure to which the material is subjected are referred to as the *cure temperature* and the *cure pressure*. The magnitude and duration of the temperatures and pressures applied during the curing process (denoted as the

cure cycle) significantly affect the performance of the finished product. Therefore, the cure cycle must be selected carefully for each application.

The standard cure cycle for polymer matrix composites is a two-step cure cycle (Figure 1.1). In such cycles the temperature of the composite is increased from room temperature to the first dwell temperature ($\approx 2°C/min$) and this temperature is held constant for the first dwell period ($\approx$ 1 hour). After that the temperature is increased ($\approx 2°C/min$) again to the second dwell temperature and held constant for the second dwell period (2-8 hours). After the second dwell, the part is cooled down to room temperature at a constant rate ($\approx 5°C/min$). Since there are two dwell periods, this type of cure cycle is referred to as a *two-step cure cycle*. The purpose of the first dwell is to allow gases (entrapped air,water, or volatiles) to escape the matrix material and to allow the matrix to flow, facilitating compaction of the part. Thus, the viscosity must be low during the first dwell. Typical viscosity versus temperature profiles of polymer matrices show that as the temperature is increased, the viscosity of the polymer decreases until a minimum viscosity is reached (Figure 1.2). As the temperature is increased further, the polymer begins to cure rapidly and the viscosity increases dramatically. The first dwell temperature must be chosen judiciously to allow the viscosity of the resin to be low while keeping the cure to a minimum. Isothermal viscosity versus time profiles are useful in determining the pot life of the polymer (Figure 1.2). The polymer pot life is the maximum length of time at a specific temperature for the polymer to

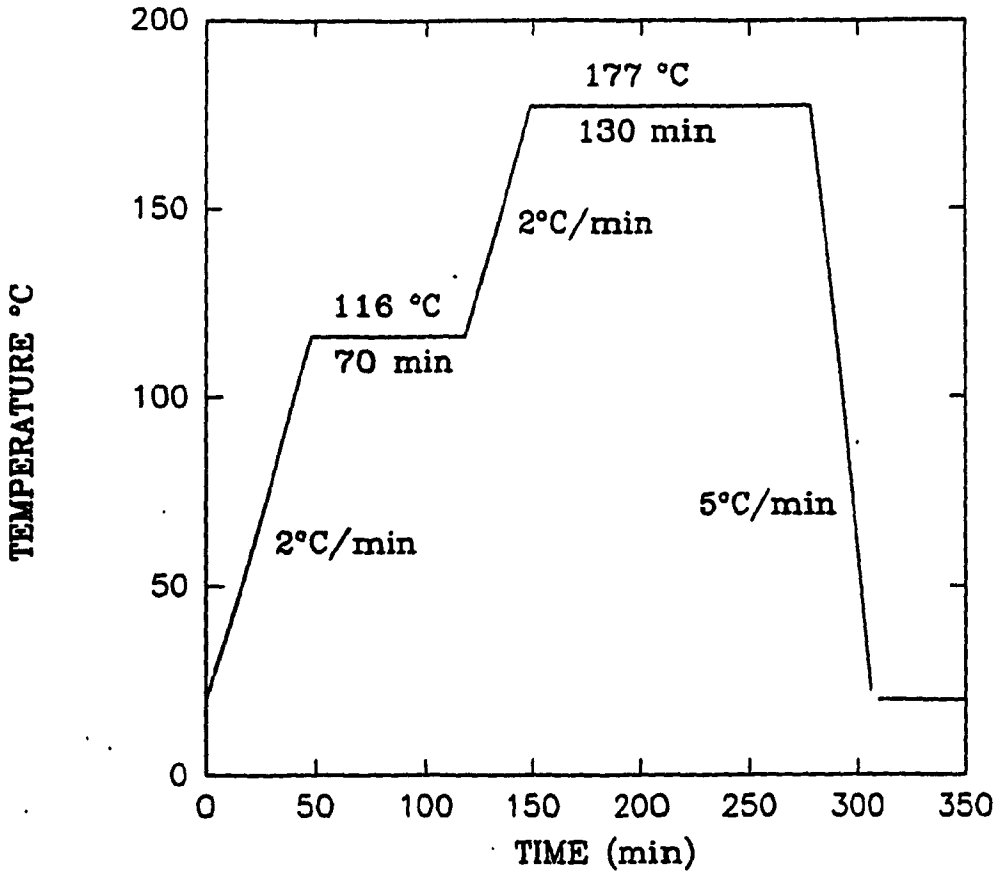

Figure 1.1: Typical two-step cure cycle for autoclave curing

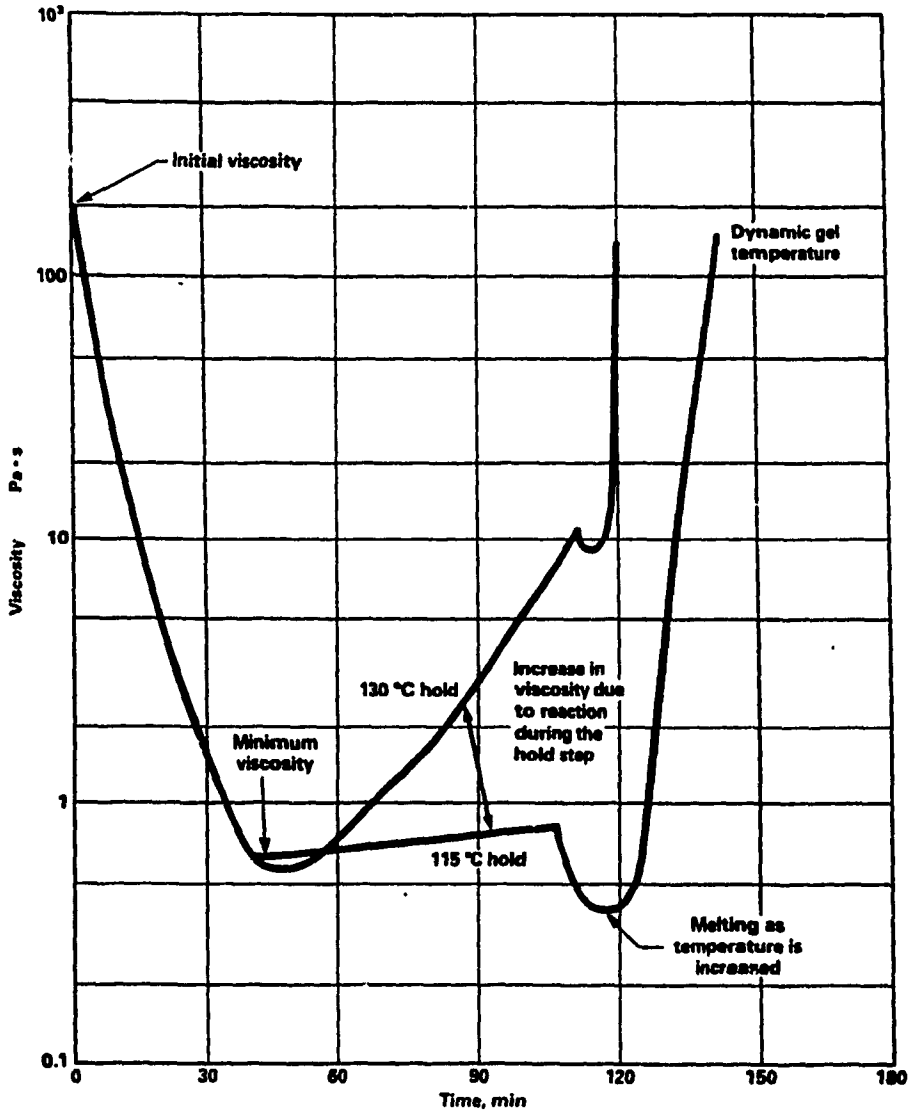

Figure 1.2: Typical viscosity variation during the two-step cure cycle (Heating rates and hold times are identical) [6].

remain fluid-like. The first dwell time must be within the pot life of the polymer at the dwell temperature.

The purpose of the second dwell is to allow cross-linking of the polymer to take place. It is here that the strength and related mechanical properties of the composite are developed. To characterize the exothermic cross-linking reaction of a thermosetting polymer matrix, a thermal cure monitoring technique such as Isothermal Differential Scanning Calorimetry (DSC) is commonly used. Two competing priorities take place in the choice of the second dwell temperature. First, a low temperature is desirable for ease of manufacturing and to reduce the effects of thermal mismatch between fiber and matrix materials. Second, the processing time should be as short as possible for economic considerations. Since low temperature requires longer dwell times, these two concern must be compromised.

Laminated composites are most commonly processed in an autoclave. In this case vacuum and pressure are applied to the part during processing. Typically, vacuum is applied to the part during the initial dwell to help facilitate removal of entrapped gases. Vacuum is discontinued after the increased viscosity of the matrix nullifies any benefit from the pressure differential experienced by the matrix. Pressure is applied to help in consolidation and ensuring fiber-matrix interaction. Pressure is removed either after significant cross-linking or after completion of the process cycle.

The proper choice of temperature and pressure histories is vitally important

in the production of high quality composite parts. The development of residual stresses, for example, is strongly influenced by processing history. Residual stresses can have a significant effect on the mechanics and performance of composite structures by inducing warpage or initiating matrix cracks and delamination [1-8]. Mechanical properties of composite laminates have been also shown to be dependent on the cure process [9, 10].

Application of thick thermosetting composites is growing in the aerospace industry and construction and military applications. To fabricate a high quality thick thermosetting composite part, the proper choice of the processing parameters during curing process is very important. There are a number of problems arising because of the low thermal conductivity and low permeability of the thick composite parts during curing. The most familiar problem is an increase in internal temperature resulting from the irreversible exothermic chemical reaction of the matrix phase. Liberated heat is slow to dissipate by conduction and may potentially raise internal part temperatures to levels risking material degradation. The second problem relates to the complex temperature and degree of cure gradients that develop in thick section during processing [11, 12, 13]. These gradients induce non-uniform curing within the part that may ultimately lead to a reduction in the overall quality and in service performance of the finished product. Non-uniform curing can result in incomplete consolidation of the part which, in turn, may lead to undesirable volume fraction gradients and entrapped volatiles or voids [13, 14].The

third problem relates to the consolidation and compaction behavior of thick thermosetting composites. When the tool temperature is increased, the temperatures at the inside and outside surface of the part increase, the local viscosity decreases and consolidation begins. However, the temperature at the center region of composite part remains low because it takes a longer time for the heat to reach to the center region by conduction. Therefore, interior viscosity can remain high during the period when the surface viscosity is low. The consolidation occurs at the outside surface (bleeder side). However, in some cases the complete through-the-thickness consolidation can not be achieved due to resin gelation. There are experimental evidences that the manufacture's recommended cure cycle may not be appropriate when curing thick composites [15, 16].

1.1 Literature Survey

The autoclave curing process of thermosetting composites has been the subject of numerous investigations. Studies of the curing process have focused on the thermal and chemical interaction, degree of cure profile, viscosity behavior, void formation and growth, and resin flow phenomena occurring in the composite under the application of a specified temperature and pressure cure cycle history. A review of the literature associated with the processing of thermosetting composites is now presented.

In general three types of investigation have been reported for the compression

molding and curing process. A few investigators [14, 22] have done simulation for the whole curing process without decoupling the heat and flow phenomena from each other. Another group of investigators[23, 44] have focused on the consolidation and compaction of composite during which the applied pressure is assumed to be constant. A few investigators [11, 13, 45, 53] have studied the thermochemical problem without considering the consolidation during the process. The survey presented here is not intended to be exhaustive, but those authors cited are felt to have made significant contributions in the area.

Loos and Springer [14] developed a comprehensive one-dimensional simulation model to describe the curing process of flat plate unidirectional graphite-epoxy composite laminates. The model integrated submodels which describe the fundamental mechanism associated with the curing process such as the thermochemical interaction, resin flow and void formation. Governing equations describing the curing process are solved with an implicit finite difference method. Temperature, degree of cure, resin flow and void size, among other processing variables are predicted as a function of the autoclave pressure and temperature cure cycle history. Experimental verification of the model was performed and results are in good agreement with simulated prediction. They developed the *sequential compaction model* to simulate the resin flow through the composite fiber bed. These submodels have been used successfully in different applications [18, 19, 20, 21].

Mallow et al. [22] developed a computer code for modeling of cure process. This model consists of five interrelated submodels named kinetic, viscosity, resin flow, heat transfer, and void growth. While the kinetic, viscosity, and void submodels are derived from experimental data, the flow and heat transfer submodels are finite difference solutions to partial differential equations in space and time.

Gutowski [26, 27] proposed a viscoelastic model for the behavior of an aligned fiber composite during the molding cycle. He suggested that the elastic effects can not ,in general, be ignored. The basic conceptual idea presented by him is that the uncured composite can be modeled as a porous, non-linear elastic media that is filled with a viscous liquid. When pressure is applied to a flat laminate of this type, it must be shared by both the resin and the fiber structure. Initially however, the applied pressure is carried solely by the resin (zero deformation). Now, if there is a lower pressure at the boundary of the composite, the pressure gradient will cause resin to flow out. This loss in resin will allow the composite to compact, thereby compressing the fiber network. As a result of this, part of the applied load is now carried by the fibers, and concurrently the resin pressure is reduced. In the extreme, when the resin is free to continuously flow out of the composite, the resin pressure must go to zero. The final fiber volume fraction of the composite is then solely determined by the deformation characteristics of the fiber structure, and has nothing to do with the resin flow process (for more details see section 2.4). Of course, there are a number of important cases where the flow process is restricted

(often due to the high viscosity), and the applied load is only partly transferred to the fibers. To get a mathematical model, he obtained a partial differential equation by combining momentum, fiber continuity, resin continuity, and Darcy's law for Newtonian fluid equations. He proposed a nonlinear stiffness parameter based on experiments in which the effect of fiber in carrying the pressure is expressed by considering the fiber volume fraction.

Dave et al. [29, 30] proposed a new three dimensional model for resin flow during composite processing. The model is based on the theory of consolidation and flow through a porous medium, which considers that the total force acting on a porous medium is countered by the sum of the opposing forces, including the force due to the spring-like effect of the fiber network and the hydrostatic force due to the pressure of the liquid within the porous medium. The flow in the laminate is described in terms of Darcy's law for Newtonian fluid in a porous medium, which requires a knowledge of the fiber network permeability and the viscosity of the flowing fluid. Unlike previous resin flow models, this model properly considers the flow in different directions to be coupled and provides a unified approach in arriving at the solution. Resin pressure profiles show that the pressure gradients in through-the-thickness and in-plane directions are not linear, unlike the assumption of linearity made in several previous resin flow models [14, 25]. By increasing the time, it has been shown that the resin pressure reaches a certain amount (ambient pressure). At this stage, all the exerted pressure is borne by the fiber structure.

Both Gutowski model [26, 27] and Dave model [29, 30] are based on the three-dimensional resin flow and one-dimensional consolidation of composite which are sometimes called *squeezed sponge model.*

Dave[32] showed that the all proposed resin model for bleeder ply molding or autoclave processing, pultrution, and resin transfer molding are special cases of a generalized flow model. He discussed the different assumptions that can be made to reduce the generalized flow model to the different available flow models. Theoretical predictions are compared with experimental data available in the literature.

Smith et.al.[34] studied and compared the sequential compaction model and squeezed sponge model for the resin flow. They have shown that the sequential compaction model is essentially a special case of the squeezed sponge model. Using the fiber bed compaction and permeability as the primary parameters in the squeezed sponge flow model, it is shown that a range of laminate compaction behavior, from sequential to uniform compaction, can be obtained. It is also shown that permeability controls the compaction time and the fiber bed behavior controls the shape of the laminate compaction response.

Lindt [35] studied the consolidation process from another point of view. An analytical solution, based on the lubrication approximation, is given for the flow associated with the consolidation of circular cylinders in a Newtonian fluid. In this model, equation of motion was integrated for the fluid flow between the cylindrical

fibers. In fact, it can be said that Lindt's approach is from microscopic point of view, while the Darcy's law approach is from macroscopic point of view.

Astrom et al. [37] reviewed most of the work done based on the Darcy's law. They concluded that although Darcy's law and the Kozeny-Carman expression for the permeability adequately describe flow of Newtonian fluids through beds of spherical particles, its commonly used equivalent form for beds of aligned fibers is much less accurate. For a given material system, the flow rate-pressure drop relationship for flow of Newtonian fluids through fiber beds may be used to obtain qualitatively accurate results, but to obtain quantitatively correct results, the shape factor and tortuosity have to be determined experimentally. Available flow rate-pressure drop relationships obtained for flow of generalized Newtonian fluid through sphere beds have been experimentally well verified. However, these relationships for flow of generalized Newtonian fluid through cylinder beds have not been verified yet. They also found that in composite processing application, the flow rates are low enough to neglect inertia effects in the flow. Whereas viscoelasticity does not normally to be considered for flow parallel to the fibers, it is suspected that viscoelastic effects may be of importance for flow perpendicular to the fibers. It means that the viscoelasticity of polymer fluids in porous media is related to the extensional nature of the flow, which results in stretching of the polymer macromolecules. In other words, the viscoelastic effects are very important in extensional flow situation, such as flow perpendicular to the fiber beds.

Gebart [38] studied the permeability of an idealized unidirectional reinforcement consisting of regularly ordered, parallel fiber. Navier-Stokes equations are integrated both for flow along and for flow perpendicular to the fibers. Two expressions for permeability along and perpendicular to the fiber have been derived. He has concluded that Darcy's law is a good approximation for the flow in Resin Transfer Moulding (RTM) when the resin behaves as a Newtonian fluid.

Skartsis et.al.[39, 40] presented a review of both theoretical and experimental studies of fluid through porous media, including fiber beds. The flow is assumed to be Newtonian. They studied the Kozeny-Carman relation and showed that one can not experimentally determine the Kozeny constant at low fiber volume fraction and use this value to describe high fiber volume fraction situations. Newtonian flow through ideal cylinder arrangements has been analyzed and measured. Their analytical and numerical solutions agreed well with experimental observation.

Kays [45] conducted a comprehensive investigation on the processing issues unique to large area thick section laminates. The baseline material system was unidirectional graphite/epoxy. Cure simulation models were developed and used in the investigation. Various autoclave procedure, cure monitoring and non-destructive evaluation techniques for thick section laminates were developed and evaluated. Interesting observations reported in the study were the development of microcracks and delaminations under certain processing conditions, indicating the importance

of processing on the cure and performance of thick section composites. Although ply-drop geometries were included in the study, cure simulation was limited to a one-dimensional through-the-thickness analysis.

Bogetti and Gillespie [11] conducted a fundamental study of process-induced residual stress in the thick-section thermosetting composites. A one-dimensional cure simulation model is employed. Residual stresses are shown to be strongly influenced by gradients in temperature and degree of cure. In another investigation, they proposed a two-dimensional cure simulation for thick thermosetting composites [13]. Temperature and degree of cure distributions within arbitrary cross-sectional geometries are predicted as a function of autoclave temperature history. The heat conduction equation for two-dimensional, transient anisotropic heat transfer is coupled to the cure kinetics of the thermosetting composite materials. Complex gradients in temperature and degree of cure are predicted and the influenced of the tools on the curing process is demonstrated. Several typical structural elements of arbitrary cross sections are analyzed to provide insight into the non-uniform curing process unique to thick-section. Spatial gradients in degree of cure are shown to be strongly dependent on part geometry, thermal anisotropy, cure kinetics and the temperature cure cycle. These spatial gradients directly influence the quality and in-service performance of the finished components by inducing warpage and residual stress during the curing process. Resin flow during the cure process has not been included in the model. Therefore, the

effect of autoclave pressure on the cure process of thick-section thermosetting composites which has an important role in the consolidation and compaction of laminates has not been studied.

Twardowski et.al.[52] addressed the curing of thick thermosetting composites. Simulation and experiments were used to investigate important processing variables. They found the followings-initial extent of reaction is relatively unimportant-consolidation is important- peak temperature sometimes originates near the surface of the laminate and propagates to the center- asymmetric temperature application changes the viscosity and the cure profile- viscosity never reaches low values uniformly through-the-thickness in laminates in excess of 10 cm thickness. The consolidation is assumed to be uniform through-the-thickness , to obey either linear change or to decay exponentially with respect to time.

Pitchumani and Yao[53] developed a non-dimensional approach to generalize the modeling of the cure of thermosetting composites, eliminating the need for a system-specific or product specific modeling. They studied the problem of selecting the best cure cycles for achieving a desired product quality. With regard to the manufacture of partially cured composite systems, optimal cure cycles which yield the homogeneous cure in the product, in the minimum possible time, are obtained as a function of the non-dimensional parameters. Design plots for the optimal cure temperature and duration were presented, and their use in practical

situations was illustrated.

In most of work done so far, either thermochemical model (heat conduction equation and kinetic equation) or resin flow model (viscosity equation and flow equation) was developed and numerically solved. Only a few investigators [14, 22] have considered both thermochemical and resin flow models simultaneously in their work. The resin flow model used by them is the sequential compaction model. However, it has been shown [26-33] that the squeezed sponge model predicts compaction of laminate accurately and has to be considered in the simulation. Thermochemical equations combined with resin flow equations (squeezed sponge model) should be solved to study the behavior of thick laminates during cure process. This type of simulation provides better results for laminate compaction.

1.2 Objectives

The cure process has a significant effect on the quality, performance, and mechanical properties of the thick-section thermosetting matrix composite materials. Therefore, the cure cycle for this type of composites should be selected carefully. Some major considerations in selecting the proper cure cycle for a given thick-section thermosetting matrix composite materials are :

- The temperature inside the material must not exceed a preset maximum value at any time during cure.

- At the end of cure, all the excess resin is squeezed out from every ply of the composite and the resin distribution is uniform.
- The material is cured uniformly and completely.
- At any time of cure, composite should have minimum spatial temperature gradient (uniform temperature in the whole composite at each moment)
- The cured composite has the lowest possible void content.
- The curing process is achieved in the shortest amount of time.

Experiment, simulation, and modeling (scaling) are three ways to study the composite behavior and to make sure that all of those mentioned considerations are achieved during curing. Performing experiment to determine optimum cure cycle for a given material particularly for thick composites requires an extensive experimental program and expensive prepreg materials.

Simulation is an efficient way to obtain the optimum processing parameters in curing. Simulation for curing process, considering the heat transfer and resin flow simultaneously, was done by a few investigators[14, 22]. The flow model used in those simulations is the sequential compaction model developed by Springer[14]. The recent research results[26-33] show that the squeezed sponge model predicts the compaction of composite more accurately and gives more realistic results. To achieve better results, particularly for the compaction and consolidation of composite, the thermochemical equations combined with squeezed sponge model should

be solved. There are some difficulties encountered in the solution due to the variable through-the-thickness composite physical properties (viscosity, permeability, and thermal conductivities). Kinetic equation is required for computer simulation. However, this equation is not available for most resins.

Another way to study the behavior of thermosetting composite (particularly thick composites) during the cure process is to design and use a model for experiment. So far, no work has been done along this line. In model work, the performance of the thick and expensive composite part (prototype) during curing is predicted from the test results on another composite part (model) which has less thickness and made of less expensive materials.

The objectives of this thesis are

- to solve the thermochemical and resin flow (squeezed sponge model) governing partial differential equations simultaneously while considering the composite physical properties as functions of fiber volume fraction.
- to perform experiment to study the curing of thick thermosetting composite parts and to verify the simulation results
- to use simulation to obtain a better understanding of the processing parameters involved in the curing of thick thermosetting composites.
- to establish the model laws for curing of thermosetting composites.

1.3 Thesis Overview

Curing of thermosetting composite parts consists of different physical phenomena such as heat transfer, chemical reaction and fluid flow. Simulation of cure process requires different models to describe each phenomenon. Those models and their related governing partial differential equations are developed in chapter 2.

Chapter 3 describes the numerical techniques used to solve the model governing equations. Method of calculation for different composite physical properties are discussed in this chapter as well. Chapter 4 explains the materials, fixtures, and instruments used in the experimental setup. In chapter 5, the experimental results are compared with simulation results. After models verification, the simulation is used to study the effect of different parameters in the curing of thick thermosetting composites. Chapter 6 describes the similarity rules and model laws for curing of thermosetting composites. In chapter 7, general conclusions about the study are presented along with an outlook for future work.

Chapter 2

Mathematical Models

To study the cure process, the development of mathematical models to describe the fundamental mechanisms involved , such as heat transfer, exothermic chemical reaction, and resin flow, is required. Such models are needed to relate the temperature and pressure applied during the cure to the thermal, chemical, and physical process occurring inside the material. The models require the knowledge of the thermal, chemical, and physical properties of the material which affect the curing process. Four models which are used to obtain governing equations describing the fundamental mechanism in curing are:

- Heat model
- Kinetic model
- Viscosity model
- Flow model

The first three models, referred to as the *Thermochemical model*, yields the temperature, the degree of cure, and the viscosity. The fourth model gives the resin pressure, the resin flow out of the composite, and the composite fiber volume fraction. The governing differential equations describing different models are coupled together and should be solved simultaneously.

2.1 Heat Model

The temperature distribution, the degree of cure of the resin, and the resin viscosity inside the composite depend on the rate at which the heat is transmitted from the environment into the material. The temperature inside the composite can be calculated using the law of conservation of energy together with an appropriate expression for the cure kinetics. By neglecting the energy transfer by convection, the energy equation with considering an internal heat generation source term can be expressed as [54]

$$-\frac{\partial q_1'}{\partial x_1}-\frac{\partial q_2'}{\partial x_2}-\frac{\partial q_3'}{\partial x_3}+\dot{g}=\rho c_p\frac{\partial T}{\partial t} \tag{2.1}$$

where q_1', q_2', and q_3' are the heat fluxes along the x_1, x_2, and x_3 axes (Figure 2.1). The term $\dot{g}$ represents internal heat generation. ρ is the composite density, and c_p is specific heat of the composite. T and t are absolute temperature and time, respectively.

The general expression for the three components of the heat flux q_1', q_2', and q_3',

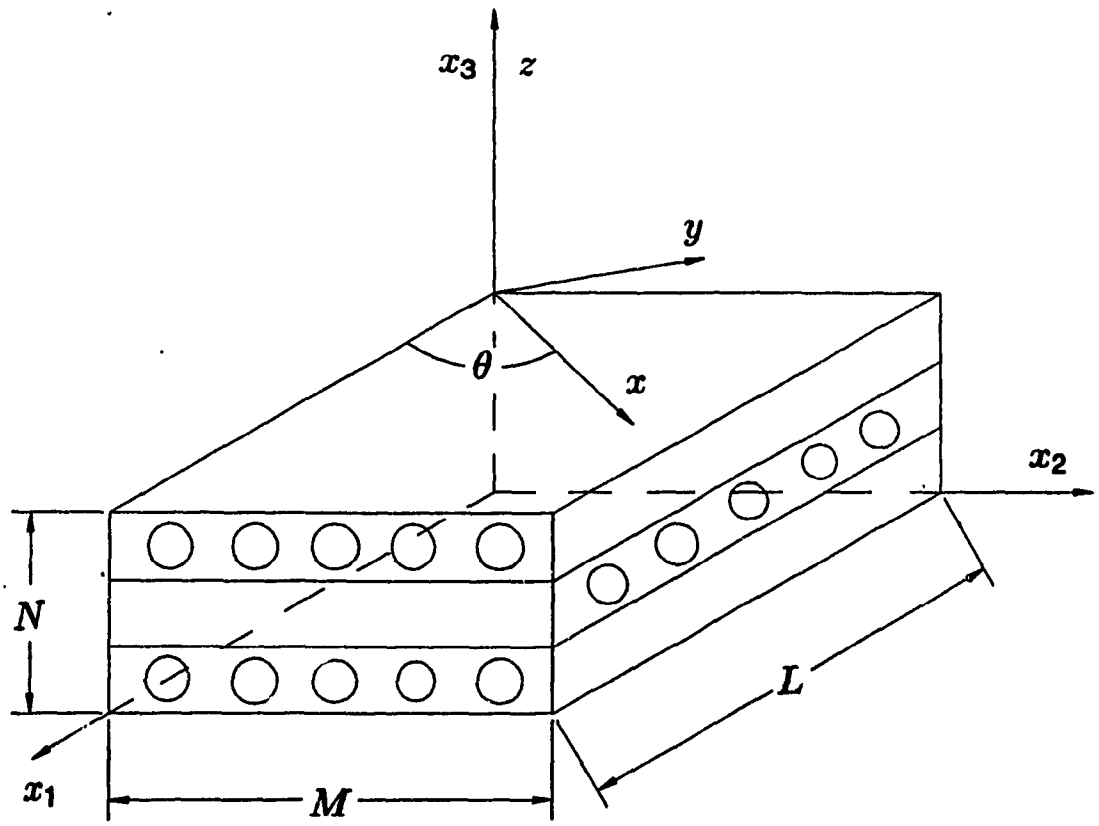

Figure 2.1: Different systems of coordinates.$x_1x_2x_3$ is the laminate system of coordinates and xyz is the ply system of coordinates (principal directions).

based on *Fourier law*, in the rectangular coordinate system are given as [54]

$$q_i' = -\sum_{j=1}^{3} k_{ij}\frac{\partial T}{\partial x_j} \qquad i = 1,2,3 \tag{2.2}$$

where k_{ij} are the coefficients of thermal conductivity tensor. The thermal conductivity is a second-rank tensor and ,therefore, can be subjected to the tensor transformation. It can be written that

$$k'_{ij} = C_{im}C_{jl}k_{ml} \qquad i,j,m,l = 1,2,3 \tag{2.3}$$

where k'_{ij} and k_{lm} are the thermal conductivities in the new and old system of coordinates, respectively. C_{ij} are the direction cosines. k_{ij} is a symmetric tensor and ,therefore, it can be written

$$k_{ij} = k_{ji} \tag{2.4}$$

One can substitute Equation (2.2) into the Equation (2.1). The result will be the following equation

$$\frac{\partial}{\partial x_1}(k_{11}\frac{\partial T}{\partial x_1} + k_{12}\frac{\partial T}{\partial x_2} + k_{13}\frac{\partial T}{\partial x_3}) + \frac{\partial}{\partial x_2}(k_{21}\frac{\partial T}{\partial x_1} + k_{22}\frac{\partial T}{\partial x_2} + k_{23}\frac{\partial T}{\partial x_3}) + \frac{\partial}{\partial x_3}(k_{31}\frac{\partial T}{\partial x_1} + k_{32}\frac{\partial T}{\partial x_2} + k_{33}\frac{\partial T}{\partial x_3}) + \dot{g} = \rho c_p\frac{\partial T}{\partial t} \tag{2.5}$$

For the flat plate composite constructed from prepreg tape with considering the selected system of coordinates (Figure 2.1), it can be shown that $k_{13} = k_{23} = 0$. Therefore, Equation (2.5) can be written as

$$\frac{\partial}{\partial x_1}(k_{11}\frac{\partial T}{\partial x_1} + k_{12}\frac{\partial T}{\partial x_2}) + \frac{\partial}{\partial x_2}(k_{21}\frac{\partial T}{\partial x_1} + k_{22}\frac{\partial T}{\partial x_2}) + \frac{\partial}{\partial x_3}(k_{33}\frac{\partial T}{\partial x_3}) + \dot{g} = \rho c_p\frac{\partial T}{\partial t} \tag{2.6}$$

This equation should be solved to get the temperature distribution inside the flat plate thermosetting composites.

Laminae thermal conductivities are usually measured along its principal directions. Thermal conductivity of each laminae in the x_1, x_2 and x_3 directions can be obtained by the transformation of the laminae thermal conductivities in the principal directions x, y, and z(Figure 2.1). Thus, it can be shown that

$$\begin{Bmatrix} k_{11} \\ k_{22} \\ k_{12} \\ k_{33} \end{Bmatrix} = \begin{bmatrix} m^2 & n^2 & 0 \\ n^2 & m^2 & 0 \\ mn & -mn & 0 \\ 0 & 0 & 1 \end{bmatrix} \begin{Bmatrix} k_x \\ k_y \\ k_z \end{Bmatrix} \tag{2.7}$$

where $m = cos\theta$ and $n = sin\theta$. θ is the angle between the principal directions with the x_1x_2 system of coordinates. k_x, k_y, and k_z are thermal conductivities in the principal directions.

Simulation, experiment, and scaling are used to study the behavior of unidirectional thick flat plate composite constructed from prepreg material. The principal directionsx, y, and z are coincident to the global coordinate x_1, x_2, and x_3 ($\theta = 0$). For this case, combination of Equations (2.6) and (2.7) yield

$$\frac{\partial}{\partial x}(k_x\frac{\partial T}{\partial x}) + \frac{\partial}{\partial y}(k_y\frac{\partial T}{\partial y}) + \frac{\partial}{\partial z}(k_z\frac{\partial T}{\partial z}) + \dot{g} = \rho c_p\frac{\partial T}{\partial t} \tag{2.8}$$

Equation (2.8) is used during the rest of the calculation. k_x, k_y, and k_z can be either constant or functions of independent variables x, y, and z.

2.1.1 Initial and Boundary conditions

The following initial and boundary conditions should be applied during the solution of Equation (2.8).

Initial condition:

$$T(x,y,z,0) = T_o \quad for \quad \begin{cases} 0 \le x \le L \\ 0 \le y \le M \\ 0 \le z \le N \end{cases} \tag{2.9}$$

where T_o is the composite initial temperature. L is plate length, M is plate width, and N is plate thickness.

Boundary conditions:

A generalized temperature boundary condition formulation is used to permit flexibility in the simulation of the autoclave curing process. Either Dirichlet, Neumann, Robin boundary conditions may be enforced on the domain boundaries. The generalized boundary condition is expressed mathematically as

$$a_1 \frac{\partial T_{bc}}{\partial n} + a_2 T_{bc} + a_3 T_a(t) = 0 \tag{2.10}$$

The surface boundary temperature is T_{bc} and n is the outward unit normal to the domain surface. The coefficient a_1, a_2, and a_3 define the effective heat transfer across the domain boundaries. The temperature $T_a(t)$ in Equation (2.10) is interpreted as the ambient autoclave temperature cure cycle. Table 2.1 summarizes the three possible boundary conditions obtainable from this generalized formulation.

Dirichlet (prescribed)	$a_1 = 0$	$a_2 = 1$	$a_3 = -1$
Neumann (insulated)	$a_1 = 1$	$a_2 = 0$	$a_3 = 0$
Robin (convective)	$a_1 = 1$	$a_2 = (\frac{h}{k})_{eff}$	$a_3 = -(\frac{h}{k})_{eff}$

Table 2.1: Generalized boundary condition coefficients

2.2 Kinetic Model

Kinetic model determines the minimum time required to cure the resin and ,therefore, to obtain sufficient physical and mechanical properties. It also determines the rate of heat generated by chemical reaction ($\dot{g}$) that appears in the heat conduction equation. *Differential Scanning Calorimetry (DSC)* is used to develop the mathematical equations for the kinetic model. Two types of scanning are used. Dynamic scans (constant heating rate) are performed to determine the resin ultimate heat of reaction H_R (the heat of reaction obtained from complete polymerization). Isothermal scans are performed to measure the heat of reaction at constant temperature. The degree of cure of the resin (denoted as the degree of cure, α) is defined as

$$\alpha = \frac{h(t)}{H_R} \tag{2.11}$$

$h(t)$ is the heat evolved from the beginning of the reaction to some intermediate time, t (Figure 2.2). For an uncured material α is equal to zero and for a completely cured material, α approaches unity. By differentiating Equation (2.11) with respect to time, the following expression can be obtained.

$$\dot{h} = \frac{d\alpha}{dt} H_R \tag{2.12}$$

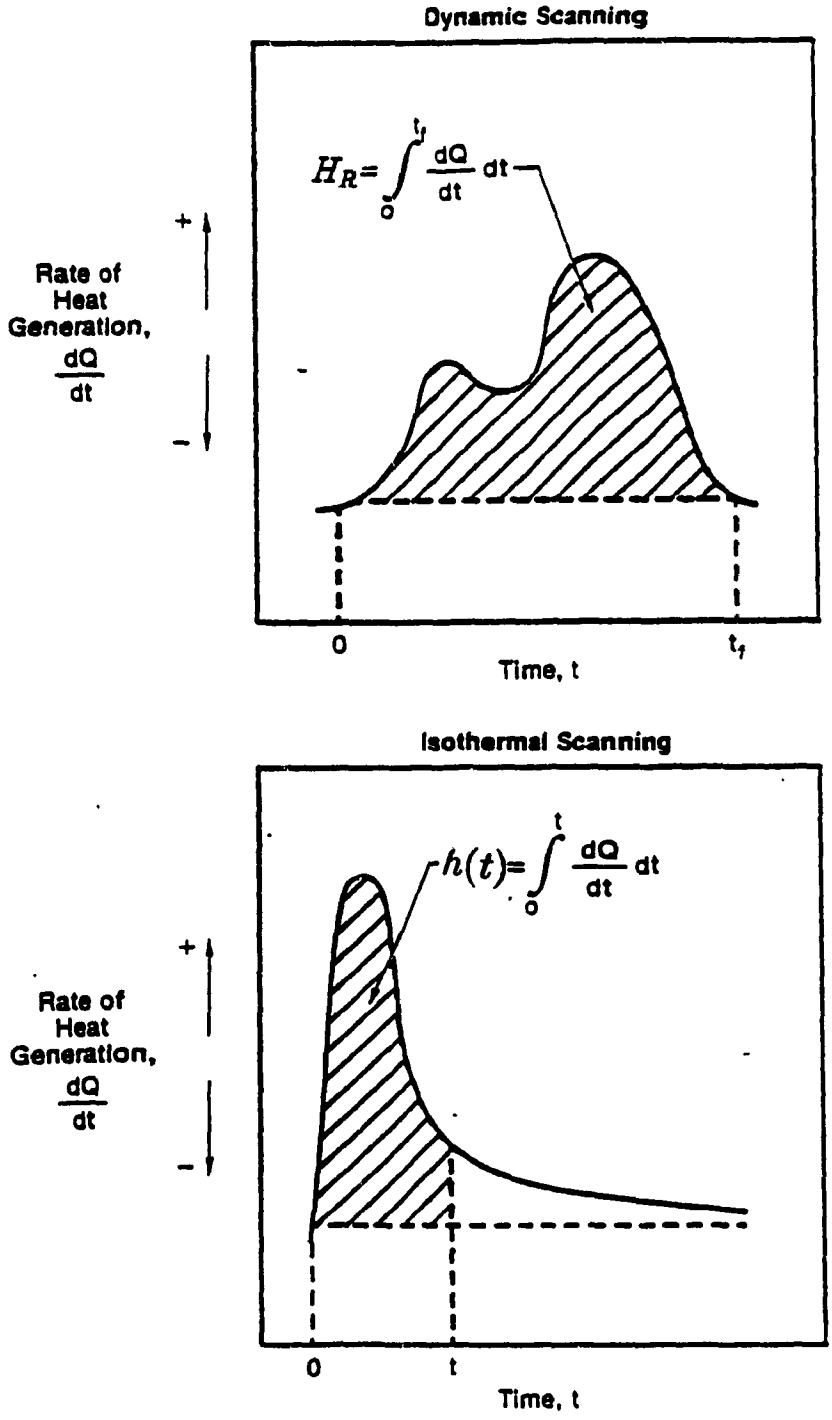

Figure 2.2: Differential Scanning Calorimetry (DSC).

$\dot{h}$ is the rate of heat generation per unit mass. Composites consist of both fiber and resin. The chemical reaction inside the resin is the only source of heat generated inside the composite during curing. Therefore, the heat generation term used in Equation (2.8) should be calculated as

$$\dot{g} = \rho_r(1 - \nu_f)\frac{d\alpha}{dt}H_R \tag{2.13}$$

$\dot{g}$ is the rate of heat generation per unit volume. ρ_r is the resin density and ν_f is the fiber volume fraction.

If diffusion of chemical species is neglected, the degree of cure at each point inside the material can be calculated once the cure rate is known in the following way

$$\alpha = \int_0^t (\frac{d\alpha}{dt})dt \tag{2.14}$$

In order to complete the model, the dependence of the cure on the temperature and on the degree of cure must be known. This dependence may be expressed symbolically as

$$\frac{d\alpha}{dt} = f(T, \alpha) \tag{2.15}$$

The functional relationship in Equation (2.15), along with the value of the heat of reaction H_R for the different materials have been determined experimentally [55, 60]. In general, it is impossible to express the kinetic equations for all resin systems in a single functional form. There exists a usual expression to obtain kinetic equation. For both epoxy and unsaturated polyester systems, the kinetic

equations in dimensional form can be expressed as[55, 56, 57, 60]

$$\frac{d\alpha}{dt} = (A_1 \exp(\frac{-E_1}{RT}) + A_2 \exp(\frac{-E_2}{RT})\alpha^a)(B - \alpha^b)(1 - \alpha^d)^c \tag{2.16}$$

where A_1 and A_2 are pre-exponential factors and E_1 and E_2 are activation energies. a, b, c, d, and B are constants. R is universal gas constant. For the case of polyester this equation can be simplified as[13, 58]

$$\frac{d\alpha}{dt} = A \exp(\frac{-E}{RT})\alpha^m (1 - \alpha)^n \tag{2.17}$$

where m and n are constants independent of temperature.

Graphite/epoxy AS4/3501-6 was used for the simulation and experiments. This is a representative epoxy system used widely in aerospace applications. The kinetic equation for the Hercules 3501-6 resin can be expressed as [56]

$$\frac{d\alpha}{dt} = \begin{cases} (K_1 + K_2\alpha)(1 - \alpha)(0.47 - \alpha) & \alpha \leq 0.3 \\ K_3(1 - \alpha) & \alpha > 0.3 \end{cases} \tag{2.18}$$

where

$$K_1 = A_1 \exp(\frac{-E_1}{RT}) \tag{2.19}$$

$$K_2 = A_2 \exp(\frac{-E_2}{RT}) \tag{2.20}$$

$$K_3 = A_3 \exp(\frac{-E_3}{RT}) \tag{2.21}$$

A_1, A_2, and A_3 are pre-exponential factors. E_1, E_2, and E_3 are the activation energies, and R is the universal gas constant.

The reaction rate is described by two different equations (Equations (2.18)). The results of the dynamic scanning measurement show that there are at least

two dominant reactions occurring during cure. These reactions (represented by two humps in dynamic scanning in Figure 2.2) can not be represented by a single equation, but must be described by different equations. This is the reason for the two equations employed here.

2.3 Viscosity Model

The coupling between thermochemical model and resin flow model is through the viscosity model. The viscosity μ of thermoset resins decreases with increasing temperature and increases with increasing degree of cure α. Since both the viscosity and degree of cure are functions of temperature and time, therefore, a relationship between μ and α can be established. The following expression can be used to describe the resin viscosity [56, 57]

$$\mu = \mu_{\infty} exp(\frac{U}{RT} + \kappa\alpha) \tag{2.22}$$

where μ_{∞} and κ are constants and U is the activation energy for viscosity.

2.4 Flow Model

Different flow models have been developed [22, 25, 30]. In this thesis, the resin flow is modeled as flow through a porous fiber bed in the case of one-dimensional consolidation with three-dimensional seepage (flow). This model is sometimes

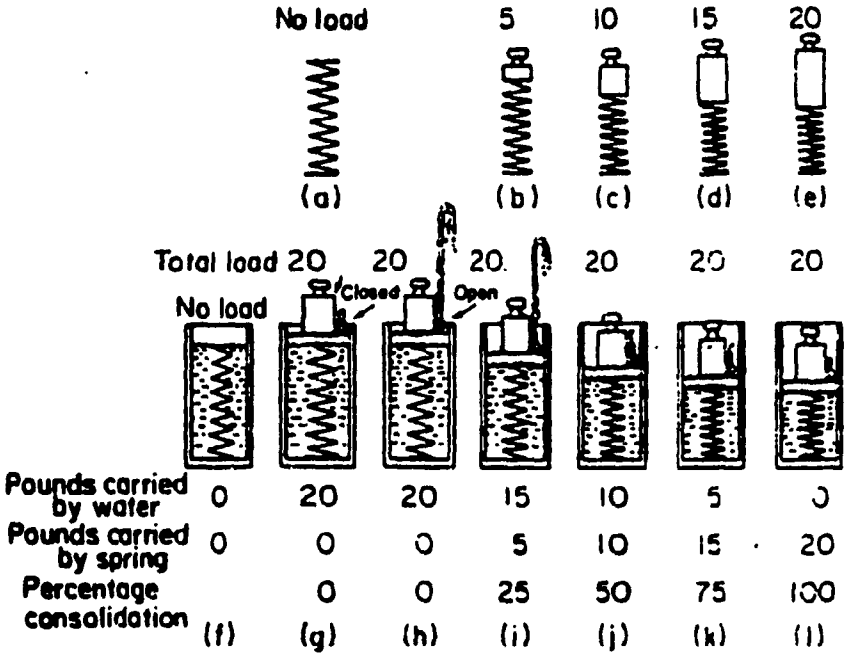

Figure 2.3: The piston and spring analogy for flow model [30].

called *Squeezed Sponge Model.* The basic idea in developing the squeezed sponge model is that the fiber bed carries some of the applied pressure (autoclave pressure). The process of consolidation based on squeezed sponge model can be described by referring to a mechanical analogy. Figure 2.3 illustrates the piston and spring analogy. In Figure 2.3 sketches a to e show the various length assumed by a spring under various loads. In the lower row of sketches the same spring is assumed to be immersed in a water-tight cylinder filled with some incompressible liquid. In sketch g,a frictionless but tightly fitted piston provided with a stopcock is placed in the cylinder and loaded with a total of $20kg$. Due to incompressibility of the liquid, no consolidation (i. e. , compression) of the spring takes place with the stopcock closed. Now at time $t = 0$, the stopcock is opened (sketch h). At the instant $t = 0$, the pressure conditions are unchanged from the condition at $t < 0$, as shown in sketch h. As time passes, more and more liquid escapes and the piston sinks lower, compressing the spring. However, at any instance, the total force acting down is always countered by the sum of the opposing forces,i. e. , the force due to the spring and the hydrostatic force due to the liquid. Since the velocity of the descending load is small, it is assumed that the load and the piston are quasistatic, which means that the sum of the forces acting downward is equal to the sum of the forces acting upward. Finally, at long time (sketch l) the spring compresses to the same length as in sketch e.

In the mechanical analogy presented above, the spring represents the com-

pressible fiber bed and the liquid represents the epoxy in the void space of the fiber bed. The stopcock opening is analogous to the permeability and the compressibility of the spring refers to the compressibility of the fiber bed. The more permeable the fiber bed, the shorter time required for consolidation.

The governing differential equation satisfying the consolidation of a porous bed with three-dimensional seepage(flow) and a one-dimensional confined compression condition (no boundary motion in x_1 or x_2 directions) is given by [29, 30, 61]

$$-\frac{\partial q_1^f}{\partial x_1}-\frac{\partial q_2^f}{\partial x_2}-\frac{\partial q_3^f}{\partial x_3}=m_v(\frac{\partial P}{\partial t}-\frac{\partial \sigma}{\partial t}) \tag{2.23}$$

where q_1^f, q_2^f, and q_3^f are the resin flow rate along the x_1, x_2, and x_3 axes. m_v represents the coefficient of the volume change which is determined by experiment. P is the resin pressure and σ is the stress externally applied to the porous medium,i. e. ,the autoclave pressure P_a. The autoclave pressure is usually constant, Therefore, the expression $\frac{\partial \sigma}{\partial t}$ can be eliminated from Equation (2.23).

Matrix flow through the fiber beds is described by *Darcy's law* which relates matrix flow rate (q^f) to matrix pressure gradient ($\frac{\partial P}{\partial x_j}$), matrix viscosity ($\mu$), and fiber bed permeability (s_{ij}). Darcy's law can be expressed as[37, 38]

$$q_i^f=-\sum_{j=1}^{3}\frac{s_{ij}}{\mu}\frac{\partial P}{\partial x_j} \qquad i=1,2,3 \tag{2.24}$$

The permeability s is the second rank tensor. Therefore, Equation (2.3) can be used to transform s_{ij} to any new system of coordinates. s is a symmetric tensor ($s_{ij}=s_{ji}$).

One can substitute Equation (2.24) into the Equation (2.23). The result will be the following equation

$$\frac{\partial}{\partial x_1}\left(\frac{s_{11}}{\mu}\frac{\partial P}{\partial x_1}+\frac{s_{12}}{\mu}\frac{\partial P}{\partial x_2}+\frac{s_{13}}{\mu}\frac{\partial P}{\partial x_3}\right)+\frac{\partial}{\partial x_2}\left(\frac{s_{21}}{\mu}\frac{\partial P}{\partial x_1}+\frac{s_{22}}{\mu}\frac{\partial P}{\partial x_2}+\frac{s_{23}}{\mu}\frac{\partial P}{\partial x_3}\right)+$$
$$\frac{\partial}{\partial x_3}\left(\frac{s_{31}}{\mu}\frac{\partial P}{\partial x_1}+\frac{s_{32}}{\mu}\frac{\partial P}{\partial x_2}+\frac{s_{33}}{\mu}\frac{\partial P}{\partial x_3}\right)=m_\nu\frac{\partial P}{\partial t} \qquad (2.25)$$

For the flat plate composite with considering the selected system of coordinates (Figure 2.1), it can be shown that $s_{13} = s_{23} = 0$. Therefore, Equation (2.25) can be written as

$$\frac{\partial}{\partial x_1}\left(\frac{s_{11}}{\mu}\frac{\partial P}{\partial x_1}+\frac{s_{12}}{\mu}\frac{\partial P}{\partial x_2}\right)+\frac{\partial}{\partial x_2}\left(\frac{s_{21}}{\mu}\frac{\partial P}{\partial x_1}+\frac{s_{22}}{\mu}\frac{\partial P}{\partial x_2}\right)+\frac{\partial}{\partial x_3}\left(\frac{s_{33}}{\mu}\frac{\partial P}{\partial x_3}\right)=m_\nu\frac{\partial P}{\partial t} \qquad (2.26)$$

This equation should be solved to get the resin pressure inside the composite.

Permeability in the x_1, x_2, and x_3 directions can be obtained by the transformation of the permeability in the principal directions x, y and z (Figure 2.1). Thus, it can be shown that

$$\begin{Bmatrix} s_{11} \\ s_{22} \\ s_{12} \\ s_{33} \end{Bmatrix} = \begin{bmatrix} m^2 & n^2 & 0 \\ n^2 & m^2 & 0 \\ mn & -mn & 0 \\ 0 & 0 & 1 \end{bmatrix} \begin{Bmatrix} s_x \\ s_y \\ s_z \end{Bmatrix} \qquad (2.27)$$

where s_x, s_y, and s_z are permeabilities in the principal directions.

Simulation, experiment, and scaling are used to study the behavior of unidirectional thick flat plate composite constructed from prepreg material. The principal directionsx, y, and z are coincident to the global coordinate x_1, x_2, and x_3 ($\theta = 0$).

Combination of Equations (2.26) and (2.27) can be written as

$$\frac{\partial}{\partial x}(\frac{s_x}{\mu}\frac{\partial P}{\partial x}) + \frac{\partial}{\partial y}(\frac{s_y}{\mu}\frac{\partial P}{\partial y}) + \frac{\partial}{\partial z}(\frac{s_z}{\mu}\frac{\partial P}{\partial z}) = m_v\frac{\partial P}{\partial t} \tag{2.28}$$

Equation (2.28) is used during the rest of the calculation.

2.4.1 Initial and Boundary conditions

Equation (2.28) should be solved under the following initial and boundary conditions.

Initial condition:

$$P(x,y,z,0) = P_a \quad for \begin{cases} 0 \le x \le L \\ 0 \le y \le M \\ 0 \le z \le N \end{cases} \tag{2.29}$$

where P_a is the autoclave pressure.

Boundary conditions:

The boundary conditions are

$$\begin{aligned} P(0,y,z,t) &= P_{bc} \quad for \quad 0 \le t \le \infty \\ P(L,y,z,t) &= P_{bc} \quad for \quad 0 \le t \le \infty \\ P(x,0,z,t) &= P_{bc} \quad for \quad 0 \le t \le \infty \\ P(x,M,z,t) &= P_{bc} \quad for \quad 0 \le t \le \infty \\ \frac{\partial P}{\partial z}(x,y,0,t) &= 0 \quad for \quad 0 \le t \le \infty \end{aligned} \tag{2.30}$$

$$P(x, y, N, t) = P_{bc} \quad for \quad 0 \leq t \leq \infty$$

where P_{bc} is the bag pressure depending on the cure cycle.

2.4.2 Equilibrium Equation

The applied pressure are borne by both fiber and resin. The equilibrium equation is defined as

$$P_a = P + P_f \tag{2.31}$$

where P_f is the pressure borne by the fiber structure. The fiber pressure is needed to calculate the coefficient of the volume change m_v.

2.4.3 Coefficient of Volume Change

To solve Equation (2.28), a relationship for the coefficient of volume change m_v is required. This coefficient can be expressed in terms of fiber volume fraction as [30]

$$m_v = \frac{\nu_o}{\nu_f^2} \frac{d\nu_f}{dP_f} \tag{2.32}$$

where ν_o is the initial fiber volume fraction. The relation between fiber volume fraction ν_f and load carried by fiber P_f is determined by experiment.

2.5 Summary

Four models (heat, kinetic,viscosity, and flow) describing the curing of thermosetting composite parts were presented. Heat conduction equation combined with kinetic equation are used to obtain the temperature and degree of cure history during curing. Resin flow based on squeezed sponge model was discussed. Flow model is used to simulate the resin flow during the cure process. So far, squeezed sponge model has been found to be the most successful model describing the resin flow through the fiber bed. Viscosity model which relates the heat equation and kinetic equation to the flow equation was discussed.

Chapter 3

Numerical Solution

Four models were developed to describe the composite behavior during curing. Equations (2.8),(2.13),(2.22), and (2.28) describing various phenomena inside the composite should be solved simultaneously to obtain the different parameters during the cure process. There is no closed form solution for this system of coupled equations. Numerical technique is required to solve this system of equations. In general, numerical techniques can be used to solve the problem with complex geometry and boundary conditions. Moreover, the numerical techniques can also account for nonlinear stress-strain behavior of the porous medium and for varying thermal conductivity, density, specific heat, permeability, applied temperature, and applied pressure during the cure process.

The Control-Volume formulation combined with Alternating Direction Explicit (ADE) method are used to discretize Equations (2.8) and (2.28). The discretization equation obtained in this manner expresses the conservation principle for heat and

flow for the finite control volume, just as the differential equation expresses it for an infinitesimal control volume [62].

The most attractive feature of the control-volume formulation is that the resulting solution would imply that the integral conservation of quantities such as mass or energy is exactly satisfied over any group of control volumes and, of course, over the whole calculation domain. This characteristic exists for any number of grid points-not just in the limiting sense when the number of grid points becomes large. Thus, even the coarse-grid solution exhibits exact integral balances.

The Alternating Direction Explicit (ADE) method which is used in the solution strategy dose not require the inversion of coefficient matrix encountered in the implicit approach. It is also preferred over the fully explicit method since it has been shown to be unconditionally stable with time step size [63].

3.1 Composite Physical Properties

Physical properties of composite are considered to be functions of fiber volume fraction ν_f. This type of calculation provides more accurate results in the simulation. Due to the nonuniform resin flow through the thickness, there would be a fiber volume fraction gradient, causing the different physical properties at different locations. Therefore, composite physical properties should be expressed in terms of fiber volume fraction and its constituent physical properties.

Hercules graphite epoxy prepreg tape, commercially called as AS4/3501-6,

is chosen due to the wealth of information available in the literature for use in the simulation. This is a representative epoxy system used widely in aerospace applications. The prepreg specifications as well as kinetic and viscosity parameters are shown in Table 3.1. The kinetic and viscosity equations are given by Equations (2.18) and (2.22), respectively.

Two sets of parameters are given for kinetic equation by Lee et.al. [56] and Martinez [51]. As is shown later in chapter 5, Martinez parameters for kinetic equation provides better simulation results for temperature in comparison with experimental results. Martinez parameters are chosen for simulation throughout of this thesis (Table 3.1).

Different curing kinetic parameters would result in different calculated values for the degree of cure α. Viscosity parameters reported by Lee et.al. [56] are obtained based on the kinetic parameters calculated by them. using Martinez kinetic parameters, the value of the constants U, d, and μ_∞ would be expected to change. However, comparison between viscosities calculated by simulation and those measured by Carpenter (see references [52] and [56]) ,as shown in Figures 3.1 and 3.2, show that combination of Lee viscosity parameters and Martinez kinetic parameters predicts viscosity well . Therefore, Lee viscosity parameters are used for simulation without any correction (Table 3.1).

Fiber radius	r_f	$3.5 \times 10^{-6} m$
Fiber density	ρ_f	$1.79 \times 10^3 \frac{kg}{m^3}$
Specific heat of fiber	c_{p_f}	$7.12 \times 10^2 \frac{J}{kg°K}$
Thermal conductivity of fiber	k_f	$26 \frac{W}{m°K}$
Resin density	ρ_r	$1.26 \times 10^3 \frac{kg}{m^3}$
Specific heat of resin	c_{p_r}	$1.26 \times 10^3 \frac{J}{kg°K}$
Thermal conductivity of resin	k_r	$0.167 \frac{W}{m°K}$
Pre-exponential factor	A_1	$5.88 \times 10^9 min^{-1}$
Pre-exponential factor	A_2	$-3.906 \times 10^9 min^{-1}$
Pre-exponential factor	A_3	$T \leq 146°C \;\; 1.57 \times 10^{15} min^{-1}$
		$T > 146°C \;\; 1.96 \times 10^5 min^{-1}$
Activation energy	E_1	$8.43 \times 10^4 \frac{J}{mol}$
Activation energy	E_2	$8.03 \times 10^4 \frac{J}{mol}$
Activation energy	E_3	$T \leq 146°C \;\; 13.6 \times 10^4 \frac{J}{mol}$
		$T > 146°C \;\; 5.66 \times 10^4 \frac{J}{mol}$
Heat of reaction	H_R	$4.73 \times 10^5 \frac{J}{kg}$
Activation energy for viscosity	U	$9.08 \times 10^4 \frac{J}{mol}$
Viscosity constant	μ_∞	$7.93 \times 10^{-14} Pa.s$
Viscosity constant	d	14.1

Table 3.1: Material properties of Hercules AS4/3501-6 [51,56].

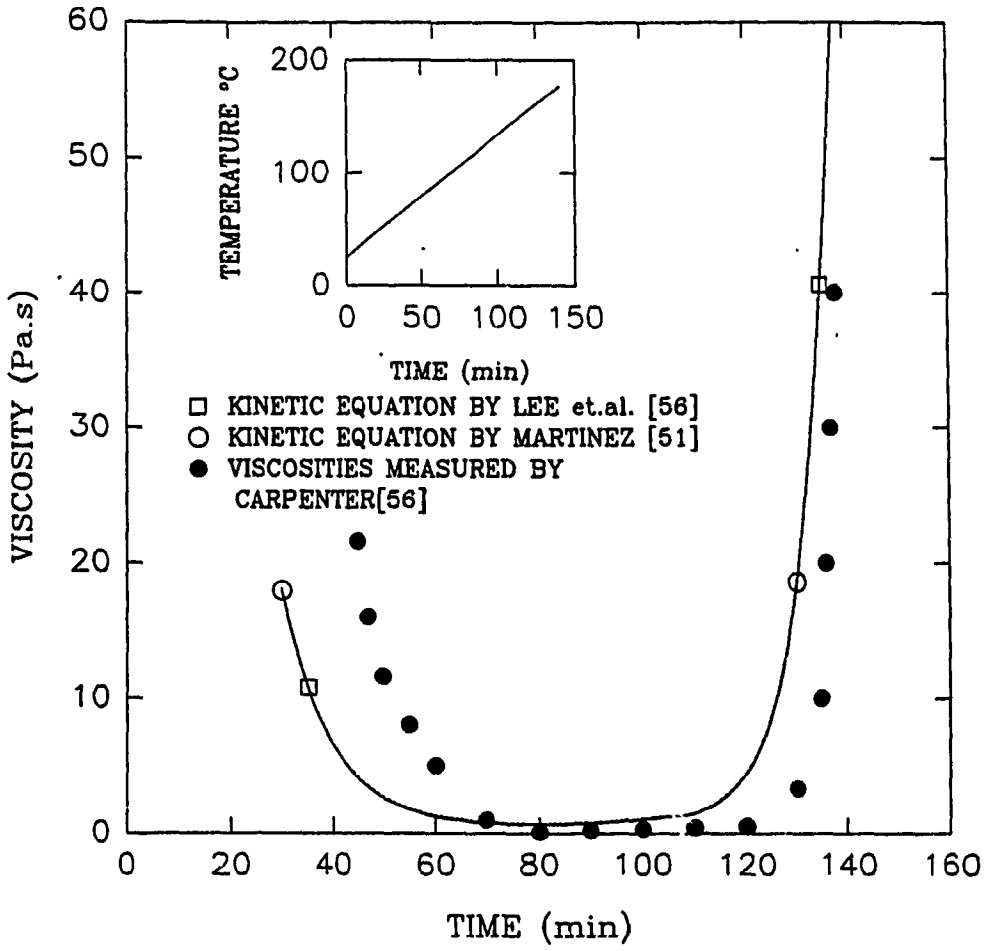

Figure 3.1: Comparison between the viscosities measured by Carpenter[56] and predicted viscosities. The inset shows the applied temperature profile (Dynamic heating).

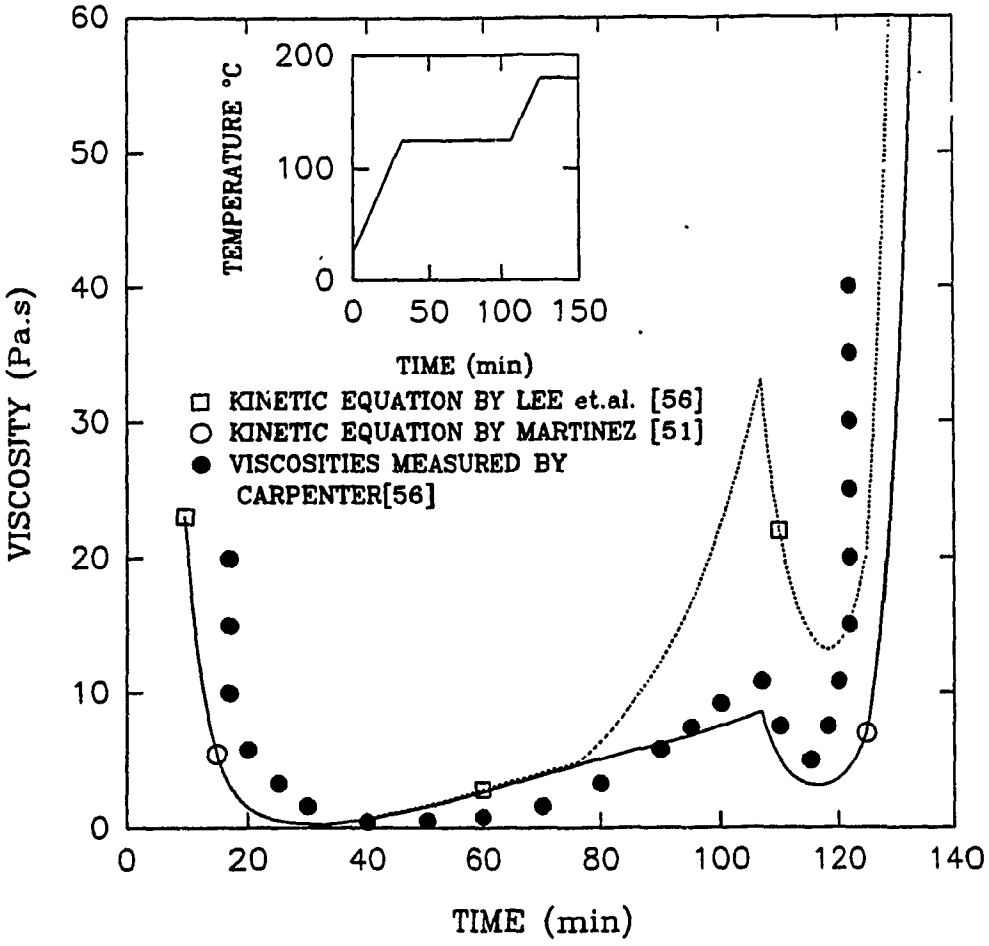

Figure 3.2: Comparison between the viscosities measured by Carpenter[56] and predicted viscosities. The inset shows the applied temperature profile.

3.1.1 Rule Of Mixture

Composite heat capacity c_p, density ρ, and thermal conductivity in the fiber direction k_x are calculated using rule of mixture. It can be written

$$\rho = \rho_f \nu_f + \rho_r(1 - \nu_f) \tag{3.1}$$

$$c_p = c_{pf}\nu_f + c_{pr}(1 - \nu_f) \tag{3.2}$$

$$k_x = k_f \nu_f + k_r(1 - \nu_f) \tag{3.3}$$

where subscripts f and r refer to fiber and resin, respectively.

3.1.2 Thermal Conductivity

There are different models to calculate thermal conductivity of composite perpendicular to the fiber direction[64, 65, 66]. To date the most successful conductivity model is that due to Springer and Tsai[64]. This model applies a series arrangement to fiber and resin normal to the fiber axis, and once a filament shape and packing arrangement is assumed, the composite conductivity can be calculated from the component conductivities. The proposed relation by Springer and Tsai to calculate thermal conductivity normal to the fibers k_z for square packing is [64]

$$\frac{k_z}{k_r} = (1 - 2\sqrt{\frac{\nu_f}{\pi}}) + \frac{1}{D}\left[\pi - \frac{4}{\sqrt{1 - (\frac{D^2\nu_f}{\pi})}} \arctan \frac{\sqrt{1 - (\frac{D^2\nu_f}{\pi})}}{1 + D\sqrt{\frac{\nu_f}{\pi}}}\right] \tag{3.4}$$

and

$$D = 2(\frac{k_r}{k_f} - 1) \tag{3.5}$$

k_r and k_f are thermal conductivities of resin and fiber respectively.

3.1.3 Permeability

Permeability is determined according to the *Kozeny-Carman* equation which can be simply written as[37, 38, 39, 40]

$$s_i = \frac{r_f^2}{4K_i}\frac{(1-\nu_f)^3}{\nu_f^2} \tag{3.6}$$

Where r_f is the fiber radius and K_i is the *Kozeny* constant. i can be x, y or z. s_x is permeability along the fiber direction and is called *Axial Permeability*. *Transverse Permeability* (s_y or s_z) represents the permeability in the direction perpendicular to the fibers. For flow through an anisotropic porous medium, like a bed of aligned fibers, the value of axial permeability is quite different from transverse permeability.

Axial permeability s_x can be well represented by Kozeny-Carman equation [28, 31, 40]. For poorly-aligned AS4 graphite fiber[31] K_x = 0.3 and for highly-aligned AS4 graphite fiber[28] K_x = 0.7 determine axial permeability accurately.

Gutowski et.al.[28] modified the Kozeny-Carman equation for transverse permeability and proposed the following expression

$$s_z = \frac{r_f^2}{4K_z'}\frac{(\sqrt{\frac{\nu_a'}{\nu_f}}-1)^3}{\sqrt{\frac{\nu_a'}{\nu_f}}+1} \tag{3.7}$$

K_z' and ν_a' are determined by fitting Equation (3.7) to the measured data. This equation agrees very closely with the standard Kozeny-Carman equation when ν_a' = 1, but gives a much lower permeability when $\nu_a' < 1$. They estimated that for highly-aligned fibers $K_z' \approx 0.2$ and ν_a' = 0.76 to 0.82.

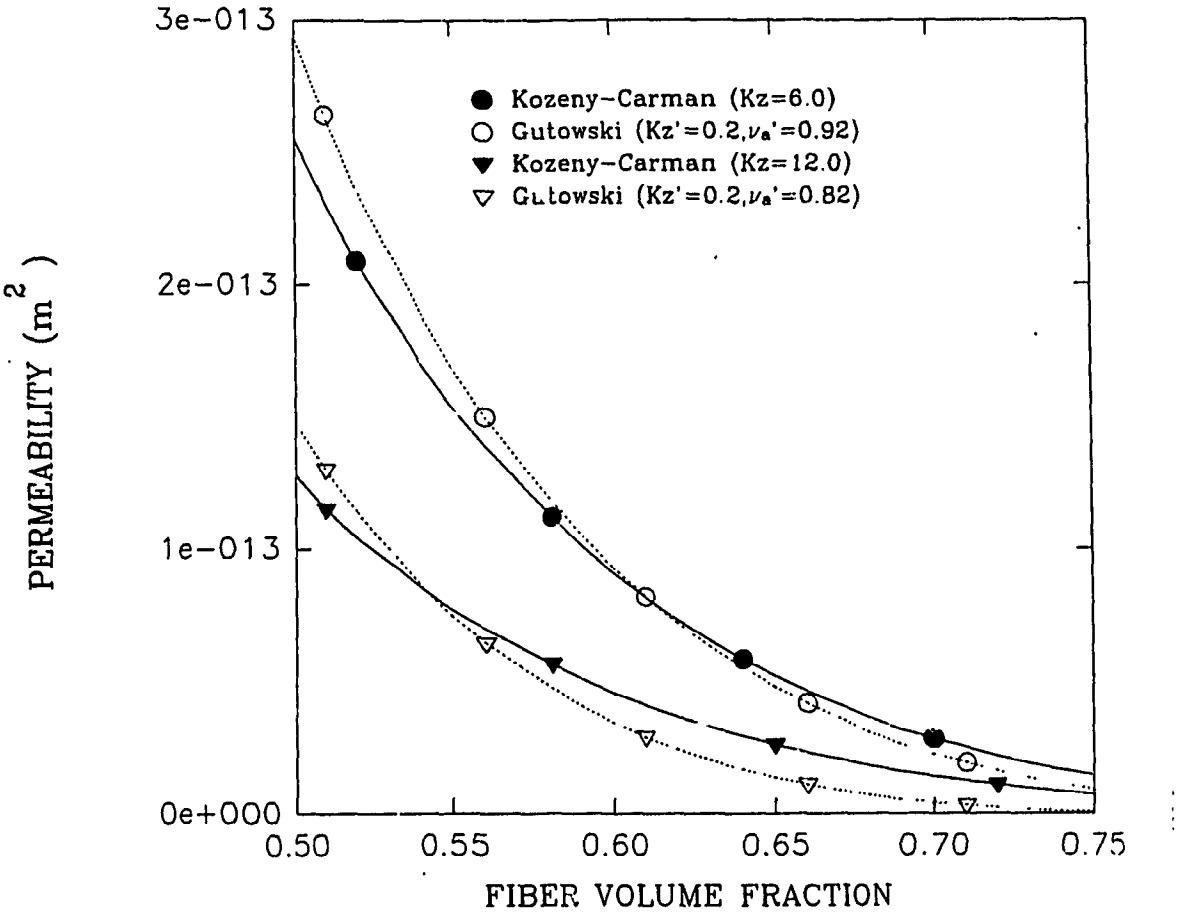

Figure 3.3: Transverse Permeability s_z vs Fiber Volume Fraction for AS4 Graphite Fibers.

For the simulation, Kozeny-Carman equation with two different values for Kozeny constant are used, depending on the fiber type. Kozeny constant is assumed to be 6 for poorly-aligned AS4 graphite fibers[31] and 12 for highly-aligned AS4 graphite fibers[40]. The permeability calculated from Equation (3.6) with $K_z = 6$ and $K_z = 12$ are equivalent with permeability calculated using Equation (3.7) with $K_z' = 0.2, \nu_a' = 0.92$ and $K_z' = 0.2, \nu_a' = 0.82$, respectively. The permeability variation vs fiber volume fraction are shown in Figure 3.3.

3.1.4 Fiber Bed Deformation

Gutowski et.al.[26, 28] evaluated the deformation properties of graphite fiber bed by compressing aligned fiber bundles impregnated with a low viscosity oil at very slow cross-head speeds. When the viscosity of impregnated oil is low and the cross-head speeds are slow, then it can be assumed that under any load, the total load is finally borne solely by the compressed fibers. The results has been presented in the form of fiber volume fraction as a function of applied pressure. This relation is required to obtain an expression for the coefficient of volume change (Equation (2.32)).

For poorly-aligned AS4 graphite fiber, it is experimentally shown that [26, 28, 31]

$$\nu_f = \begin{cases} 6.915 \times 10^{-7} P_f + 0.53 & 00000 \leq P_f \leq 68707 Pa \\ 0.1094 \log_{10} P_f + 0.0486 & 68707 \leq P_f \leq 1030612 Pa \end{cases} \tag{3.8}$$

and therefore

$$\frac{d\nu_f}{dP_f} = \begin{cases} 6.915 \times 10^{-7} & 00000 \leq P_f \leq 68707 Pa \\ \frac{0.0475}{P_f} & 68707 \leq P_f \leq 1030612 Pa \end{cases} \tag{3.9}$$

For highly-aligned AS4 graphite fiber, it is experimentally shown that [28, 40]

$$\nu_f = \begin{cases} 7.560 \times 10^{-7} P_f + 0.58 & 00000 \leq P_f \leq 68707 Pa \\ 0.1197 \log_{10} P_f + 0.0596 & 68707 \leq P_f \leq 721430 Pa \end{cases} \tag{3.10}$$

and therefore

$$\frac{d\nu_f}{dP_f} = \begin{cases} 7.560 \times 10^{-7} & 00000 \leq P_f \leq 68707 Pa \\ \frac{0.0519}{P_f} & 68707 \leq P_f \leq 721430 Pa \end{cases} \tag{3.11}$$

3.2 One-Dimensional Analysis

One-dimensional through-the-thickness (z direction) analysis is usually used to simulate the curing of both thin and thick composite parts, assuming no heat transfer and resin flow in other directions (x and y). The governing partial differential equations (Equations (2.8) and (2.28)) developed for cure analysis can be simplified to describe this type of analysis, eliminating those terms which represent the other directions (x and y).

3.2.1 Heat Model

The governing Equation (2.8) for one-dimensional through-the-thickness (Figure 3.4) can be simplified as

$$\frac{\partial}{\partial z}(k_z\frac{\partial T}{\partial z}) + \dot{g} = \rho c_p \frac{\partial T}{\partial t} \tag{3.12}$$

$\dot{g}$ should be calculated by using Equation (2.13). Solution to Equations (2.13) and (3.12) can be obtained once the initial and boundary conditions are specified. The initial and boundary conditions are

Initial Conditions:

$$\left.\begin{aligned} T(z,0) = T_o \quad & 0 \le z \le N \\ \alpha = 0 \quad & t < 0 \end{aligned}\right\} \tag{3.13}$$

where N is the laminate thickness and T_o is the initial temperature in the composite.

Boundary Conditions:

$$\left.\begin{aligned} T = T_a(t) \quad & at \quad z = 0 \\ T = T_a(t) \quad & at \quad z = N \end{aligned}\right\} t \ge 0 \tag{3.14}$$

where T_a is autoclave temperature (cure cycle). T_a can be either a constant or a function of time.

Solutions to Equations (2.13),(3.12),(3.13), and (3.14) yield the temperature T, the cure rate $\frac{d\alpha}{dt}$, and the degree of cure α as functions of position and time inside the composite.

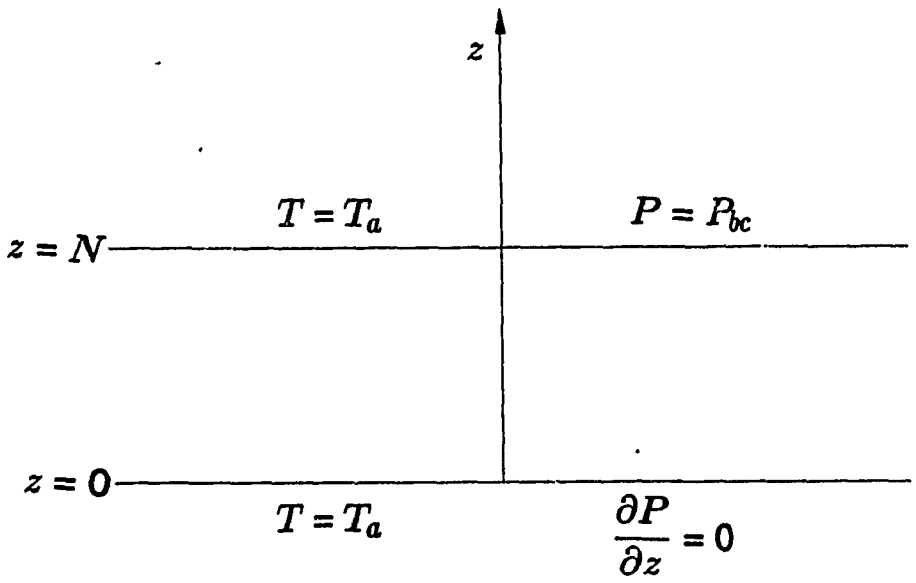

Figure 3.4: One-dimensional through-the-thickness analysis: composite geometry and boundary conditions.

3.2.2 Discretization Procedure For Heat Model

The one-dimensional case has been considered. The physical domain is divided by a number of control volumes N_{cv} (see Figure 3.5). By integration over each control volume and using the Alternating Direction Explicit method for the solution, the discretized equations can be derived.

To get the discretized equation based on control volume approach, Equation (3.12) should be integrated over the whole control volume (Figure 3.6). Therefore, it can be written

$$\int_t^{t+\delta t}\int_z^{z+\delta z}\frac{\partial}{\partial z}(k_z\frac{\partial T}{\partial z})dzdt+\int_t^{t+t}\int_z^{z+\delta z}\dot{g}dzdt=\int_t^{t+\delta t}\int_z^{z+\delta z}(\rho c_p\frac{\partial T}{\partial t})dzdt \qquad (3.15)$$

Consider the first term of Equation (3.15). After integration with respect to z, it can be shown that

$$\int_t^{t+\delta t}\int_z^{z+\delta z}\frac{\partial}{\partial z}(k_z\frac{\partial T}{\partial z})dzdt=\int_t^{t+\delta t}((k_z\frac{\partial T}{\partial z})_{z+\delta z}-(k_z\frac{\partial T}{\partial z})_z)dt \qquad (3.16)$$

For simplicity, $n+1$ denotes time level $t+\delta t$ and n time level t. If the alternating direction explicit method is used, the integration (3.16) can be done in two steps.

Step 1 (Forward Sweep):

$$\int_t^{t+\delta t}\int_z^{z+\delta z}\frac{\partial}{\partial z}(k_z\frac{\partial T}{\partial z})dzdt=((k_z\frac{\partial T}{\partial z})^n_{z+\delta z}-(k_z\frac{\partial T}{\partial z})^{n+1}_z)\delta t \qquad (3.17)$$

Suppose u is the pseudo-temperature solution of Equation (3.12) and suppose k_z is constant between two consecutive time steps. Equation (3.17) can be written

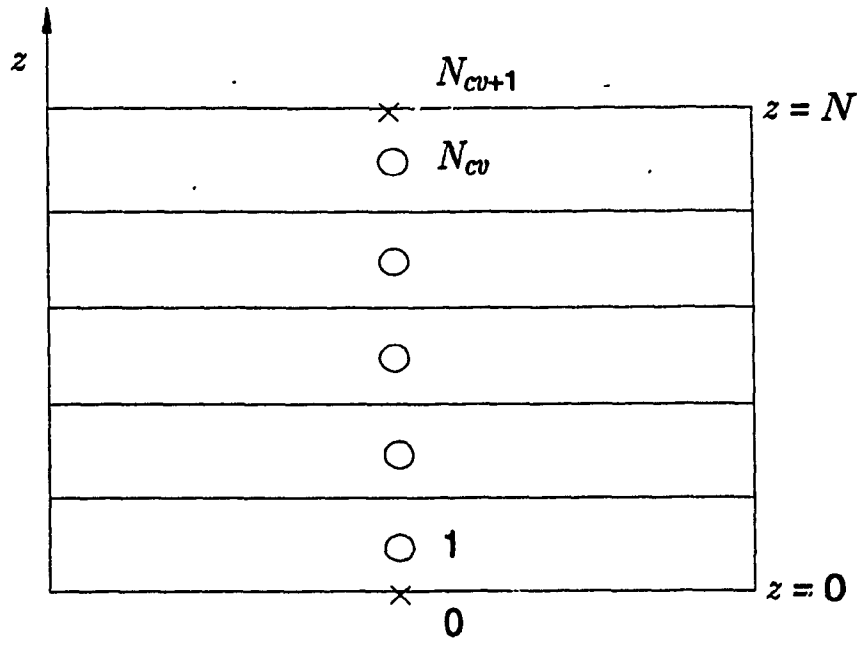

Figure 3.5: One-dimensional Through-the-Thickness analysis: computational domain.

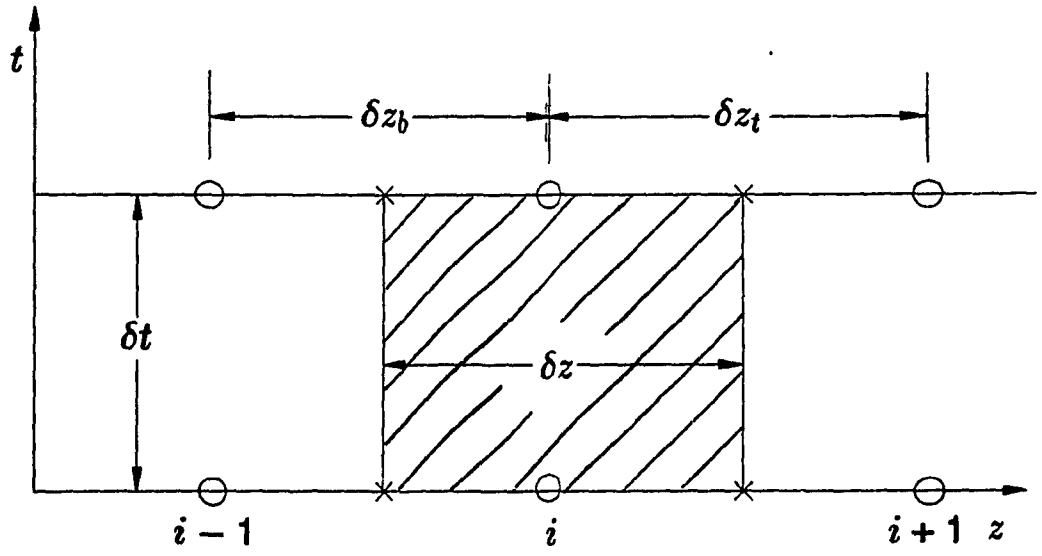

Figure 3.6: Control Volumes for one-dimensional discretization.

as

$$\int_t^{t+\delta t}\int_z^{z+\delta z}\frac{\partial}{\partial z}(k_z\frac{\partial T}{\partial z})dzdt = \frac{k_z\delta t}{\delta z_t}(u_{i+1}^n - u_i^n) - \frac{k_z\delta t}{\delta z_b}(u_i^{n+1} - u_{i-1}^{n+1}) \qquad (3.18)$$

Step 2 (Backward Sweep):

$$\int_t^{t+\delta t}\int_z^{z+\delta z}\frac{\partial}{\partial z}(k_z\frac{\partial T}{\partial z})dzdt = ((k_z\frac{\partial T}{\partial z})_{z+\delta z}^{n+1} - (k_z\frac{\partial T}{\partial z})_z^n)\delta t \qquad (3.19)$$

Suppose v is the pseudo-temperature solution of the Equation (3.12). Therefore, Equation (3.19) can be written as

$$\int_t^{t+\delta t}\int_z^{z+\delta z}\frac{\partial}{\partial z}(k_z\frac{\partial T}{\partial z})dzdt = \frac{k_z\delta t}{\delta z_t}(v_{i+1}^{n+1} - v_i^{n+1}) - \frac{k_z\delta t}{\delta z_b}(v_i^n - v_{i-1}^n) \qquad (3.20)$$

Now consider the heat source term in the Equation (3.15). Assuming the constant heat source between two consecutive time steps, it can be shown that

$$\int_t^{t+\delta t}\int_z^{z+\delta z}\dot{g}dzdt = (\dot{g})^{(n)}\delta z\delta t \qquad (3.21)$$

Note that the superscript n in Equation (3.21) represents the time level of $\dot{g}$, and not $\dot{g}$ in the power of n. Combination of Equations (2.13) and (3.21) gives the final expression for the heat source term as

$$\int_t^{t+\delta t}\int_z^{z+\delta z}\dot{g}dzdt = \rho_r(1-\nu_f^{(n)})H_R(\frac{d\alpha}{dt})^{(n)}\delta z\delta t \qquad (3.22)$$

Integration of the right hand side of Equation (3.15), assuming constant density and specific heat between two consecutive time steps, will result in

Forward Sweep

$$\int_t^{t+\delta t}\int_z^{z+\delta z}(\rho c_p\frac{\partial T}{\partial t})dzdt = \rho c_p\delta z(u_i^{n+1} - u_i^n) \qquad (3.23)$$

Backward Sweep

$$\int_t^{t+\delta t}\int_z^{z+\delta z}(\rho c_p\frac{\partial T}{\partial t})dzdt = \rho c_p\delta z(v_i^{n+1} - v_i^n) \tag{3.24}$$

Substitute Equations (3.18),(3.22) and (3.23) into the Equation (3.15), the final expression for u_i at the time step $t + \delta t$ during a forward sweep is given by

$$(1 + a_2)u_i^{n+1} = (1 - a_1)u_i^n + a_1u_{i+1}^n + a_2u_{i-1}^{n+1} + a_3 \qquad i = 1, \cdots, N_{cv} \tag{3.25}$$

$$u_o^{n+1} = T_a^{n+1} \quad , \quad u_{N_{cv}+1}^n = T_a^n \tag{3.26}$$

where

$$a_1 = \frac{k_z\delta t}{\rho c_p\delta z\delta z_t} \tag{3.27}$$

$$a_2 = \frac{k_z\delta t}{\rho c_p\delta z\delta z_b} \tag{3.28}$$

$$a_3 = \frac{\rho_r(1 - \nu_f^{(n)})H_R(\frac{d\alpha}{dt})^{(n)}\delta t}{\rho c_p} \tag{3.29}$$

If all control volumes have the same sizes ($\delta z = \delta z_t = \delta z_b$), it can be shown

$$a_1 = a_2 = \frac{k_z\delta t}{\rho c_p(\delta z)^2} \tag{3.30}$$

The u_{i-1}^{n+1} (u_{i-1} at time step $t + \delta t$) on the right-hand side of Equation (3.25) has already been computed during the same time step. Similarly, combination of Equations (3.15), (3.20),(3.22), and (3.24) are used to express v_i at new time step . The final expression for v_i will be

$$(1 + a_1)v_i^{n+1} = (1 - a_2)v_i^n + a_2v_{i-1}^n + a_1v_{i+1}^{n+1} + a_3 \qquad i = N_{cv}, \cdots, 1 \tag{3.31}$$

$$v_o^n = T_a^n \quad , \quad v_{N_{cv}+1}^{n+1} = T_a^{n+1} \tag{3.32}$$

The v_{i+1}^{n+1} (v_{i+1} at time step $t+\delta t$) on the right-hand side of Equation (3.31) is already computed during the same time step.

The temperature at each control volume at the new time level can be calculated as

$$T_i^{n+1} = \frac{1}{2}(u_i^{n+1} + v_i^{n+1}) \tag{3.33}$$

3.2.3 Flow Model

The governing Equation (2.28) for one-dimensional through-the-thickness (Figure 3.4) can be simplified as

$$\frac{\partial}{\partial z}(\frac{s_z}{\mu}\frac{\partial P}{\partial z}) = m_v \frac{\partial P}{\partial t} \tag{3.34}$$

The initial and boundary conditions which are required to solve Equation (3.34) are

Initial Conditions:

$$P(z,0) = P_a \qquad 0 \le z \le N \tag{3.35}$$

where P_a is the initial resin pressure inside the composite (autoclave pressure).

Boundary Conditions:

$$\left.\begin{aligned} \frac{\partial P}{\partial z} &= 0 \quad at \quad z = 0 \\ P &= P_{bc}(t) \quad at \quad z = N \end{aligned}\right\} t \ge 0 \tag{3.36}$$

where P_{bc} is the bag pressure. The boundary condition $\frac{\partial P}{\partial z} = 0$ means that the tool plate is impermeable and resin can not move through the tool plate. Consolidation and therefore resin flow usually happens at the first dwell temperature during which vacuum is drawn on the bag to remove the air bubbles and volatiles and therefore $P_{bc} = 0$ (absolute pressure).

3.2.4 Discretization Procedure For Flow Model

The procedure explained in the heat equation discretization can be repeated to get the discretized equation for the flow equation. There is no source term in the flow equation which makes it easier for the solution. The boundary condition at $z = 0$ is different from the heat equation. Denoting u and v to represent pressure in this case, the final discretized equations for the flow model are

$$(1 + a_2)u_i^{n+1} = (1 - a_1)u_i^n + a_1 u_{i+1}^n + a_2 u_{i-1}^{n+1} \qquad i = 1, \cdots, N_{cv} \tag{3.37}$$

$$u_o^{n+1} = u_1^{n+1} \quad , \quad u_{N_{cv}+1}^n = P_{bc}^n \tag{3.38}$$

and

$$(1 + a_1)v_i^{n+1} = (1 - a_2)v_i^n + a_2 v_{i-1}^n + a_1 v_{i+1}^{n+1} \qquad i = N_{cv}, \cdots, 1 \tag{3.39}$$

$$v_o^n = v_1^n \quad , \quad v_{N_{cv}+1}^{n+1} = P_{bc}^{n+1} \tag{3.40}$$

where

$$a_1 = \frac{s_z \delta t}{m_v \mu \delta z \delta z_t} \tag{3.41}$$

$$a_2 = \frac{s_z \delta t}{m_v \mu \delta z \delta z_b} \tag{3.42}$$

If all control volumes have the same size ($\delta z_t = \delta z_b = \delta z$), it can be shown that

$$a_1 = a_2 = \frac{s_z \delta t}{m_v \mu (\delta z)^2} \tag{3.43}$$

The resin pressure at each control volume at the new time level can be calculated as

$$P_i^{n+1} = \frac{1}{2}(u_i^{n+1} + v_i^{n+1}) \tag{3.44}$$

3.2.5 Closed-Form Solution For Flow Model

Closed-form solution are applicable to Equation (3.34) when the following parameters are constant during the flow process : s_z, m_v, μ, and N. Obviously the bed thickness, N, decreases due to seepage. However to obtain an analytical solution it is assumed that the change in bed thickness is negligible when compared to the original thickness of the laminate. To get the closed-form series solution, it is necessary that the boundary conditions during the flow process be either $P_{bc}(t) = 0$ or $grad(P) = 0$ (Figure 3.4). Under the above conditions, the closed-form solution for one-dimensional flow is given by [30]

$$P(z,t) = \frac{4P_a}{\pi} \sum_{j=1}^{\infty} \frac{(-1)^{j-1}}{2j-1} cos(\frac{(2j-1)\pi z}{2N}) exp(\frac{-(2j-1)^2 \pi^2 T_v}{4}) \tag{3.45}$$

where

$$T_v = \frac{s_z t}{\mu m_v N^2} \tag{3.46}$$

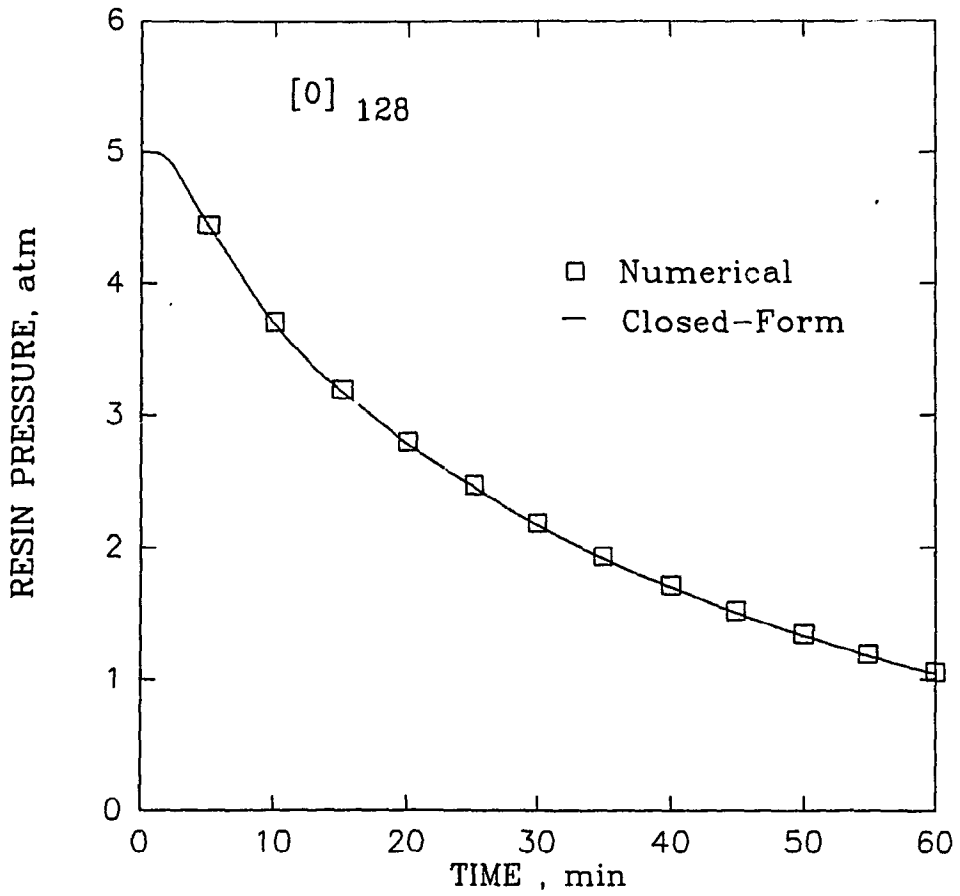

Figure 3.7: Variation of resin pressure with time at the midpoint of the laminate

Thickness of prepreg	t_p	$1.651 \times 10^{-4} m$
Permeability	s_z	$6.46 \times 10^{-13} m^2$
Coefficient of volume change	m_v	8.8×10^{-7}
Resin viscosity	μ	$10 Pa.s$
Initial resin pressure	P_a	$5 atm$

Table 3.2: Material properties for flow model

To show the accuracy of the numerical technique, the numerical results are compared with the closed-form solution. The input data used in the simulation are summarized in Table (3.2).

Resin pressure at the midpoint of the laminate were compared with the numerical solutions obtained using the control-volume ADE method (Figure 3.7). The time increment has been taken to unity (t = 1sec). After 3600 time steps (t = 60min), the maximum error is 1.1 percent . Results confirm the accuracy of the new numerical solution for the curing simulation.

3.3 Two-Dimensional Analysis

3.3.1 Heat Model

The governing equation (2.8) for two-dimensional analysis (Figure 3.8) can be written as

$$\frac{\partial}{\partial x}(k_x\frac{\partial T}{\partial x}) + \frac{\partial}{\partial z}(k_z\frac{\partial T}{\partial z}) + \dot{g} = \rho c_p\frac{\partial T}{\partial t} \tag{3.47}$$

The initial conditions are

$$\left.\begin{aligned} T(x,z,0) &= T_o \\ \alpha(x,z,0) &= 0 \end{aligned}\right\} \quad \begin{aligned} 0 \le x \le L \\ 0 \le z \le N \end{aligned} \tag{3.48}$$

For the flat plate composite, the boundary conditions are

$$\left.\begin{aligned} T(0,z,t) = T(L,z,t) &= T_a(t) \\ T(x,0,t) = T(x,N,t) &= T_a(t) \end{aligned}\right\} t \ge 0 \tag{3.49}$$

Equations (2.13) and (3.47) subjected to the above mentioned initial and boundary conditions need to be solved to obtain temperature and degree of cure distribution inside composite.

3.3.2 Discretized Equation For Heat Model

The same procedure explained before for the discretization of one-dimensional heat equation is applied to discretize Equation (3.47). The only difference is that the integration should be done in the x direction as well as the z direction (Figure

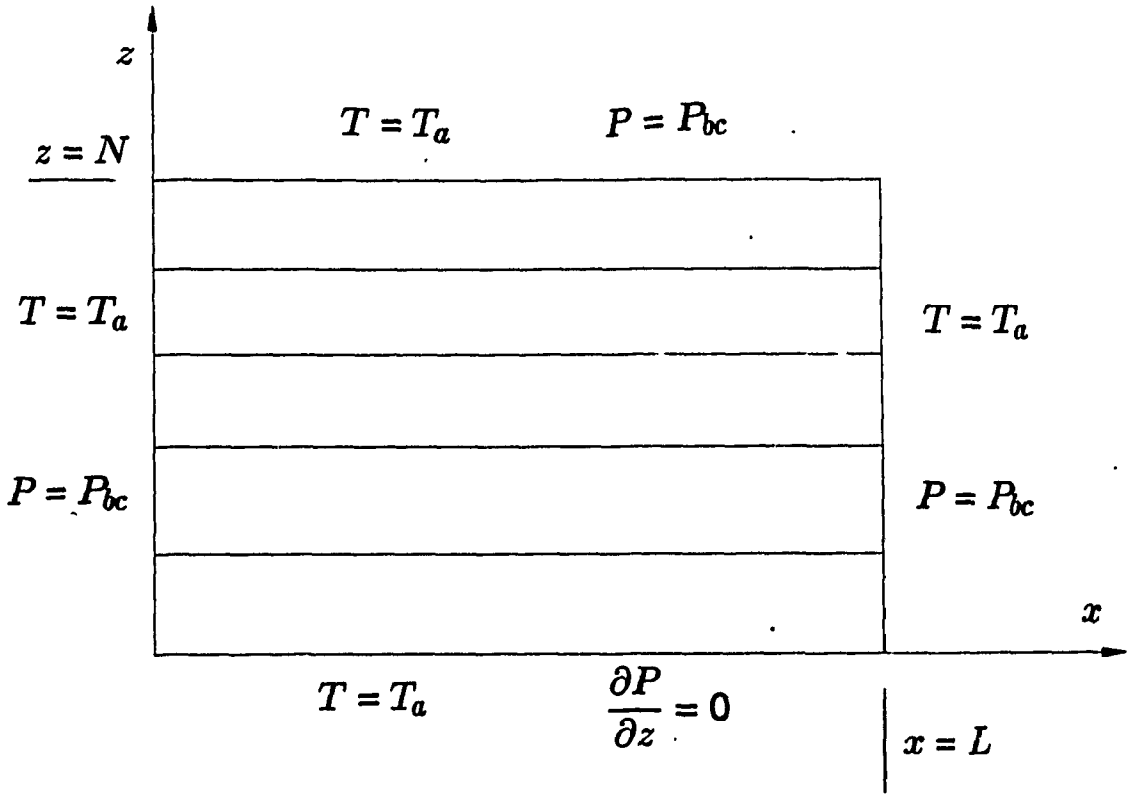

Figure 3.8: Two-dimensional analysis: composite geometry and boundary conditions.

3.9). Therefore, it can be written

$$\int_t^{t+\delta t}\int_x^{x+\delta x}\int_z^{z+\delta z}\frac{\partial}{\partial x}(k_x\frac{\partial T}{\partial x})dzdxdt+\int_t^{t+\delta t}\int_z^{z+\delta z}\int_x^{x+\delta x}\frac{\partial}{\partial z}(k_z\frac{\partial T}{\partial z})dxdzdt+$$
$$\int_t^{t+t}\int_x^{x+\delta x}\int_z^{z+\delta z}\dot{g}dzdxdt=\int_t^{t+\delta t}\int_x^{x+\delta x}\int_z^{z+\delta z}(\rho c_p\frac{\partial T}{\partial t})dzdxdt \quad (3.50)$$

The first term of Equation (3.50) can be integrated with respect to z as

$$\int_t^{t+\delta t}\int_x^{x+\delta x}\int_z^{z+\delta z}\frac{\partial}{\partial x}(k_x\frac{\partial T}{\partial x})dzdxdt=\int_t^{t+\delta t}\int_x^{x+\delta x}\frac{\partial}{\partial x}(k_x\frac{\partial T}{\partial x})\delta zdxdt \quad (3.51)$$

δz is shown in Figure 3.10. Integration of Equation (3.51) with respect to x results in

$$\int_t^{t+\delta t}\int_x^{x+\delta x}\int_z^{z+\delta z}\frac{\partial}{\partial x}(k_x\frac{\partial T}{\partial x})dzdxdt=\int_t^{t+\delta t}((k_x\frac{\partial T}{\partial x})_{x+\delta x}-(k_x\frac{\partial T}{\partial x})_x)\delta zdt \quad (3.52)$$

Using alternating direction explicit method, integration (3.52) can be done in two steps.

Step 1 (Forward Sweep):

$$\int_t^{t+\delta t}\int_x^{x+\delta x}\int_z^{z+\delta z}\frac{\partial}{\partial x}(k_x\frac{\partial T}{\partial x})dzdxdt=((k_x\frac{\partial T}{\partial x})^n_{x+\delta x}-(k_x\frac{\partial T}{\partial x})^{n+1}_x)\delta z\delta t \quad (3.53)$$

Suppose u is the pseudo-temperature solution of Equation (3.47). Equation (3.53) can be written as

$$\int_t^{t+\delta t}\int_x^{x+\delta x}\int_z^{z+\delta z}\frac{\partial}{\partial x}(k_x\frac{\partial T}{\partial x})dzdxdt=\frac{k_x\delta z\delta t}{\delta x_r}(u^n_{i+1,j}-u^n_{i,j})-\frac{k_x\delta z\delta t}{\delta x_l}(u^{n+1}_{i,j}-u^{n+1}_{i-1,j}) \quad (3.54)$$

δx_r and δx_l are shown in Figure 3.10.

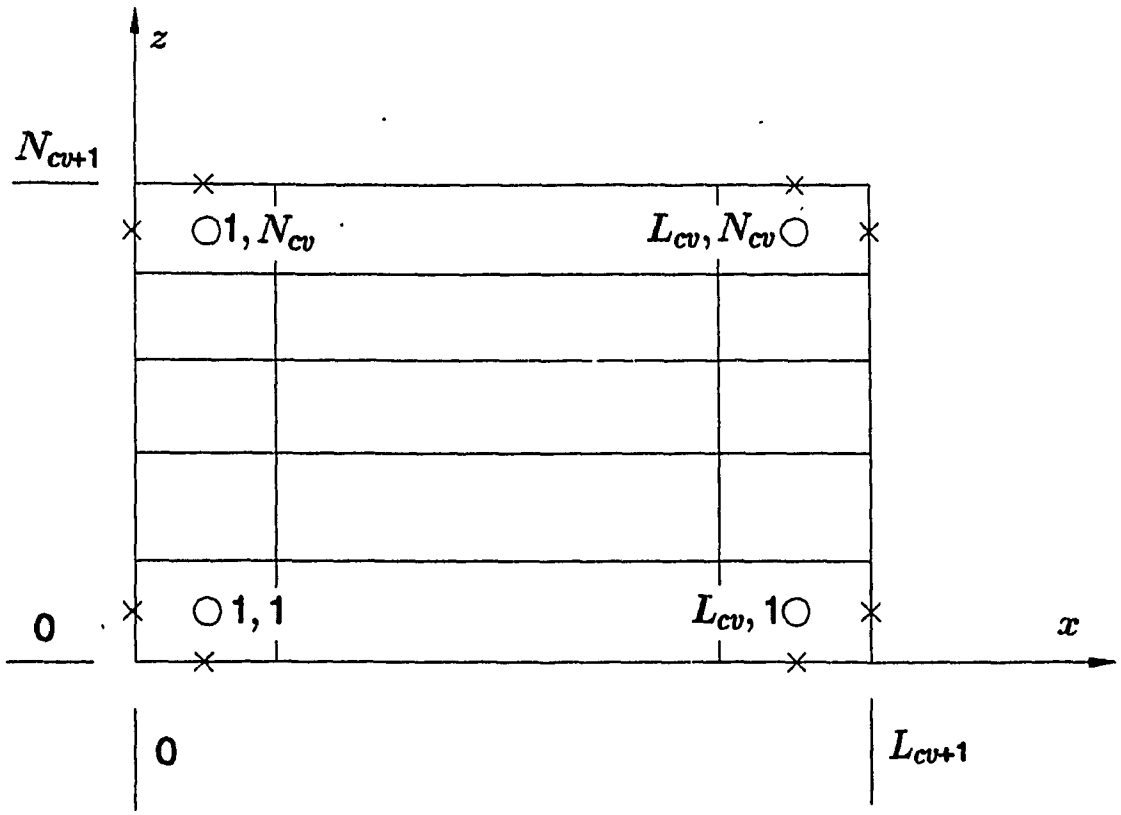

Figure 3.9: Two-dimensional analysis: computational domain.

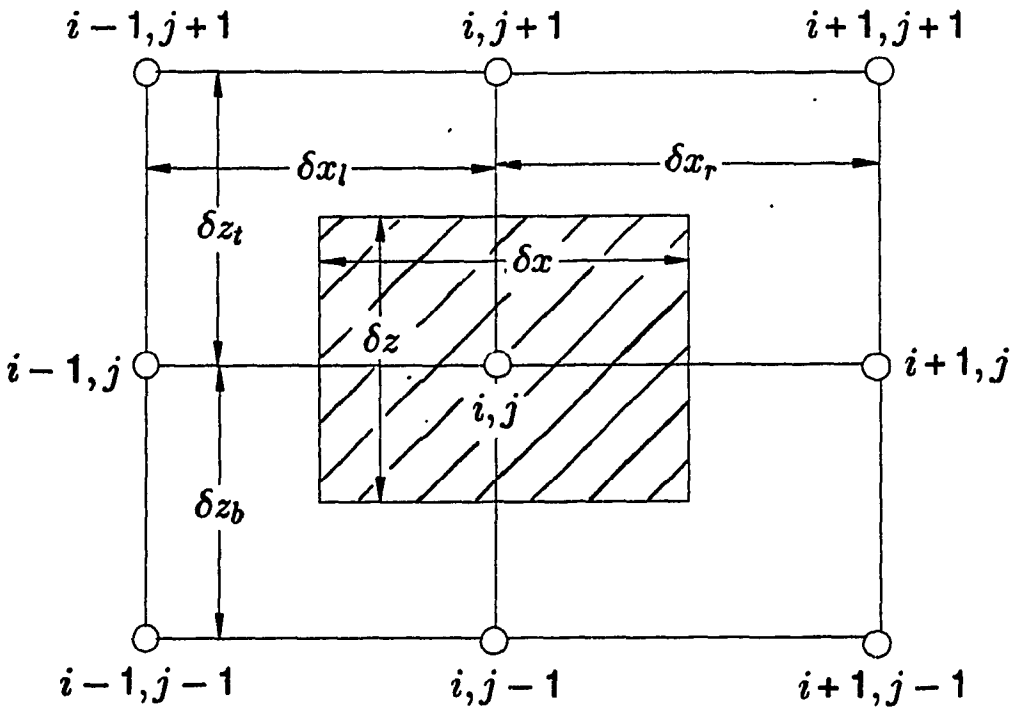

Figure 3.10: Control-volumes for two-dimensional discretization.

Step 2 (Backward Sweep):

$$\int_t^{t+\delta t}\int_x^{x+\delta x}\int_z^{z+\delta z}\frac{\partial}{\partial x}(k_x\frac{\partial T}{\partial x})dzdxdt = ((k_x\frac{\partial T}{\partial x})^{n+1}_{x+\delta x} - (k_x\frac{\partial T}{\partial x})^n_x)\delta z\delta t \qquad (3.55)$$

Suppose v is the pseudo-temperature solution of Equation (3.47). Therefore, Equation (3.55) can be written as

$$\int_t^{t+\delta t}\int_x^{x+\delta x}\int_z^{z+\delta z}\frac{\partial}{\partial x}(k_x\frac{\partial T}{\partial x})dzdxdt = \frac{k_x\delta z\delta t}{\delta x_r}(v^{n+1}_{i+1,j} - v^{n+1}_{i,j}) - \frac{k_x\delta z\delta t}{\delta x_l}(v^n_{i,j} - v^n_{i-1,j}) \qquad (3.56)$$

Consider the second term of Equation (3.50). Integration with respect to x results in

$$\int_t^{t+\delta t}\int_z^{z+\delta z}\int_x^{x+\delta x}\frac{\partial}{\partial z}(k_z\frac{\partial T}{\partial z})dxdzdt = \int_t^{t+\delta t}\int_z^{z+\delta z}\frac{\partial}{\partial z}(k_z\frac{\partial T}{\partial z})\delta xdzdt \qquad (3.57)$$

δx is shown in Figure 3.10. Equation (3.57) can be integrated with respect to z as

$$\int_t^{t+\delta t}\int_z^{z+\delta z}\int_x^{x+\delta x}\frac{\partial}{\partial z}(k_z\frac{\partial T}{\partial z})dxdzdt = \int_t^{t+\delta t}((k_z\frac{\partial T}{\partial z})_{z+\delta z} - (k_z\frac{\partial T}{\partial z})_z)\delta xdt \qquad (3.58)$$

Again Equation (3.58) can be integrated with respect to time in two steps.

Step 1 (Forward Sweep):

$$\int_t^{t+\delta t}\int_z^{z+\delta z}\int_x^{x+\delta x}\frac{\partial}{\partial z}(k_z\frac{\partial T}{\partial z})dxdzdt = ((k_z\frac{\partial T}{\partial z})^n_{z+\delta z} - (k_z\frac{\partial T}{\partial z})^{n+1}_z)\delta x\delta t \qquad (3.59)$$

and therefore

$$\int_t^{t+\delta t}\int_z^{z+\delta z}\int_x^{x+\delta x}\frac{\partial}{\partial z}(k_z\frac{\partial T}{\partial z})dxdzdt = \frac{k_z\delta x\delta t}{\delta z_t}(u^n_{i,j+1} - u^n_{i,j}) - \frac{k_z\delta x\delta t}{\delta z_b}(u^{n+1}_{i,j} - u^{n+1}_{i,j-1}) \qquad (3.60)$$

δz_t and δz_b are shown in Figure 3.10.

Step 2 (Backward Sweep):

$$\int_t^{t+\delta t}\int_z^{z+\delta z}\int_x^{x+\delta x}\frac{\partial}{\partial z}(k_z\frac{\partial T}{\partial z})dxdzdt = ((k_z\frac{\partial T}{\partial z})^{n+1}_{z+\delta z} - (k_z\frac{\partial T}{\partial z})^n_z)\delta x\delta t \tag{3.61}$$

and therefore

$$\int_t^{t+\delta t}\int_z^{z+\delta z}\int_x^{x+\delta x}\frac{\partial}{\partial z}(k_z\frac{\partial T}{\partial z})dxdzdt = \frac{k_z\delta x\delta t}{\delta z_t}(v^{n+1}_{i,j+1} - v^{n+1}_{i,j}) - \frac{k_z\delta x\delta t}{\delta z_b}(v^n_{i,j} - v^n_{i,j-1}) \tag{3.62}$$

Assuming constant heat source between two consecutive time steps and Equation (2.13), the third term of Equation (3.50) can be written as

$$\int_t^{t+\delta t}\int_x^{x+\delta x}\int_z^{z+\delta z}\dot{g}dzdxdt = \rho_r(1-\nu_f^{(n)})H_R(\frac{d\alpha}{dt})^{(n)}\delta x\delta z\delta t \tag{3.63}$$

The right-hand side of Equation (3.50) can be integrated in two steps as

Forward Sweep

$$\int_t^{t+\delta t}\int_x^{x+\delta x}\int_z^{z+\delta z}\rho c_p\frac{\partial T}{\partial t}dzdxdt = \rho c_p\delta x\delta z(u^{n+1}_{i,j} - u^n_{i,j}) \tag{3.64}$$

Backward Sweep

$$\int_t^{t+\delta t}\int_x^{x+\delta x}\int_z^{z+\delta z}\rho c_p\frac{\partial T}{\partial t}dzdxdt = \rho c_p\delta x\delta z(v^{n+1}_{i,j} - v^n_{i,j}) \tag{3.65}$$

Substitute Equations (3.54),(3.60),(3.63),and (3.64) into Equation (3.50), the final expression for $u_{i,j}$ at time step $t + \delta t$ for an interior node during a forward

sweep can be derived as

$$(1+a_2+a_4)u_{i,j}^{n+1} = (1-a_1-a_3)u_{i,j}^{n} + a_1 u_{i+1,j}^{n} + a_2 u_{i-1,j}^{n+1} + a_3 u_{i,j+1}^{n} + a_4 u_{i,j-1}^{n+1} + a_5 \quad (3.66)$$

$$i = 1, \cdots, L_{cv} \qquad j = 1, \cdots, N_{cv}$$

where

$$\begin{aligned} a_1 &= \frac{k_x \delta t}{\rho c_p \delta x \delta x_r} \\ a_2 &= \frac{k_x \delta t}{\rho c_p \delta x \delta x_l} \\ a_3 &= \frac{k_z \delta t}{\rho c_p \delta z \delta z_t} \\ a_4 &= \frac{k_z \delta t}{\rho c_p \delta z \delta z_b} \\ a_5 &= \frac{\rho_r (1-\nu_f^{(n)}) H_R (\frac{d\alpha}{dt})^{(n)} \delta t}{\rho c_p} \end{aligned} \quad (3.67)$$

The $u_{i-1,j}^{n+1}$ and $u_{i,j-1}^{n+1}$ on the right-hand side of Equation (3.66) all have previously been calculated during the same time step $(n+1)$. The following expressions are used to describe the boundary conditions for the solution (boundary nodes)

$$\left.\begin{aligned} u_{i,0}^{n+1} = u_{0,j}^{n+1} = T_a^{n+1} \\ u_{i,N_{cv}+1}^{n} = u_{L_{cv}+1,j}^{n} = T_a^{n} \end{aligned}\right\} \begin{aligned} i &= 1, \cdots, L_{cv} \\ j &= 1, \cdots, N_{cv} \end{aligned} \quad (3.68)$$

Similarly, combination of Equations (3.50),(3.56),(3.62), (3.63), and (3.65) is used to derive an expression for $v_{i,j}$ at time step $t+\delta t$ for an interior node during a backward sweep as

$$(1+a_1+a_3)v_{i,j}^{n+1} = (1-a_2-a_4)v_{i,j}^{n} + a_1 v_{i+1,j}^{n+1} + a_2 v_{i-1,j}^{n} + a_3 v_{i,j+1}^{n+1} + a_4 v_{i,j-1}^{n} + a_5 \quad (3.69)$$

$$i = L_{cv}, \cdots, 1 \qquad j = N_{cv}, \cdots, 1$$

The $v^{n+1}_{i+1,j}$ and $v^{n+1}_{i,j+1}$ on the right-hand side of Equation (3.69) are those previously computed during the same time step $(n+1)$. The boundary nodes for the solution of backward sweep equation are

$$\left.\begin{aligned} v^{n}_{i,0} = v^{n}_{0,j} = T^{n}_{a} \\ v^{n+1}_{i,N_{cv}+1} = v^{n+1}_{L_{cv}+1,j} = T^{n+1}_{a} \end{aligned}\right\} \begin{array}{l} i = L_{cv}, \cdots, 1 \\ j = N_{cv}, \cdots, 1 \end{array} \tag{3.70}$$

The temperature at each control volume at the new time level can be calculated as

$$T^{n+1}_{i,j} = \frac{1}{2}(u^{n+1}_{i,j} + v^{n+1}_{i,j}) \tag{3.71}$$

3.3.3 Flow Model

The flow governing equation for two-dimensional analysis (Figure 3.8) can be expressed as

$$\frac{\partial}{\partial x}(\frac{s_x}{\mu}\frac{\partial P}{\partial x}) + \frac{\partial}{\partial z}(\frac{s_z}{\mu}\frac{\partial P}{\partial z}) = m_v\frac{\partial P}{\partial t} \tag{3.72}$$

The initial condition is

$$P(x,z,0) = P_a \left\{ \begin{array}{l} 0 \le x \le L \\ 0 \le z \le N \end{array} \right. \tag{3.73}$$

and boundary conditions are

$$\left.\begin{aligned} P(0,z,t) = P(L,z,t) = P_{bc} \\ \tfrac{\partial P}{\partial z}(x,0,t) = 0 \\ P(x,N,t) = P_{bc} \end{aligned}\right\} \begin{array}{l} 0 \le x \le L \\ 0 \le z \le N \end{array} \tag{3.74}$$

3.3.4 Discretized Equation For Flow Model

The discretization equation for two-dimensional flow can be obtained from heat discretized equation, eliminating the heat generation source term ($a_5 = 0$). Denoting u and v to represent pseudo-pressure in this case, for forward sweep, it can be written

$$(1 + a_2 + a_4)u_{i,j}^{n+1} = (1 - a_1 - a_3)u_{i,j}^{n} + a_1 u_{i+1,j}^{n} + a_2 u_{i-1,j}^{n+1} + a_3 u_{i,j+1}^{n} + a_4 u_{i,j-1}^{n+1} \quad (3.75)$$

$$i = 1, \cdots, L_{cv} \qquad j = 1, \cdots, N_{cv}$$

where

$$\begin{aligned} a_1 &= \frac{s_x}{\mu}\frac{\delta t}{m_v \delta x \delta x_r} \\ a_2 &= \frac{s_x}{\mu}\frac{\delta t}{m_v \delta x \delta x_l} \\ a_3 &= \frac{s_z}{\mu}\frac{\delta t}{m_v \delta z \delta z_t} \\ a_4 &= \frac{s_z}{\mu}\frac{\delta t}{m_v \delta z \delta z_b} \end{aligned} \quad (3.76)$$

The boundary nodes are

$$\left.\begin{aligned} u_{i,0}^{n+1} = u_{0,j}^{n+1} &= P_{bc}^{n+1} \\ u_{i,N_{cv}+1}^{n} = u_{L_{cv}+1,j}^{n} &= P_{bc}^{n} \end{aligned}\right\} \begin{aligned} &i = 1, \cdots, L_{cv} \\ &j = 1, \cdots, N_{cv} \end{aligned} \quad (3.77)$$

Similarly, for an interior node during backward sweep, it can be shown to be

$$(1 + a_1 + a_3)v_{i,j}^{n+1} = (1 - a_2 - a_4)v_{i,j}^{n} + a_1 v_{i+1,j}^{n+1} + a_2 v_{i-1,j}^{n} + a_3 v_{i,j+1}^{n+1} + a_4 v_{i,j-1}^{n} \quad (3.78)$$

$$i = L_{cv}, \cdots, 1 \qquad j = N_{cv}, \cdots, 1$$

The boundary nodes for the solution of backward sweep equation are

$$\begin{aligned} v^n_{i,0} = v^n_{0,j} = P^n_{bc} \quad & \begin{cases} i = L_{cv}, \cdots, 1 \\ j = N_{cv}, \cdots, 1 \end{cases} \\ v^{n+1}_{i,N_{cv}+1} = v^{n+1}_{L_{cv}+1,j} = P^{n+1}_{bc} \quad & \end{aligned} \tag{3.79}$$

The pressure at each control volume at the new time level can be calculated as

$$P^{n+1}_{i,j} = \frac{1}{2}(u^{n+1}_{i,j} + v^{n+1}_{i,j}) \tag{3.80}$$

3.4 Solution Techniques

At the beginning of the solution ($t = 0$), the degree of cure and temperature are defined as

$$\alpha^\circ = 0 \qquad T^\circ = T_\circ \tag{3.81}$$

Therefore, one can calculate $(\frac{d\alpha}{dt})^\circ = f(T^\circ, \alpha^\circ)$. For the next time step, the degree of cure will be calculated by the following relation

$$\alpha^{n+1} = \alpha^n + (\frac{d\alpha}{dt})^n \delta t \tag{3.82}$$

There are two problems that should be taken care of during the numerical solution. First the composite thickness at each time step should be recalculated. Equation (2.28) applies to a quasistatic condition and the motion of the boundary condition needs to be accounted for during numerical computation. Secondly, the coefficients a_i in Equations (3.27),(3.28), (3.41),(3.42),(3.67), and (3.76) are

functions of fiber volume fraction. There are different fiber volume fractions in two adjacent control volumes. Therefore, the heat flux and fluid flow calculated across the same boundary between two adjacent cells will have different values in each cell during numerical computation. To overcome this difficulty, analogy to electric current relation is used. Considering Fourier's law of conduction, the thermal resistance R_k inside a cell between the center node and the boundary can be expressed as (Figure 3.11)

$$R_{k_i} = \frac{\delta z_i}{2k_{z_i}} \tag{3.83}$$

The same analogy can be applied to Darcy's law to obtain the flow resistance R_s inside a cell between the center node and the boundary as

$$R_{s_i} = \frac{\mu_i \delta z_i}{2s_{z_i}} \tag{3.84}$$

Therefore, the effective thermal and flow resistance between two nodes i and $i+1$ can be written as (series resistances)

$$(k_z)_{eff} = \frac{k_{z_i} k_{z_{i+1}} (\delta z_i + \delta z_{i+1})}{k_{z_{i+1}} \delta z_i + k_{z_i} \delta z_{i+1}} \tag{3.85}$$

$$(\frac{s_z}{\mu})_{eff} = \frac{s_{z_i} s_{z_{i+1}} (\delta z_i + \delta z_{i+1})}{s_{z_{i+1}} \delta z_i \mu_i + s_{z_i} \delta z_{i+1} \mu_{i+1}} \tag{3.86}$$

To satisfy the mass and energy conservation laws, k_z and $\frac{s_z}{\mu}$ in Equations (3.27),(3.28), (3.41),(3.42),(3.67), and (3.76) should be replaced by $(k_z)_{eff}$ and $(\frac{s_z}{\mu})_{eff}$,respectively, during numerical computation.

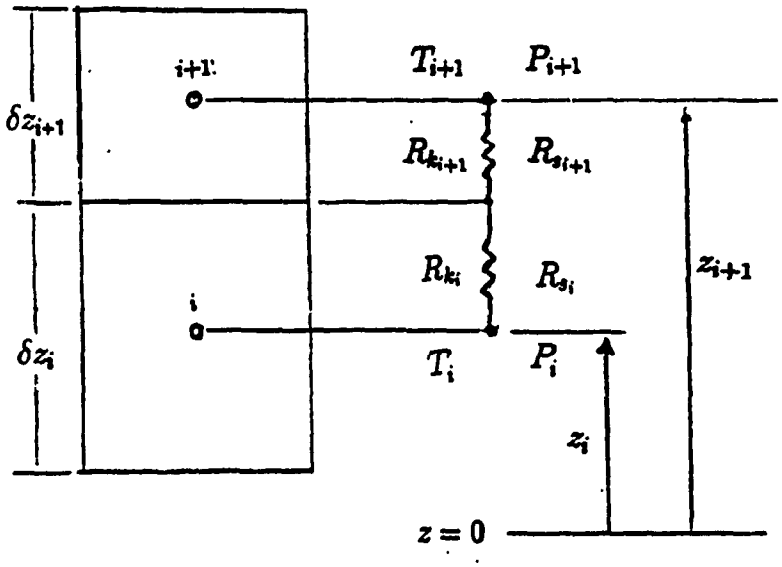

Figure 3.11: Thermal and flow resistance

3.5 Summary

Numerical method was developed to discretize the governing partial differential equations describing the cure process. Control-volume approach combined with Alternating Direction Explicit method (ADE) were used in discretization. Different expressions employed to calculate composite physical properties during numerical computation were discussed

Chapter 4

Experimental Setup

Experimental results are required to validate any process model. Experimental apparatus and procedure which were used to measure the temperature and fiber volume fraction as well as experimental results are described in this chapter. The material system which was studied is AS4/3501-6, a commercial graphite epoxy prepreg from Hercules. The thickness of each ply is approximately 0.16 mm and it has 36 percent resin content by weight.

Experiment was performed to study the one-dimensional curing of thick composites. Since both temperature overshoot and non-uniform through-the-thickness compaction were observed, it was decided to study the different ways to solve those problems. Two-dimensional experiment was performed to show the heat transfer effect along the fibers to reduce the temperature overshoot inside laminate. Prebleeding technique was used to achieve the uniform distribution of fibers through-the-thickness. Two experiments were performed to study the prebleeding

effect on fabrication of thick composites.

4.1 One-Dimensional Experiment

This experiment was performed to study the laminate behavior during curing under one-dimensional through-the-thickness assumptions. The heat and resin allowed to move through-the-thickness, perpendicular to the fiber direction.

4.1.1 Experimental Tooling Set-up

A cross-sectional view through-the-thickness of the tooling set-up is shown in Figure 4.1. A unidirectional flat laminate 7.6 cm by 7.6 cm consists of 330 layers was produced by hand lay-up. Two K-type thermocouples were placed at top of laminate (between layer 329 and layer 330) and middle of laminate (between layer 165 and 166). The thermocouples were wrapped in a small layer of peel ply to prevent short-circuiting noise due to the graphite fiber conductivity. Four sides of the laminate were positioned against $4cm$ width ceramic blocks, which acts as a dam to prevent resin loss as well as to reduce the heat movement through the edges. This arrangement closely resembles the one-dimensional through-the-thickness analysis more valid . The laminate sides were wrapped tightly in a nylon film to help in preventing resin loss. Eighteen layers of polyester bleeder materials supplied from Air-Tech International were placed on top of the laminate to absorb

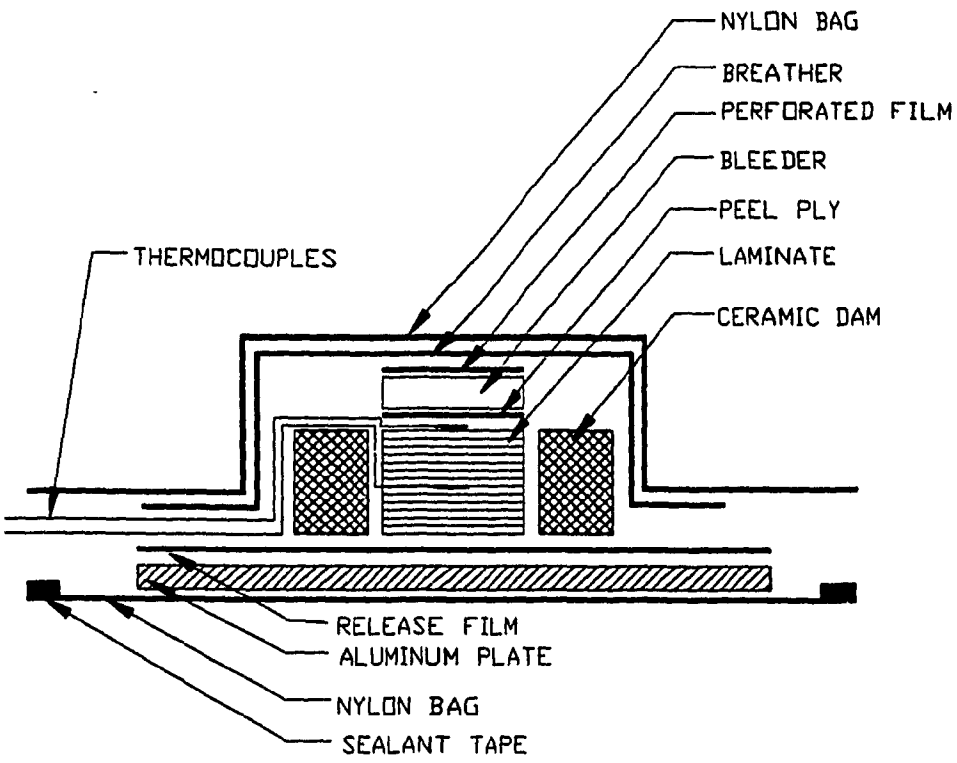

Figure 4.1: Experimental Tooling Setup (Bleed setup).

the resin. Two perforated nylon and a polyester breather material were placed on top of the bleeder to give the air an escape path when vacuum is applied. The assembly was covered with a nylon film and sealed. Vacuurn was applied inside the vacuum bag. The whole assembly was placed in an autoclave. This type of set-up can be referred to as bleed processing since the resin is intentionally removed during cure.

4.1.2 Cure Cycle

A modified cure cycle based on the recommended cure cycle by the manufacturer for thick parts of AS4/3501-6 [52] was applied. A pressure of 0.584MPa(85psi) was applied inside autoclave, with vacuum drawn on the charge. The temperature was raised to 115°C. The laminate was then soaked for 120min at this temperature based on the lagging thermocouple (the last thermocouple which indicates the target temperature is called lagging thermocouple). The temperature was then raised to 150°C and the laminate soaked at this temperature for 90min based on the lagging thermocouple. The final stage includes heating the laminate to 177°, with a 120min soak period based on the lagging thermocouple. A 120min soak is used to obtain heat deflection temperature of 190°C, a 240min soak results in heat deflection temperature of 210°C, while 360min of soaking gives a further improvement of only 2°C [52]. The part was then allowed to cool to ambient temperature overnight before removal.

4.1.3 Experimental Results

The temperature as a function of time was measured at the top layer (layer 329) and middle layer (layer165) of the 330-layer laminate. Results of temperature measurement are shown in Figure 4.2. Temperature at top of laminate is larger than temperature at the middle of laminate. The insulating effect of bleeder plies is the main reason for this phenomena. Therefore, due to the presence of bleeder plies, the maximum temperature may not happen at the composite center. Since temperature at the bottom of laminate (next to the aluminium plate) is shown to follow closely the temperature of the autoclave [51] and looking at Figure 4.2, the temperature distribution through the thickness is unsymmetric.

Autoclave pressure was set to $0.584 MPa(85psi)$. However, during the cure process the measured pressure was $0.549 MPa(80psi)$. Since the laminate was thick and no caul plate was used, compaction of laminate was nonuniform around the edges (approximately $1.5cm$ from edges). A uniform thickness was obtained (4.5 by 4.5 cm) at the middle of laminate. The final thickness at the middle was $4.5cm$. Fourteen layers of bleeder were completely filled with resin. Some of the resin around the thermocouple location passed all the bleeder layers and get into the breather.

The final part was cut to study the fiber distribution through-the-thickness. Laminate was polished using four sandpaper grades (240, 320, 400, and 600) and 1 micron Alumina powder. The laminate photomicrograph at different locations (see

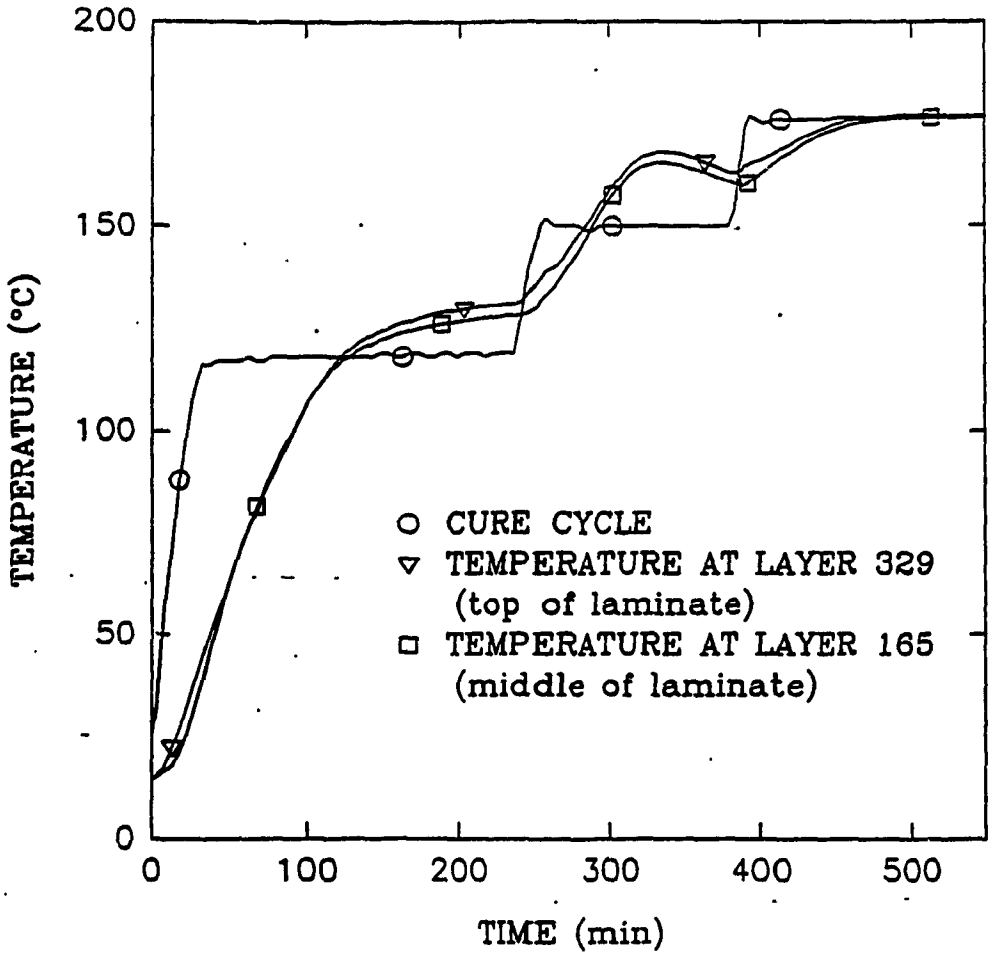

Figure 4.2: Measured temperature at different locations for one-dimensional experiment (330-layer laminate) .

Figure 4.3) are shown in Figures 4.4, 4.5, and 4.6. There were a few void locations observed at top ten layers as shown in Figure 4.7. Composite compaction at top layers was better than the bottom layers. There was a nonuniform compaction and fiber volume fraction distribution which makes the laminate imperfect.

The fiber volume fraction can be determined from the photomicrograph [67]. This can be done by counting the number of fibers in a selected area and calculating the total fiber area from their average diameter. The fiber volume fraction is determined as

$$v_f = \frac{A_f}{A} \tag{4.1}$$

where A_f and A are the total fiber area and the area of the selected region of the micrograph, respectively. Using this technique, fiber volume fraction was obtained at top, middle, and bottom of laminate. At each photomicrograph, three regions of 2.5 cm by 2.5 cm were selected and the number of fibers (NF) were counted. One region was selected from resin rich area and one from fiber rich area. The third region was selected from the area which fiber and resin are relatively distributed uniformly. Results are shown in table 4.1.

4.2 Two-Dimensional Experiment

This experiment was designed to show the effect of heat transfer through the sides of thick composite (sides which are perpendicular to the fiber direction in unidirectional plate) in curing. The heat was allowed to move through the thickness

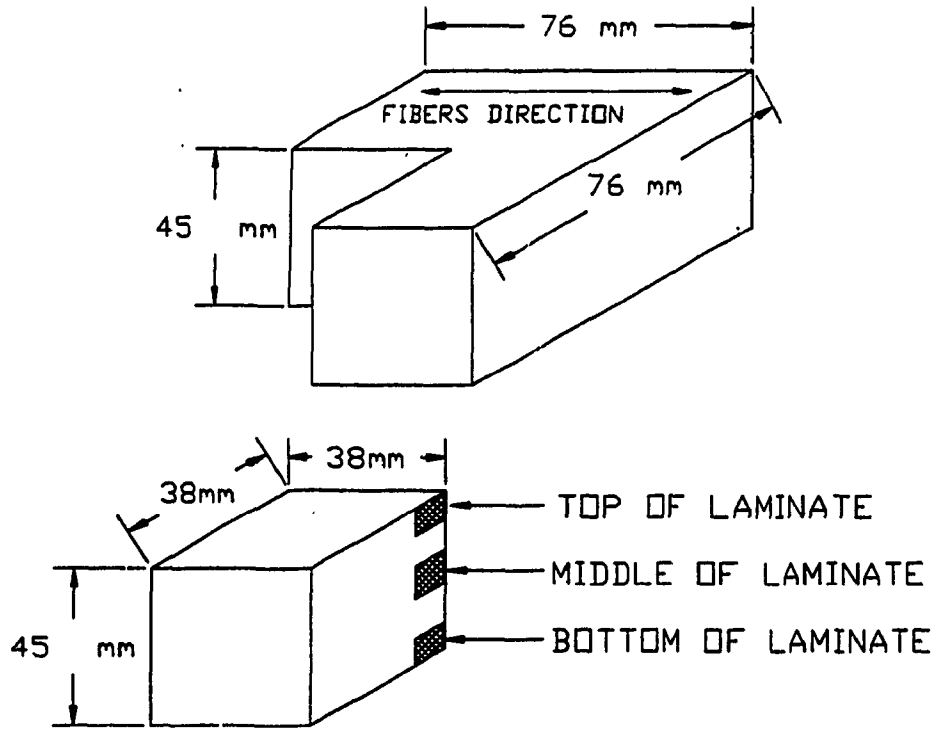

Figure 4.3: Location of different regions used to take photomicrograph (One-dimensional experiment and 330-layer laminate).

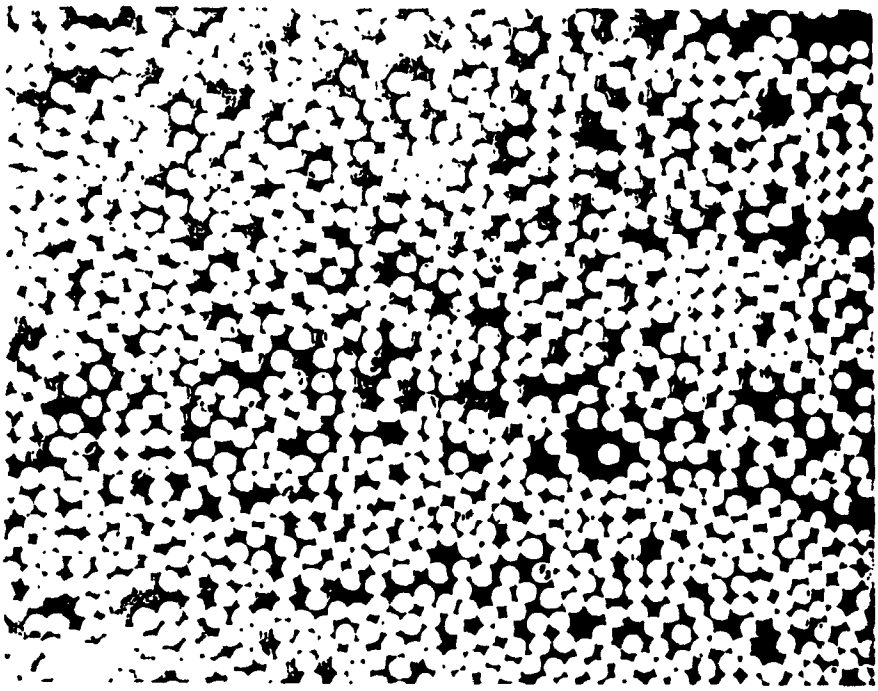

Figure 4.4: Cross-section photomicrograph (399X) at the top of laminate close to bleeder side (One-dimensional experiment and 330-layer laminate).

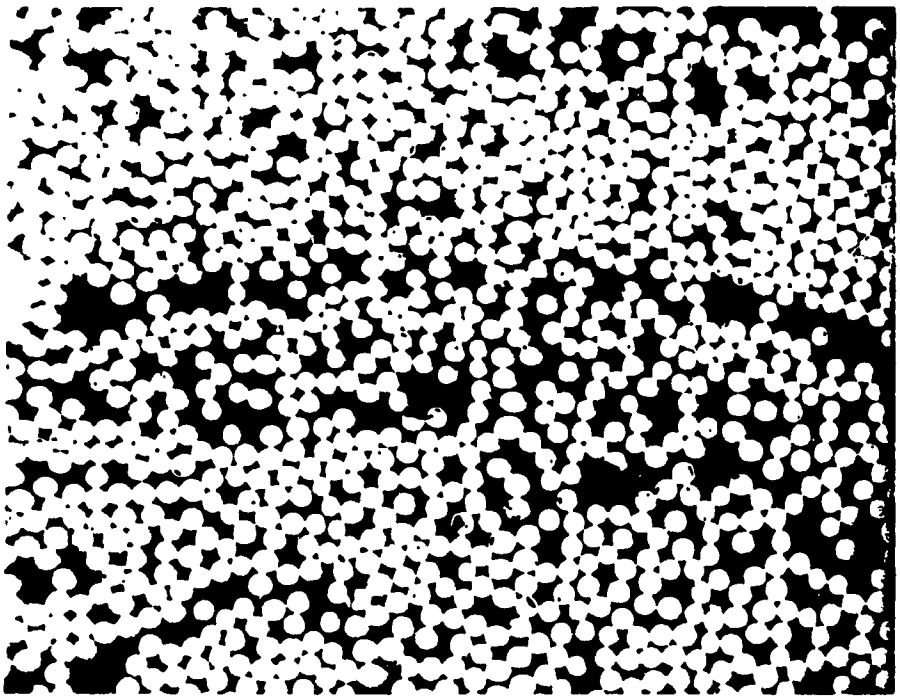

Figure 4.5: Cross-section photomicrograph (399X) at the middle of laminate (One-dimensional experiment and 330-layer laminate).

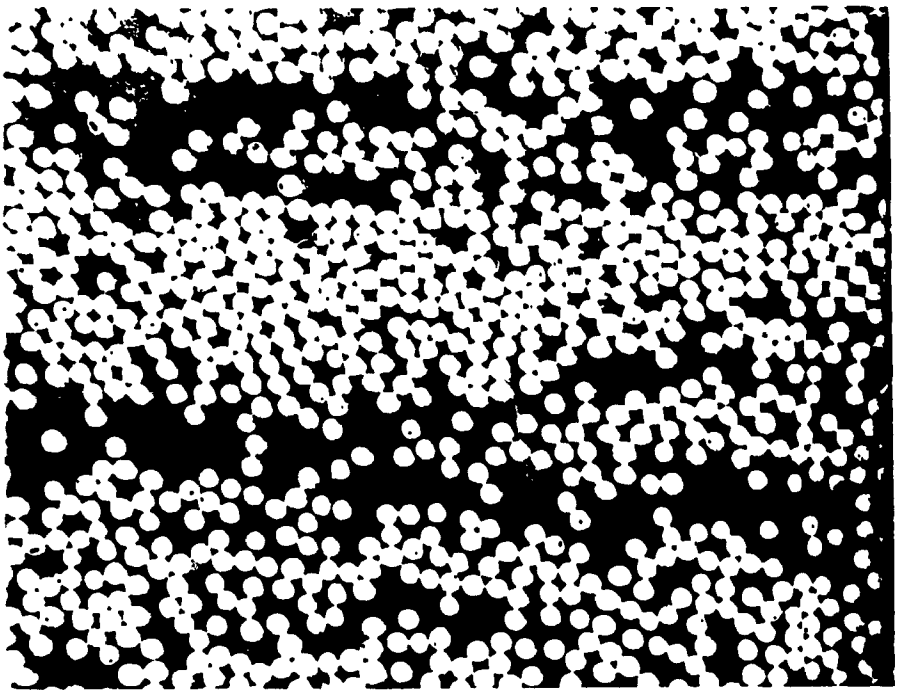

Figure 4.6: Cross-section photomicrograph (399X) at the bottom of laminate close to Aluminum plate (One-dimensional experiment and 330-layer laminate).

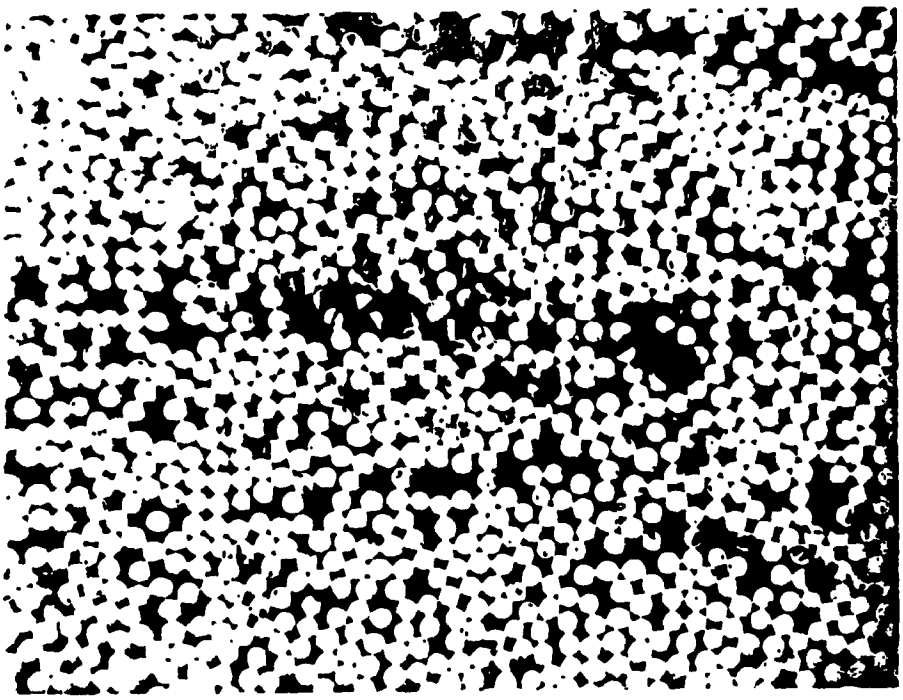

Figure 4.7: Cross-section photomicrograph (399X) at the top ten layers of laminate (One-dimensional experiment and 330-layer laminate).

TOP		MIDDLE		BOTTOM	
NF	ν_f	NF	ν_f	NF	ν_f
60	0.59	54	0.53	45	0.44
66	0.65	58	0.57	56	0.55
69	0.68	67	0.66	66	0.65
Ave.	0.64	Ave.	0.58	Ave.	0.55

Table 4.1: Fiber volume fraction at different locations (one-dimensional experiments and 330-layer laminate).

and through the two other sides. It was intended to allow the resin to move only through the thickness.

4.2.1 Experimental Tooling Set-up

Tooling set-up used was the same as one-dimensional experiment. The only difference was to use the aluminum plate at two edges instead of ceramic insulation. These two aluminum plates were located perpendicular to the fiber directions, allowing heat to travel along the fiber directions. It should be noted that the thermocouples should be located perpendicular to the fiber direction. Cure cycle for one-dimensional experiment which was described before was used for this experiment as well.

4.2.2 Experimental Results

The temperature as a function of time was measured at two different locations (top and middle) inside a 330-ply composite. Results of the temperature measurement are shown in Figure 4.8. Like one-dimensional case, the temperature at top is larger than temperature at the middle. The maximum temperature may not happen at the laminate center. Comparison between Figures 4.2 and 4.8 shows that heat can travel much faster inside the composite in two-dimensional case. At the first dwell of cure cycle, the temperature based on lagging thermocouple reached to 116°C in 85min, 35min faster than one-dimensional case. The high thermal conductivity of composite along the graphite fibers causes the heat to move much faster. The temperature overshoot at the second dwell of cure cycle is lower than the one-dimensional case. Therefore, two-dimensional curing reduces the cure cycle time as well as the temperature overshoot at the second dwell period of cure cycle.

It was intended to let the resin move only through-the-thickness. However, due to the small gap between aluminum plate and laminate sides, some resin was pushed out through these gaps. All eighteen layers of polyester bleeder were full of resin. The final laminate thickness was 40 mm.

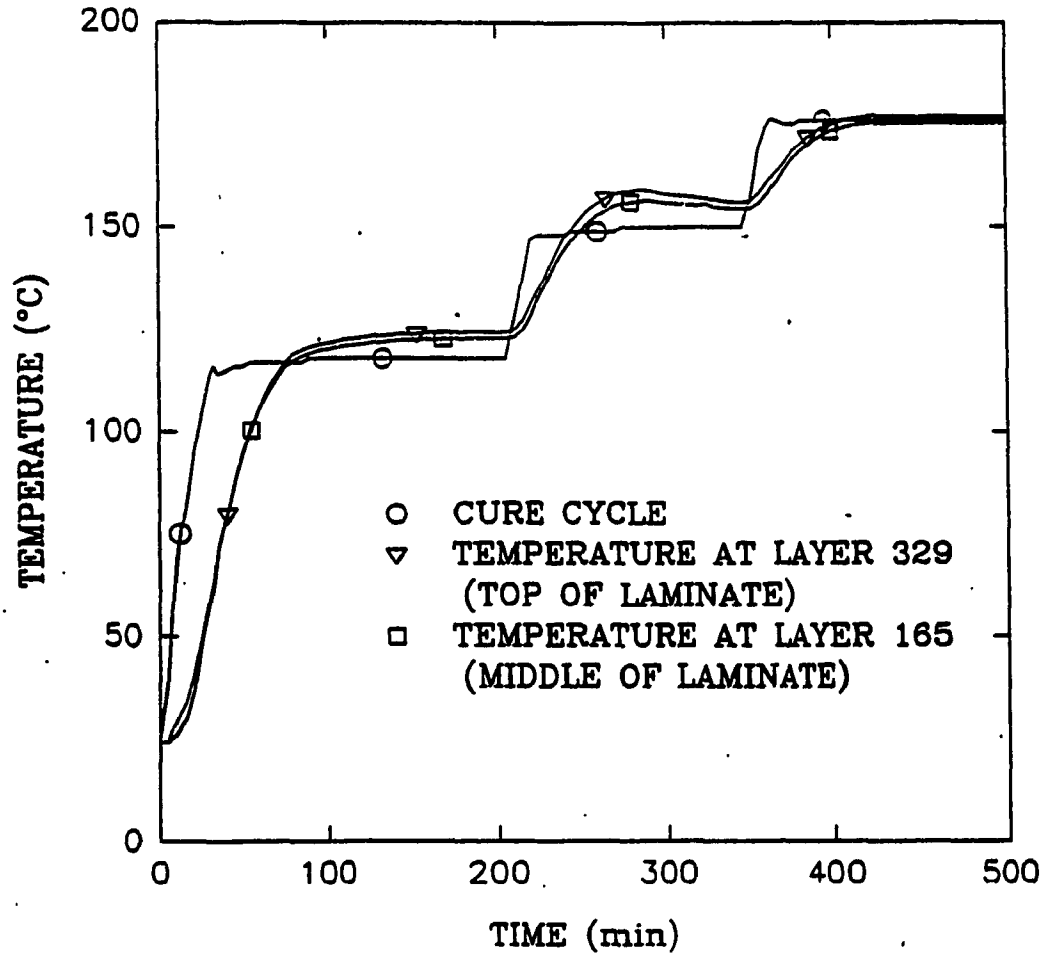

Figure 4.8: Measured temperature at different locations for two-dimensional experiment (330-layer laminate).

4.3 Prebleeding Experiment

While cure cycle recommended for thick laminate can solve the temperature overshoot problem (Figures 4.2 and 4.8), complete through-the-thickness consolidation may not be achieved (Figures 4.4, 4.5 and 4.6). In prebleeding experiment, thick laminate is divided to a number of sublaminates. Each sublaminate is subjected to the consolidation cure cycle to produce the fully-compacted and partially cured sublaminates. Those sublaminates are put together to make the thick laminate. The thick composite is exposed to the second cure cycle to complete the cure process. Therefore, the uniform fiber distribution is achieved.

4.3.1 Experimental Tooling Setup

Fabrication of thick laminate using prebleeding technique consists of two steps, prebleeding and final curing. Ten sublaminates, each consists of 32 layers, were prepared by hand lay-up. The bleed setup (Figure 4.1) was used for the prebleeding step. Six layers of polyester bleeder were used. The sides of sublaminates were wrapped tightly by Teflon film and then placed against the ceramic dams. All ten sublaminates were placed inside autoclave simultaneously and prebleeding cure cycle was applied. After completion of prebleeding stage, those ten sublaminates were put together to fabricate a thick composite. A K-type thermocouple was placed at the middle of laminate. Again the laminate sides were wrapped tightly with Teflon film to prevent any resin loss. No-bleed setup (Figure 4.9) was used

for this stage. None of the resin is intentionally removed during cure in no-bleed setup.

4.3.2 Cure Cycle

Two cure cycles were designed based on the manufacturer recommended cure cycle. First cure cycle was applied to the prebleeding stage. A pressure of $0.584 MPa (85 psi)$ was applied and vacuum was drawn on the bagged charge. The temperature was raised to $116°C$ and sublaminates were soaked for 70 min at this temperature. The pressure and vacuum were released and the charge was allowed to cool down to room temperature.

Second cure cycle was applied for the final curing of thick laminate. Again, $0.584 MPa$ pressure was applied, with vacuum drawn in the charge. The temperature was increased to $116°C$ and laminate was soaked for 60 min at this temperature based on the lagging thermocouple. The temperature was increased to $150°C$. The charge was soaked at this temperature for 90 min based on the lagging thermocouple. The temperature was then increased to $177°C$. The part was soaked at this temperature for 120 min, again based on the lagging thermocouple.

4.3.3 Experimental Results

Temperature was measured at the middle of laminate during the final cure. Result is shown in Figure 4.10. Temperature overshoot is less in comparison to full-bleed

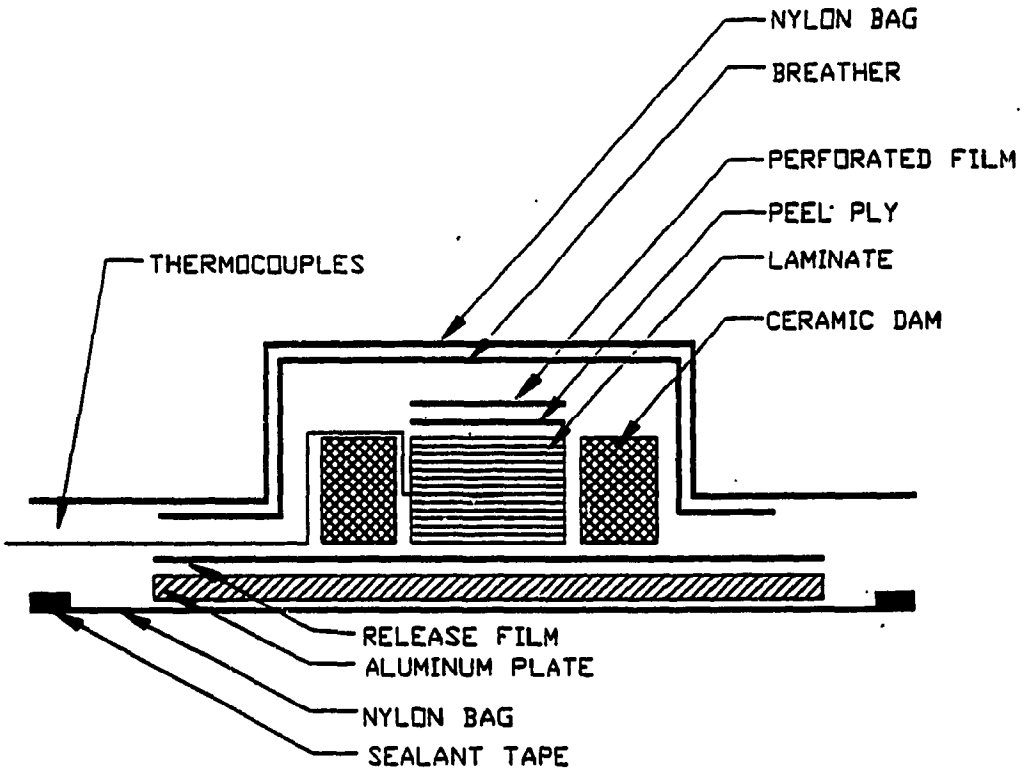

Figure 4.9: No-bleed tooling setup

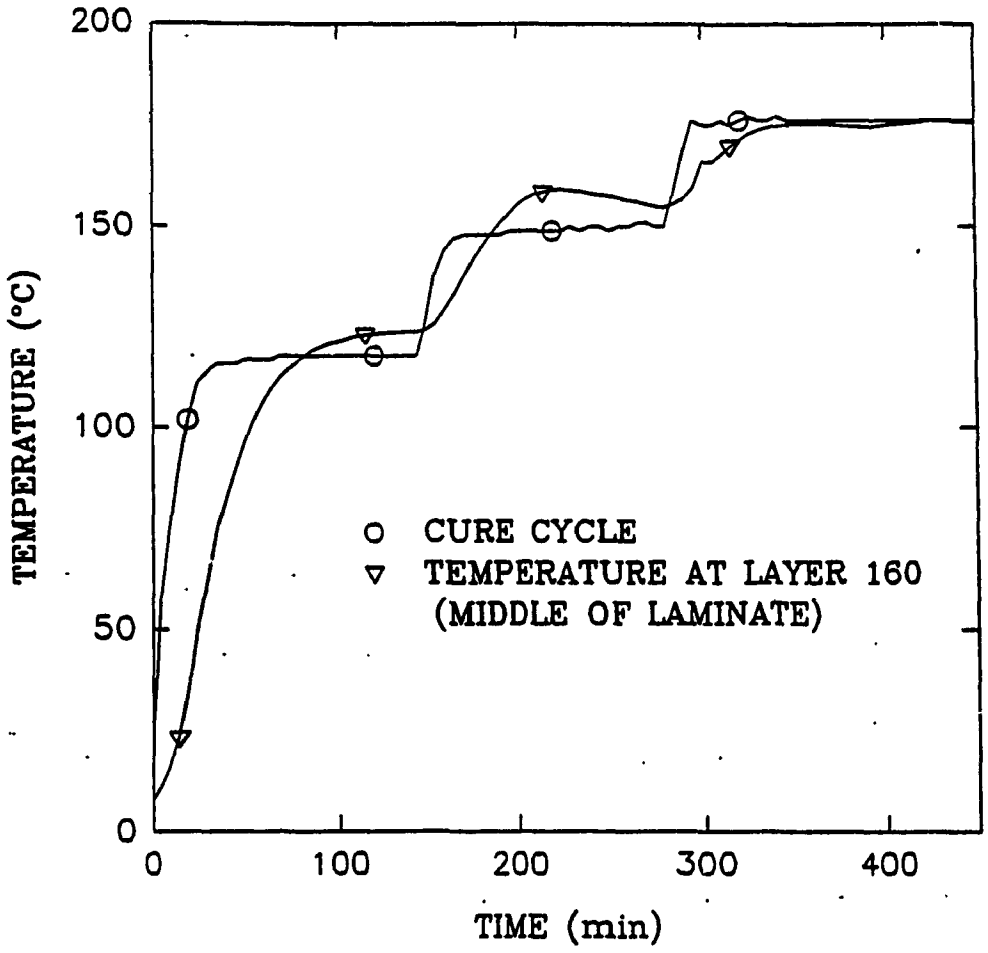

Figure 4.10: Measured temperature at the middle of 320-layer laminate- Prebleeding experiment.

setup (Figure 4.2). There are three reasons for decrease of temperature overshoot. First, all layers are completely compacted in the prebleeding stage and ,therefore, less resin remains inside laminate during the final cure, producing less heat. The second one is thickness of laminate. Since compaction is already done on all layers, the final thickness of 320-layer laminate is less. Finally application of no-bleed setup during the final curing and eliminating the thick bleeder layers from setup help heat to dissipate faster from center region of laminate.

Autoclave pressure was 0.549MPa. All bleeder plies were full with resin during the prebleeding experiment. The measured thickness of sublaminates after prebleeding stage was between 4.55 mm and 4.60 mm. It was expected to have sublaminates with thickness around 3.8 mm. As discussed in chapter 2, the fiber has spring-like behavior. During the dwell period of prebleeding cure cycle, resin moves out and fibers start to contact each others. The autoclave pressure transfers to fibers and resin pressure drops. At the end of dwell period, resin is partially cured. However, due to the high temperature (116°C), the resin is still liquid. Releasing pressure and vacuum at this time causes fibers move to upward due to their springback behavior. Therefore, the sublaminate thicknesses were more than expected.

The final thickness after complete curing was 38 mm. The laminate was cut and prepared for microscope inspection. The photomicrographs at different locations (see Figure 4.11) are shown in Figures 4.12, 4.13, and 4.14. Examination

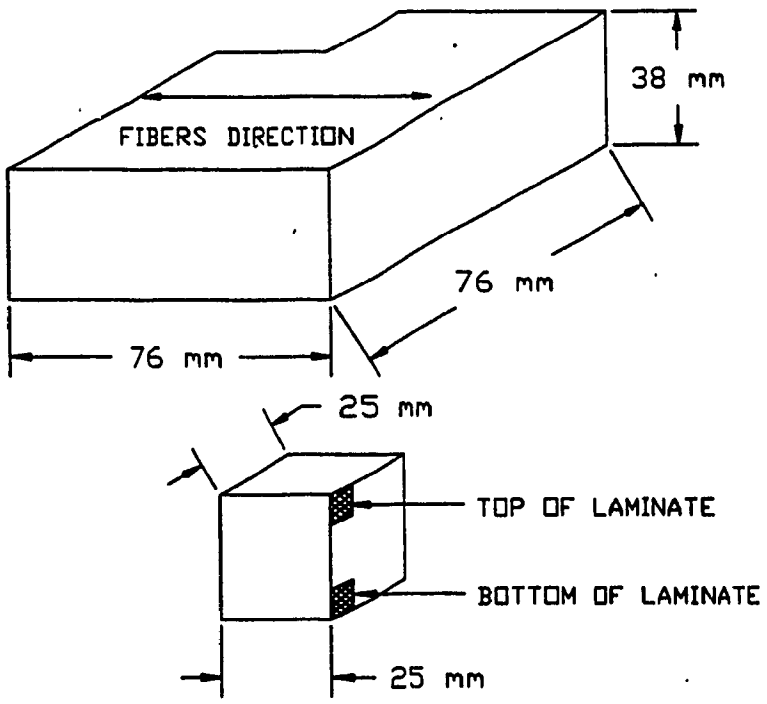

Figure 4.11: Location of different regions used to take photomicrograph (prebleeding experiment and 320-layer laminate).

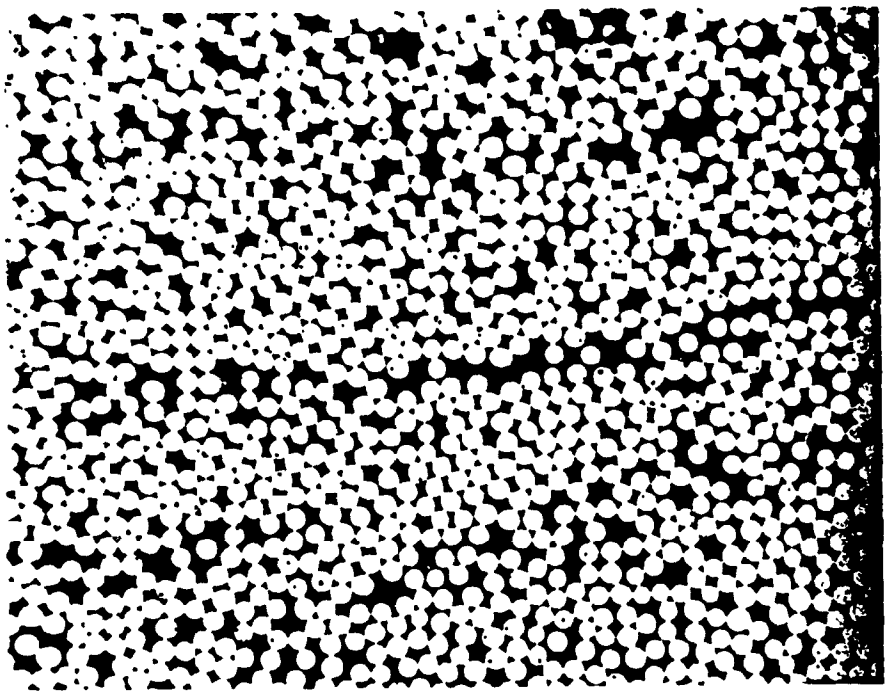

Figure 4.12: Cross-section photomicrograph (399X) at the top of laminate (pre-bleeding experiment and 320-layer laminate).

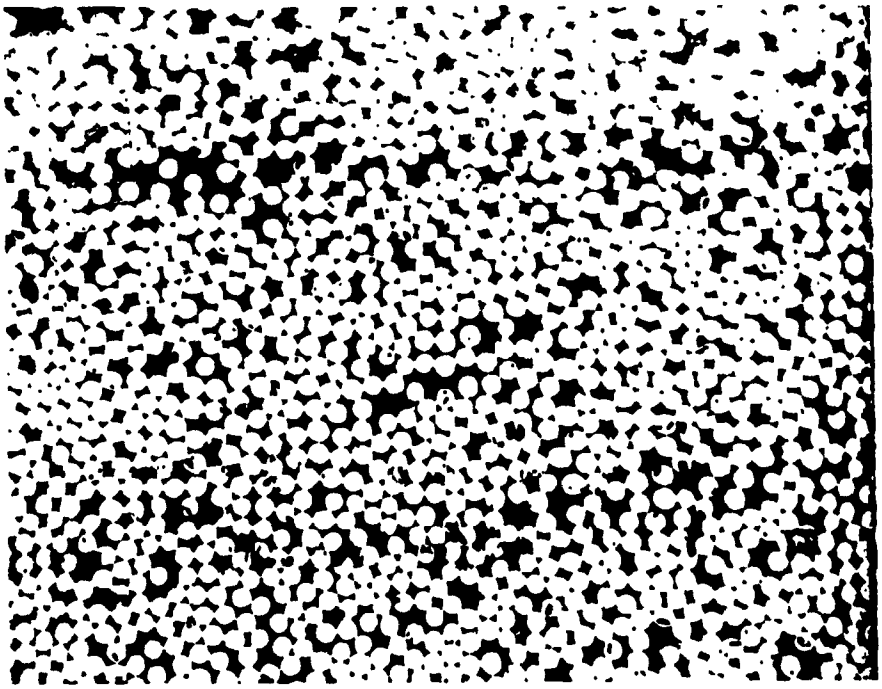

Figure 4.13: Cross-section photomicrograph (399X) at the bottom of laminate (prebleeding experiment and 320-layer laminate).

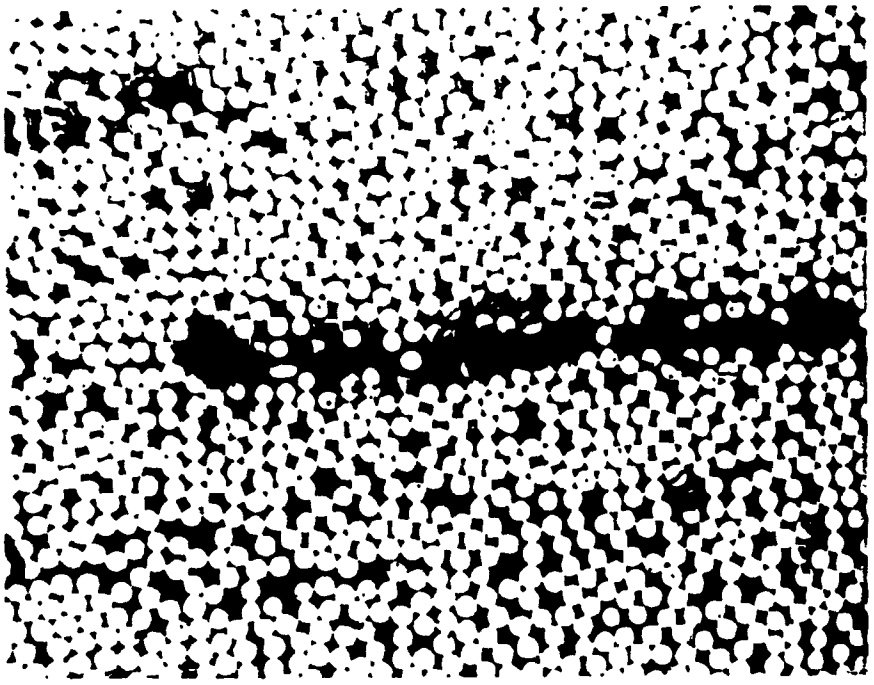

Figure 4.14: Void (399X) inside the laminate (prebleeding experiment and 320-layer laminate).

of the cross-section under the microscope showed that fibers uniformly distributed through-the-thickness of 320-layer laminate with small resin rich area. However, there were a few voids observed especially at resin rich area (Figure 4.14). Examining the fabrication process, two problems were found in prebleeding stage. Six layers of polyester bleeder absorb too much resin, decreasing the resin pressure rapidly. There was moisture which is present in the resin during the prepreg production and lay-up procedure. At high temperature , the resin should be under sufficient pressure to prevent nucleation of dissolved water in the resin on graphite fiber surface. This phenomenon was well-described by Dave et.al. [29]. Since resin pressure dropped too much because of too many bleeder plies and therefore too much resin absorption, voids are formed.

Releasing pressure and vacuum at the end of dwell period of prebleeding cure cycle was the next problem. The fiber moves upward due to their springback behavior and air gets into the sublaminates.

The measured fiber volume fraction at top and bottom of laminate are given in table 4.2.

4.3.4 Modified Fabrication Procedure

To fabricate a void-free thick laminate, a new experiment was designed and performed. Six sublaminates each consists of 20 layers were made by hand lay-up. All six sublaminates were prepared by bleed setup (Figure 4.1). Two bleeder plies

TOP		BOTTOM	
NF	ν_f	NF	ν_f
70	0.69	74	0.73
68	0.67	69	0.68
67	0.66	67	0.66
Ave.	0.67	Ave.	0.69

Table 4.2: Fiber volume fraction at different locations (Prebleeding experiments and 320-layer laminate).

were used for each sublaminate. All sublaminates were subjected to the modified prebleeding cure cycle. This prebleeding cure cycle was the same as before except that the pressure and vacuum were held until the charge cooled down (around 30°C). All six modules were put together and laminate sides were wrapped tightly in teflon film. The no-bleed setup (Figure 4.9) was used to prepare the laminate for final curing.

The final thickness was 14.8 mm. Photomicrograph of cross-section are shown in Figures 4.15, 4.16, and 4.17. The fiber distribution is uniform throughout the laminate. Some resin rich areas were observed (Figure 4.17). No void was observed. Using area method, the fiber volume fraction was measured. The results are shown in table 4.3.

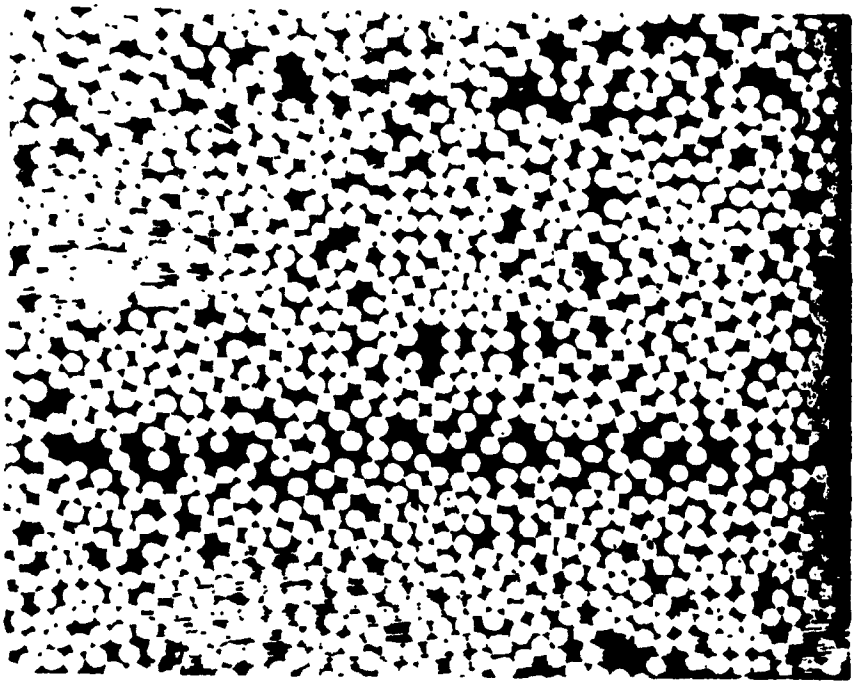

Figure 4.15: Cross-section photomicrograph (399X) at the top of laminate (Pre-bleeding experiment and 120-layer laminate).

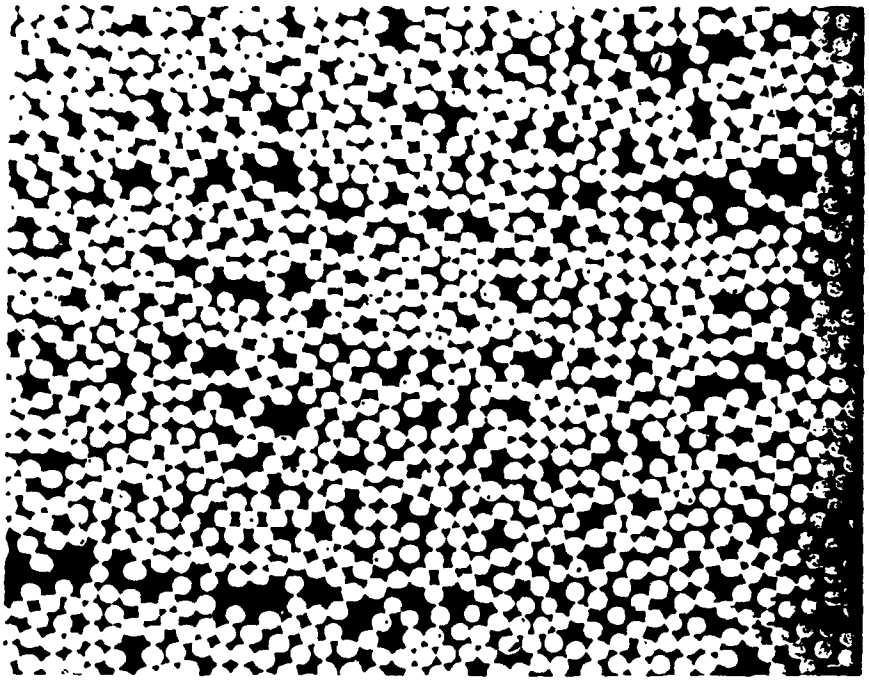

Figure 4.16: Cross-section photomicrograph (399X) at the bottom of laminate (Prebleeding experiment and 120-layer laminate).

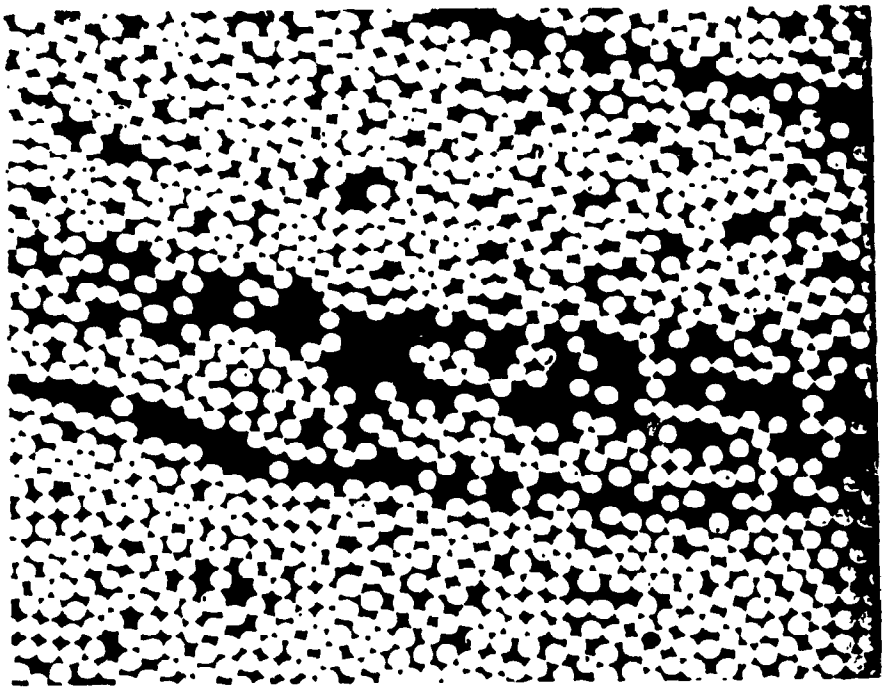

Figure 4.17: Resin rich area (399X) inside the laminate (prebleeding experiment and 120-layer laminate).

TOP		BOTTOM	
NF	ν_f	NF	ν_f
66	0.65	64	0.63
66	0.65	69	0.68
65	0.64	67	0.66
Ave.	0.65	Ave.	0.65

Table 4.3: Fiber volume fraction at different locations (Prebleeding experiments and 120-layer laminate).

4.4 Summary

One-dimensional through-the-thickness experiment for thick composite (330-layer) was performed. The bleed setup was used. Two problems were found, temperature overshoot at second dwell temperature and incomplete through-the-thickness consolidation. The temperature at top of laminate was observed to be higher than at the middle of laminate. Therefore, maximum temperature may not happen at the center of laminate.

To reduce the temperature overshoot, the two-dimensional experiment was designed and performed. The bleed setup was used. The two-dimensional curing decreases the temperature overshoot as well as cure time.

Prebleeding experiment was designed and performed to achieve complete through-the-thickness consolidation. Thick laminate was divided into thin sublam-

inates. After prebleeding the sublaminates using bleed setup, the sublaminates were put together and completely cured (using no-bleed setup). Uniform compaction was obtained.

Chapter 5

Experimental and Simulation Results

Experimental results are compared with simulation results in this chapter. After verification of model and numerical solutions, simulation is used to study the thick laminate behavior during cure process. The simulation results can also be compared with other investigators' results [13, 22, 27, 51, 52]. However, no comparison was made with those results, due to the lack of information about their setup. Two main problems are investigated. Mechanism and effect of consolidation on laminate curing are discussed as well as different ways to achieve complete through-the-thickness consolidation. Tooling effect on curing of thick composite is studied.

Two computer codes based on discretization equations derived in chapter 3 are

Density	1300 $\frac{kg}{m^3}$
Specific Heat	1600 $\frac{J}{kg\,^\circ K}$
Thermal Conductivity	0.17 $\frac{W}{m\,^\circ K}$

Table 5.1: Typical physical properties of polyester [68,69].

developed for one-dimensional and two-dimensional simulation studies. Equation (3.8) is employed in the simulation.

5.1 One-dimensional Results

Tooling setup used for the simulation is shown in Figure 5.1. The polyester bleeder thickness measured after experiment was 5.5 mm from which 3.8 mm was filled with resin and the rest was dry. The polyester physical properties used in the simulation are given in Table 5.1. the calculated bleeder fiber volume fraction was 0.3.

Bleeder physical properties are calculated based on the laminate compaction during curing. It is assumed that the resin which moves to the bleeder is distributed uniformly throughout the 3.8 mm bleeder plies. Bleeder density and specific heat are calculated using rule of mixture. It is assumed that initial bleeder thermal conductivity (k_{bi}) is 0.01 $\frac{W}{m^\circ K}$ (typical thermal conductivity for insulating materials) and during the consolidation stage it reaches to its final value (k_{bf}) of 0.17 $\frac{W}{m^\circ K}$ (Polyester and epoxy 3501-6 have almost the same thermal conductivity). The

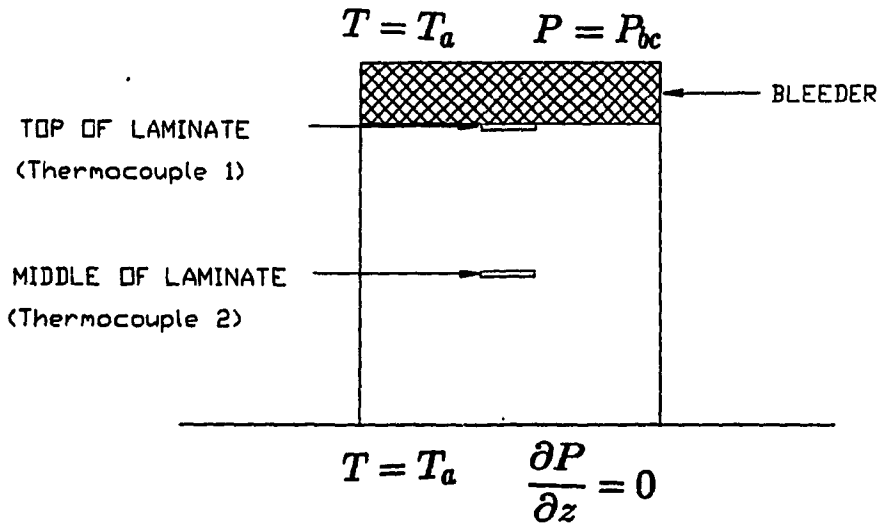

Figure 5.1: Tooling setup used for simulation (One-dimensional analysis and 330-layer laminate).

variation of bleeder thermal conductivity can be expressed as a function of laminate compaction. The following equation is used for the simulation

$$k_b = k_{bi} + \frac{(k_{bf} - k_{bi})L_t}{L_f} \tag{5.1}$$

where k_b is bleeder thermal conductivity. L_t is the laminate thickness reduction at each time step and L_f is the total laminate thickness reduction after curing.

Simulation and experimental results for temperature measurement at top and middle of laminate are shown in Figures 5.2 and 5.3. The predicted temperatures are in good agreement with measured temperatures except at first dwell period. The peak temperatures at second dwell period are almost the same for both experiment and simulation.

There are two possibilities to explain the mismatch between actual and predicted temperature. The thermal properties of polyester bleeder were not given by manufacturer and ,therefore, they were taken as typical properties obtained from handbooks (Table 5.1). Simulation shows that among the bleeder physical properties, initial thermal conductivity has more effect in the simulation. Different initial thermal conductivities were examined (0.001 to 0.3). However, the mismatch between the measured and predicted temperatures were always observed. Therefore, it is not the only reason of mismatch.

Examination of Figures 5.2 and 5.3 suggests that the kinetic equation has to be improved. The rate of reaction predicted by kinetic equation is higher than the actual reaction. In the simulation, the reaction proceeds faster than the actual

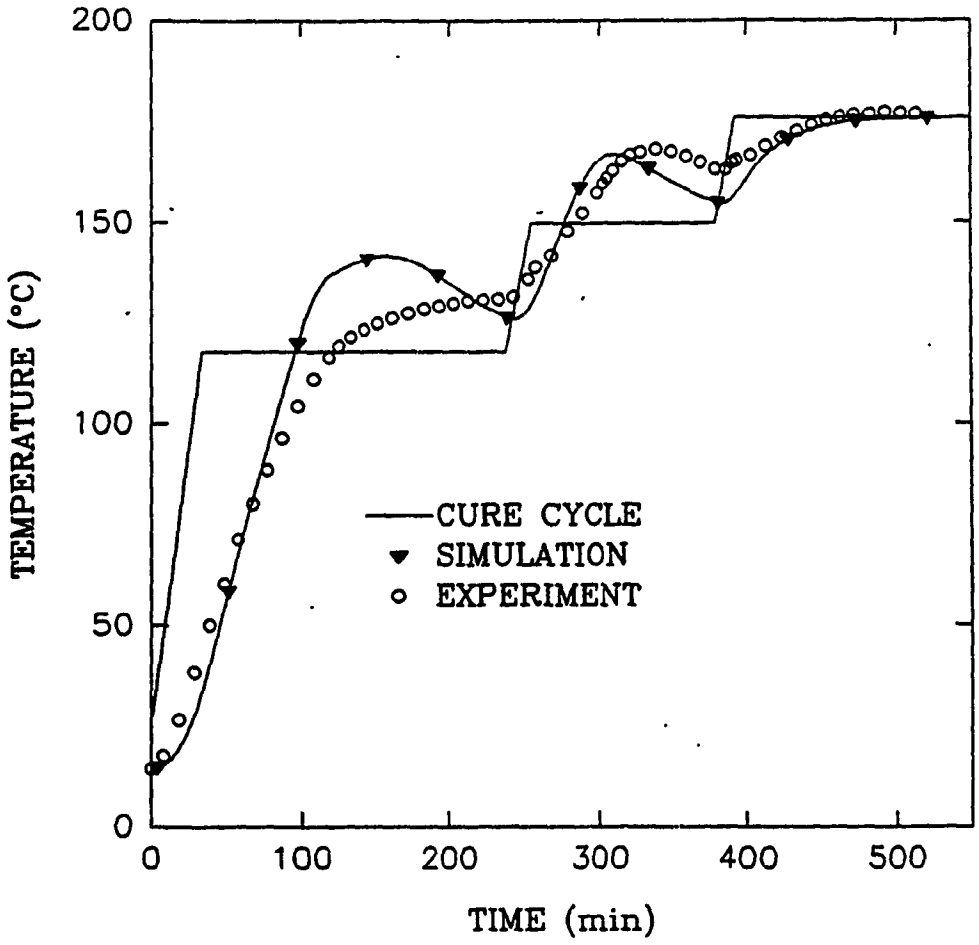

Figure 5.2: Comparison between measured and predicted temperature at top of laminate (One-dimensional analysis and 330-layer laminate).

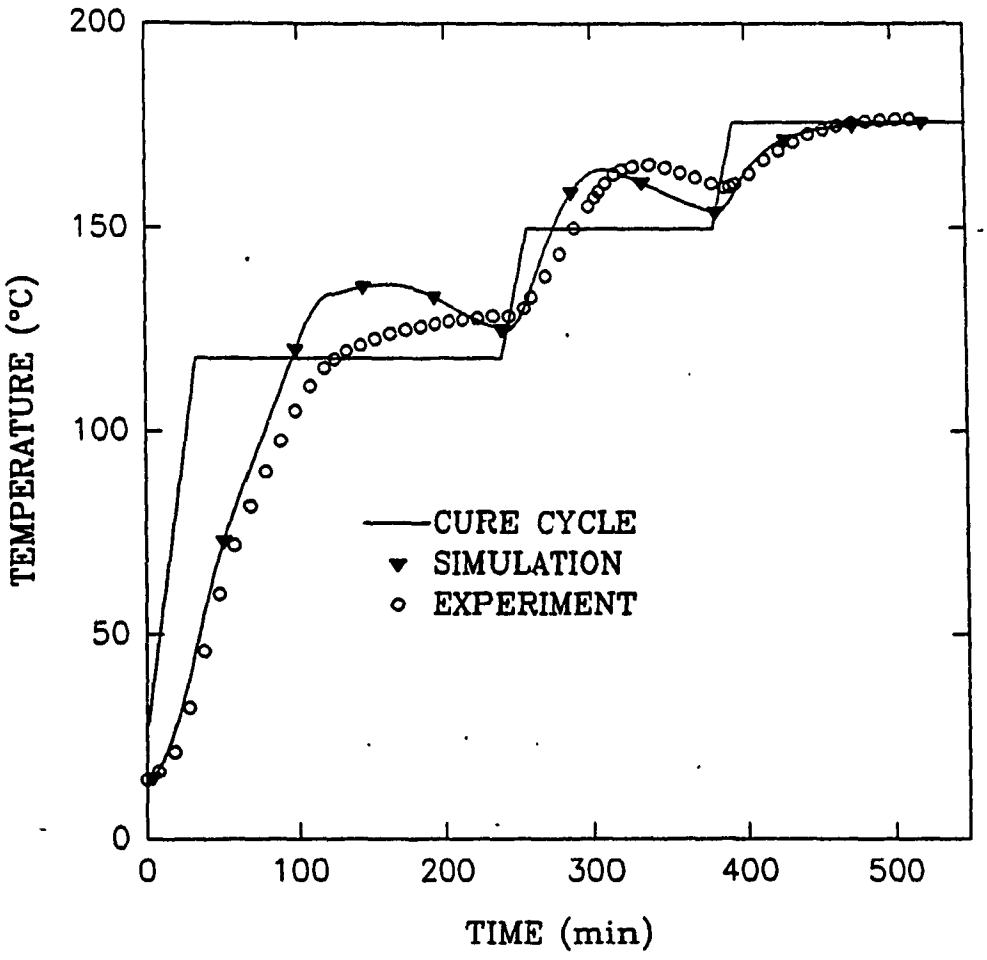

Figure 5.3: Comparison between measured and predicted temperature at middle of laminate (One-dimensional analysis and 330-layer laminate).

reaction, generating heat faster. The generated heat does not have enough time to reach to the surface and to dissipate. The internal energy increases, raising the laminate temperature. Due to the lower bleeder thermal conductivity at the first ramp and dwell period of cure cycle, higher rate of heat generation in simulation causes higher mismatch between predicted and actual temperature. It can be concluded that the kinetic equation proposed by Lee et.al. [56] and modified by Martinez [51] for epoxy 3501-6 overestimates the rate of chemical reaction and should be improved.

Both experiment and simulation show that the temperature distribution through-the-thickness is not symmetric (Figure 5.4). In fact, due to the insulating behavior of bleeder plies, temperature at top of laminate is greater than the temperature at the middle.

The simulation results for laminate compaction is shown in Figure 5.5. The measured thickness after curing was 45 mm which is in good agreement with simulation. The predicted and calculated fiber volume fraction distribution through-the-thickness are shown in Figure 5.6. The fiber distribution is not uniform. Fully compacted thick laminate can not be fabricated by this technique. Good agreement between predicted and calculated fiber volume fraction is obtained. Maximum error (at the middle of laminate) is about eight percent.

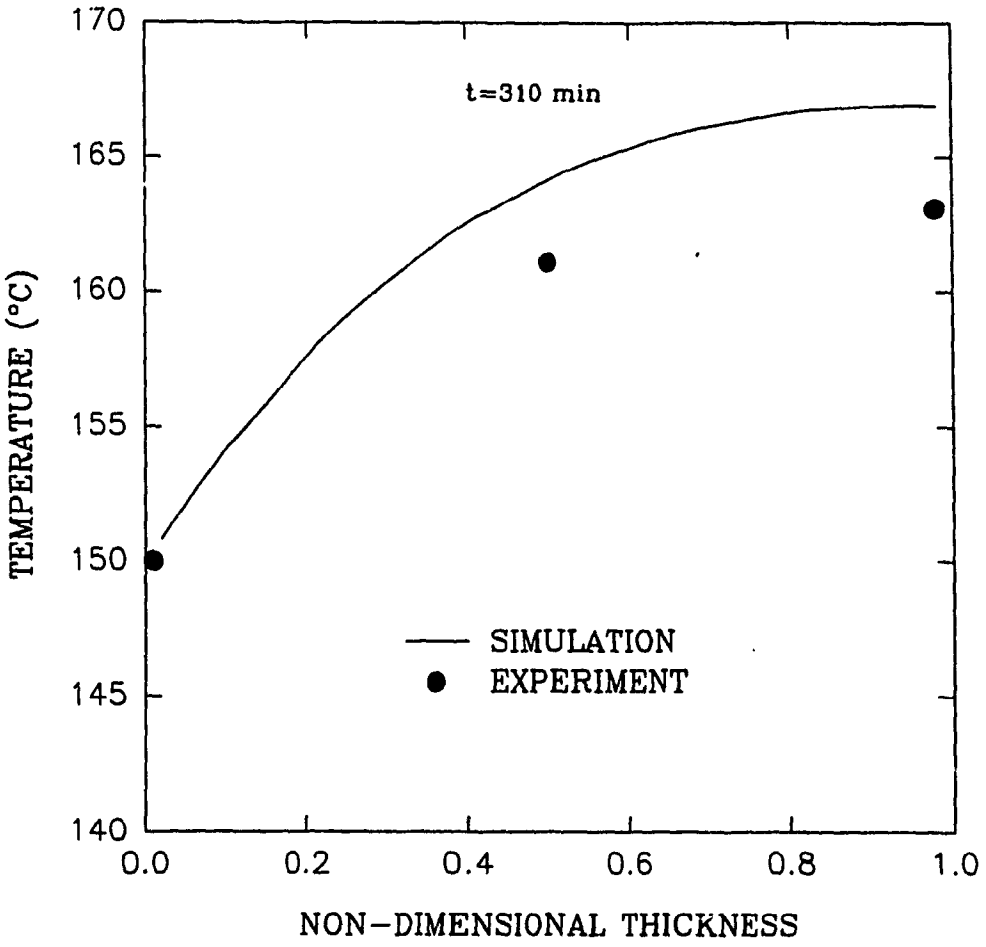

Figure 5.4: Temperature distribution through-the-thickness (One-dimensional analysis and 330-layer laminate).

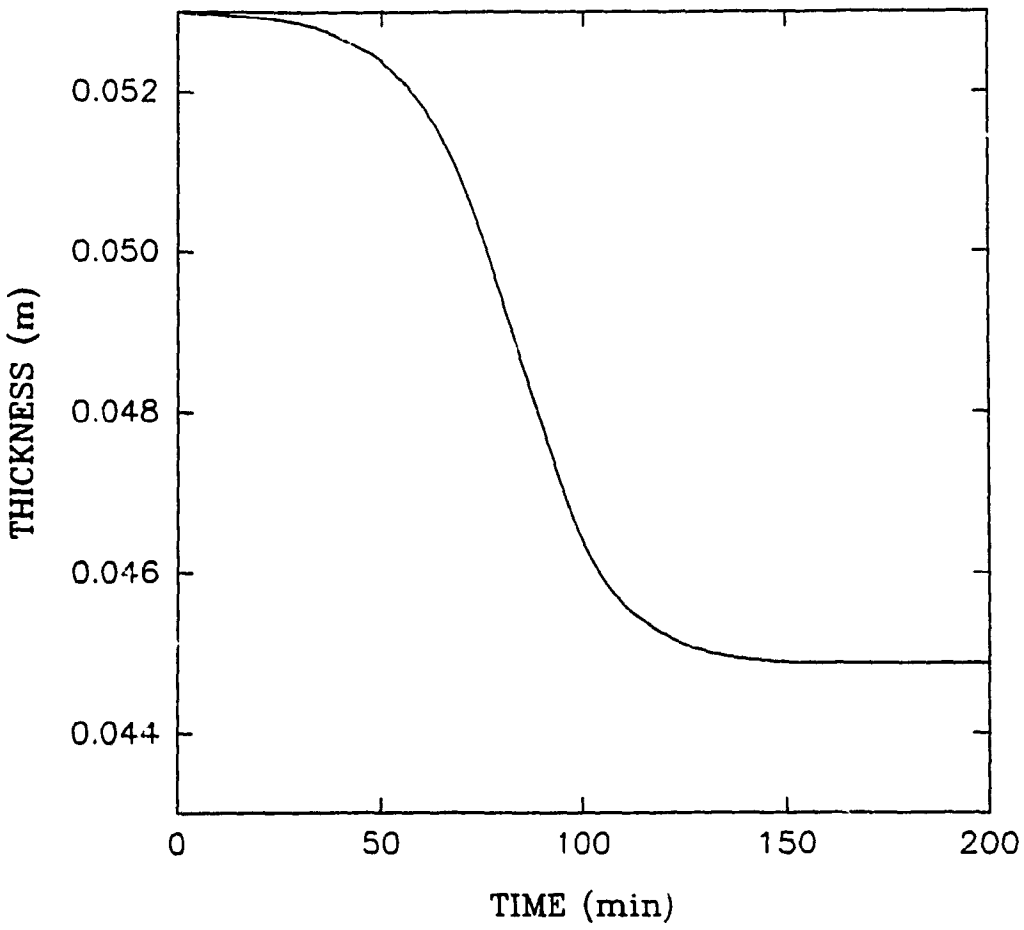

Figure 5.5: Laminate compaction evolution (One-dimensional analysis and 330-layer laminate).

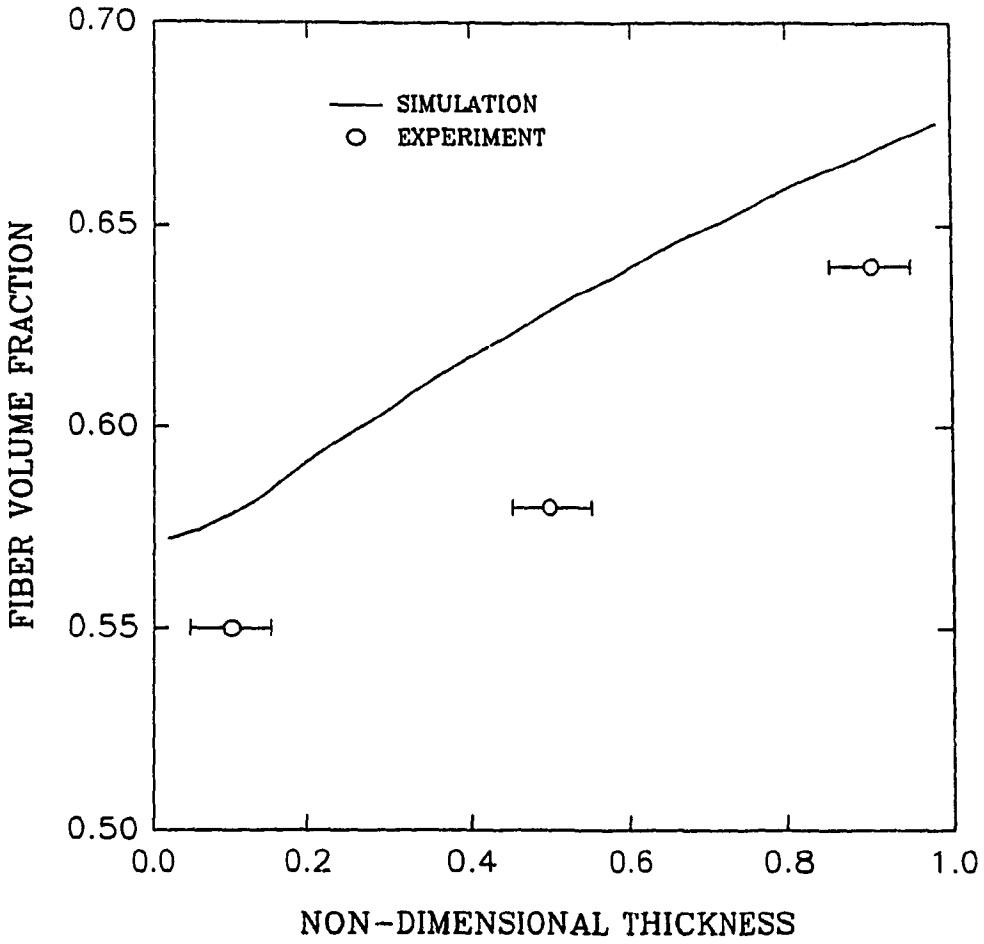

Figure 5.6: Fiber volume fraction distribution through-the-thickness (One-dimensional analysis and 330-layer laminate).

5.2 Two-dimensional Results

As explained before, this experiment was designed to have two-dimensional heat transfer and one-dimensional resin flow. However, both heat transfer and resin flow were two-dimensional during experiment. Simulation is done for this case. Tooling setup used in the simulation is shown in Figure 5.7. Based on the laminate cross-section examination, one layer of resin with thickness 0.5 mm was assumed at the laminate sides in simulation. The bleeder thickness was 5 mm and all bleeders were filled with resin. Bleeder thermal conductivity is calculated using Equation (5.1). Kozeny constant for permeability calculation along the fibers direction is assumed to be 0.3. The predicted and measured temperature are shown in Figures 5.8 and 5.9. Again, it seems that the kinetic equation overestimates the rate of reaction.

5.3 Prebleeding Results

Two simulations are required to study prebleeding process. First, The prebleeding cure cycle is applied to the sublaminates. The same tooling setup as shown in Figure 5.1 was used. The simulation shows that at the end of curing sublaminates degree of cure is 0.3 and each sublaminate is fully compacted with uniform fiber volume fraction equal to 0.68. Since there is no compaction allowed in the final cure cycle, the laminate final fiber volume fraction is 0.68. This value for ν_f and

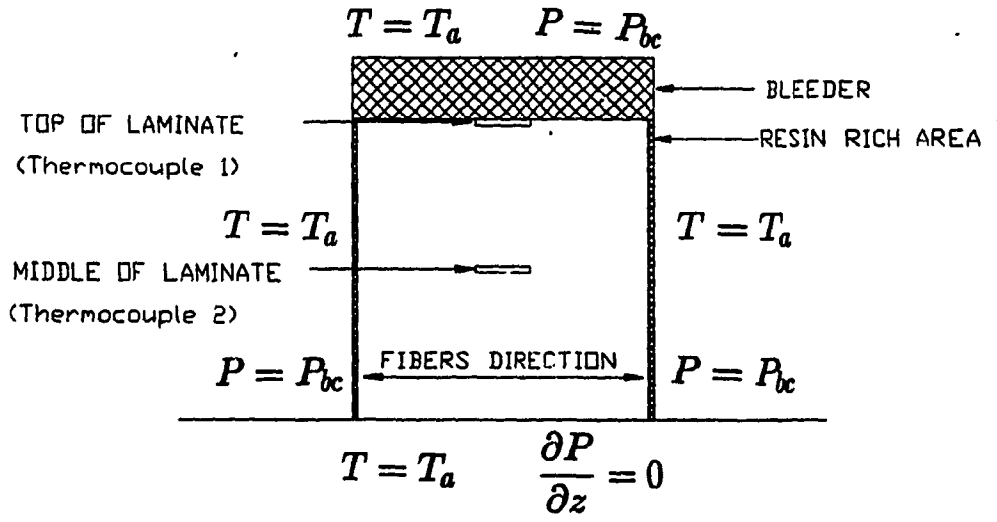

Figure 5.7: Tooling setup used for simulation (Two-dimensional analysis and 330-layer laminate).

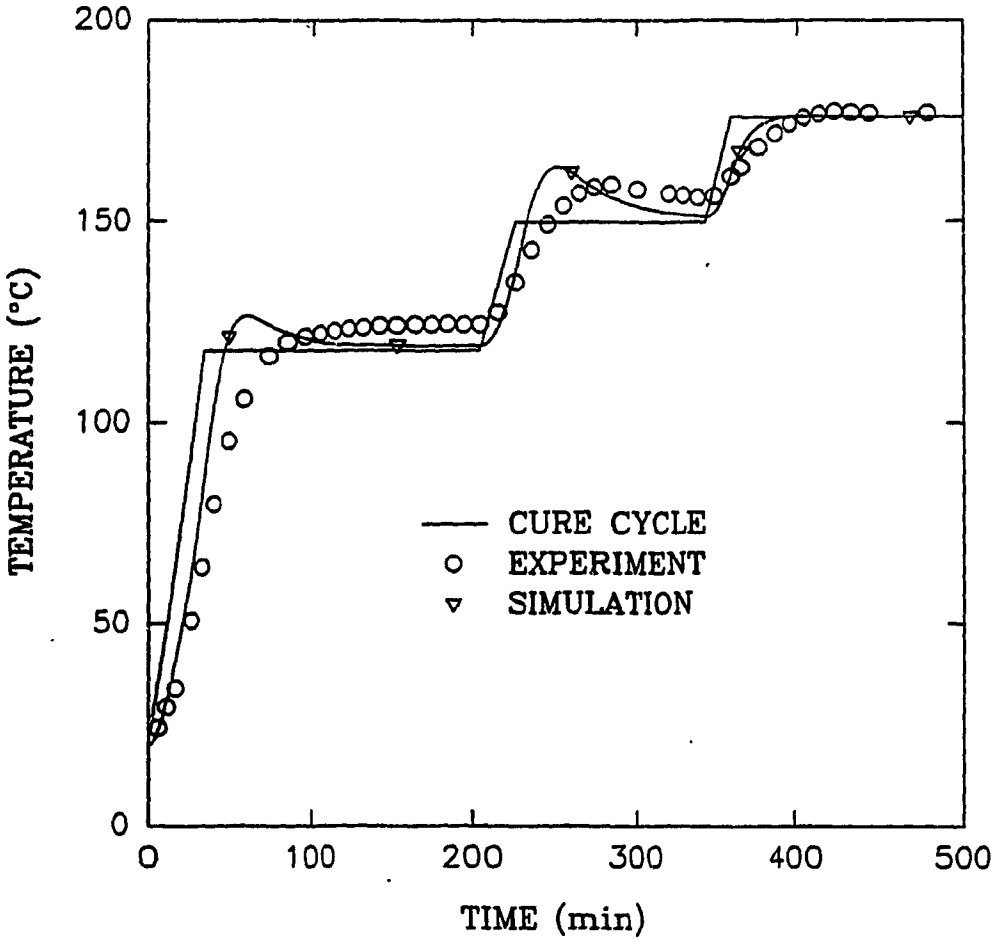

Figure 5.8: Comparison between measured and predicted temperature at top of laminate (Two-dimensional analysis and 330-layer laminate).

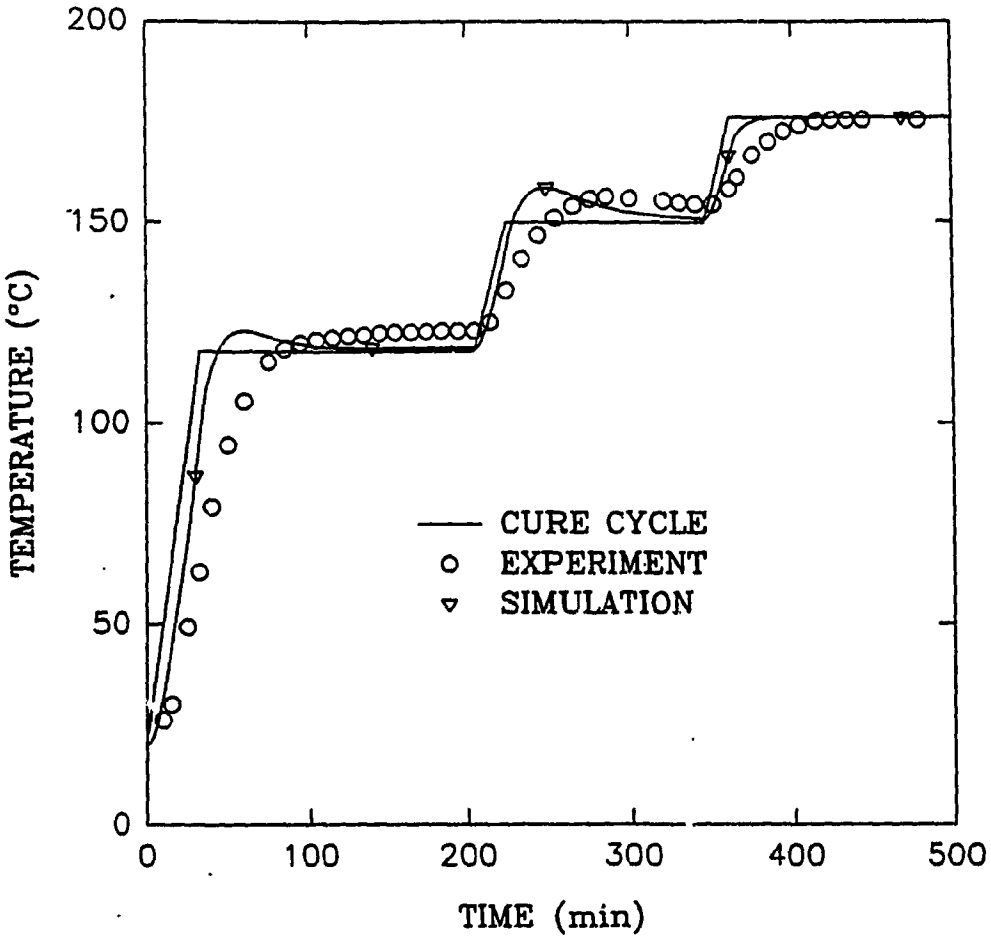

Figure 5.9: Comparison between measured and predicted temperature at middle of laminate (Two-dimensional analysis and 330-layer laminate).

those obtained by experiment (Table 4.2) are in good agreement.

The next simulation is performed using the modified cure cycle for final curing as explained before. Initial conditions are

$$\alpha_0 = 0.3$$

$$v_f = 0.68$$

No compaction is allowed. Tooling setup shown in Figure 5.1 is used with 0.5 mm breather thickness. The actual and predicted temperature at the middle of laminate is shown in Figure 5.10. Like before, due to the higher rate of reaction in simulation, a mismatch between predicted and actual temperature is observed.

5.4 Simulation Results

Experimental results were compared with simulation and good agreement was observed. In this section, the simulation is used to study different mechanisms and phenomena that occurred inside thick laminate during curing. One-dimensional through-the-thickness assumptions are used [78].

Three different cure cycles are used for the simulation. These cure cycles are shown in Figures 1.1 (cure cycle 1) ,5.11,5.12. It is assumed that a pressure of 0.584 MPa (85 psi) is applied over the composite and vacuum is drawn on the bagged charge. The same pressure cycle is employed for all three cure cycles.

Different simulations were conducted to find out the optimum time and space

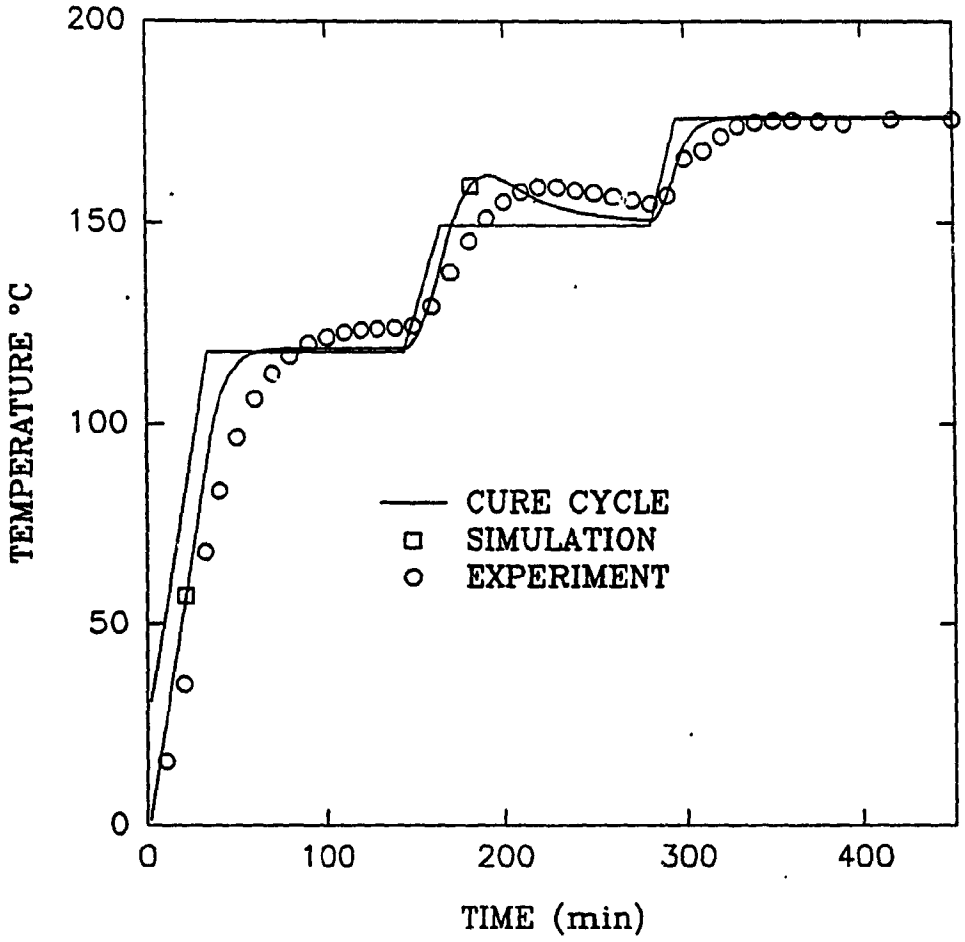

Figure 5.10: Comparison between measured and predicted temperature at middle of laminate (Prebleeding experiment and 320-layer laminate).

step sizes. A time step size of one second and space step size of two millimeters were selected for the simulation throughout this thesis. Larger step sizes may be used with less accuracy in the results.

5.4.1 Consolidation effect

Simulation results show that consolidation is an important processing variable. Consolidation and compaction have a major role in the temperature overshoot at the center of composite during curing. Two cure cycles 1 and 2 are used for the curing simulation of a laminate with 5 cm thickness. The results are shown in Figures 5.13 and 5.14 for cure cycle 1 and 2, respectively. With considering for consolidation in the simulation, maximum temperature at the middle of laminate is reduced by almost 32°C in cure cycle 1 and 21°C in cure cycle 2 in comparison to the simulation results without considering consolidation. There are three main reasons for this improvement. Heat is generated inside the composite by exothermic chemical reaction of the resin. During the consolidation significant amount of resin is taken out of the interior region of laminate. Maximum chemical reaction usually happens after the consolidation is finished. At this time, less resin remains inside composite and therefore less heat will be generated which causes less increase in the composite internal energy. The second reason is that the consolidation causes the fiber volume fraction inside the laminate to increase. Composite thermal conductivity increases with increasing fiber volume fraction which helps heat to

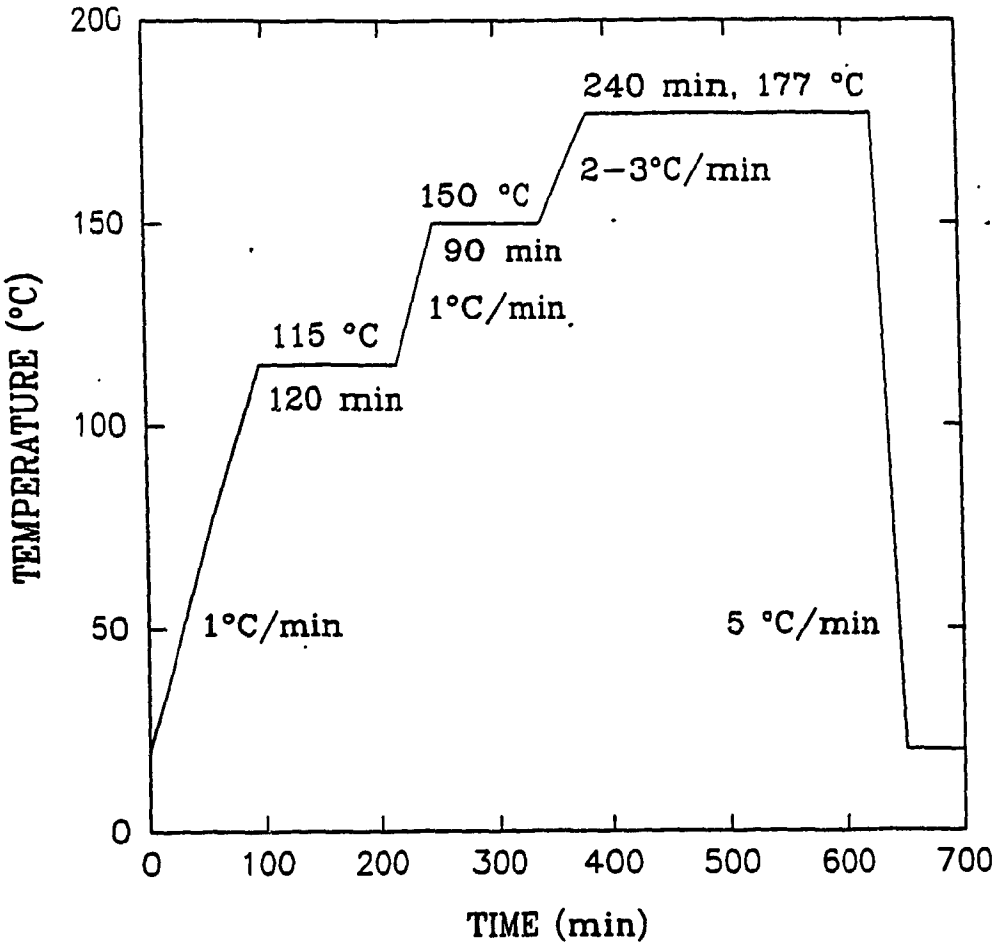

Figure 5.11: Cure cycle 2-Recommended by manufacturer for thick composites [52].

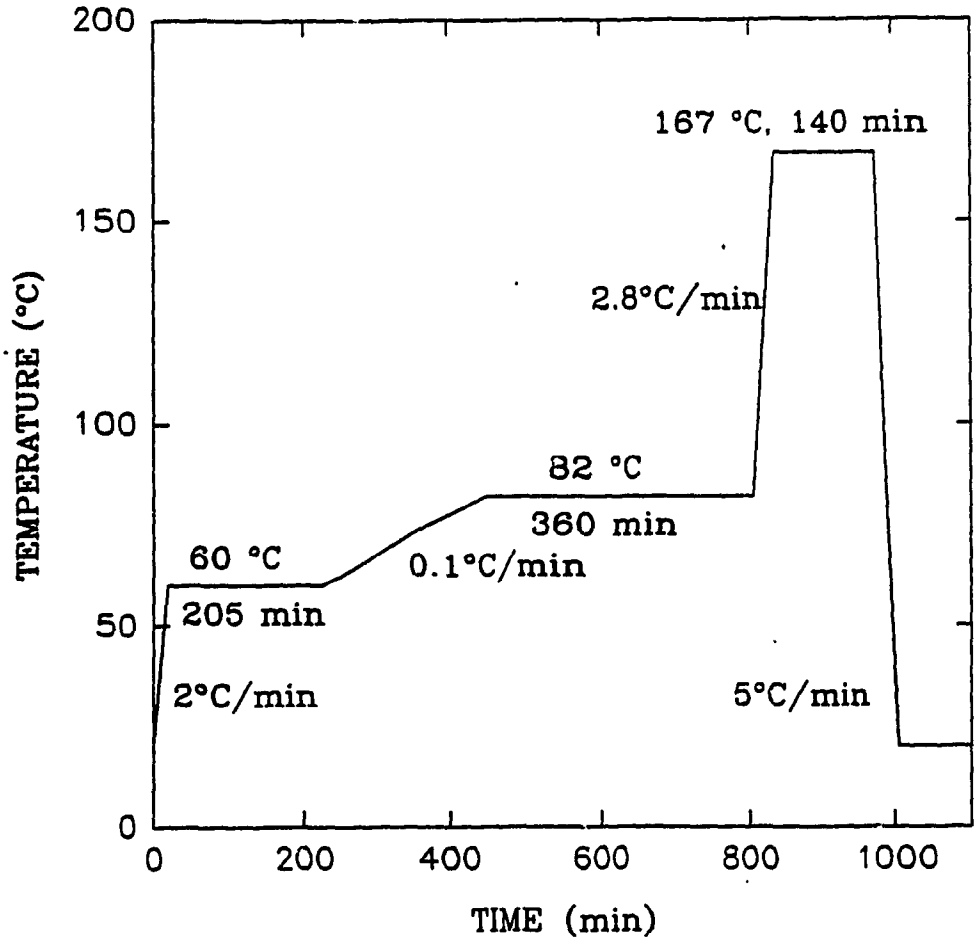

Figure 5.12: Cure cycle 3-Recommended for thick composites [49].

be dissipated faster. Finally, the temperature overshoot usually happens at the second cure cycle temperature ramp when consolidation is completed and the laminate thickness is decreased. Therefore the generated heat at the middle of laminate should travel less distance to reach the surface and then to dissipate.

5.4.2 Composite thickness variation

The consolidation process causes the composite thickness to reduce during the cure process. The variation of thickness with respect to time is shown for three different cure cycles in Figure 5.15. The variation of thickness with respect to time is an indication of compaction during the cure process. It should be noted that this variation does not give any information about the uniformity of compaction through the thickness. However as will be discussed later, simulation can be used to determine the fiber volume fraction distribution through-the-thickness at any time step.

The fastest compaction happens for cure cycle 1. The different heating rates at the first temperature ramp is responsible for the lower rate of compaction in cure cycle 2 in comparison with cure cycle 1. When the second temperature ramp is started in both cure cycle 1 and 2, resin is still liquid (Figure 5.16). Increasing temperature causes viscosity to drop, therefore the rate of compaction is increased for some time before the resin begins to gel. Hjellming and Walker[49] proposed cure cycle 3 to get maximum compaction during curing of thick composites. However,

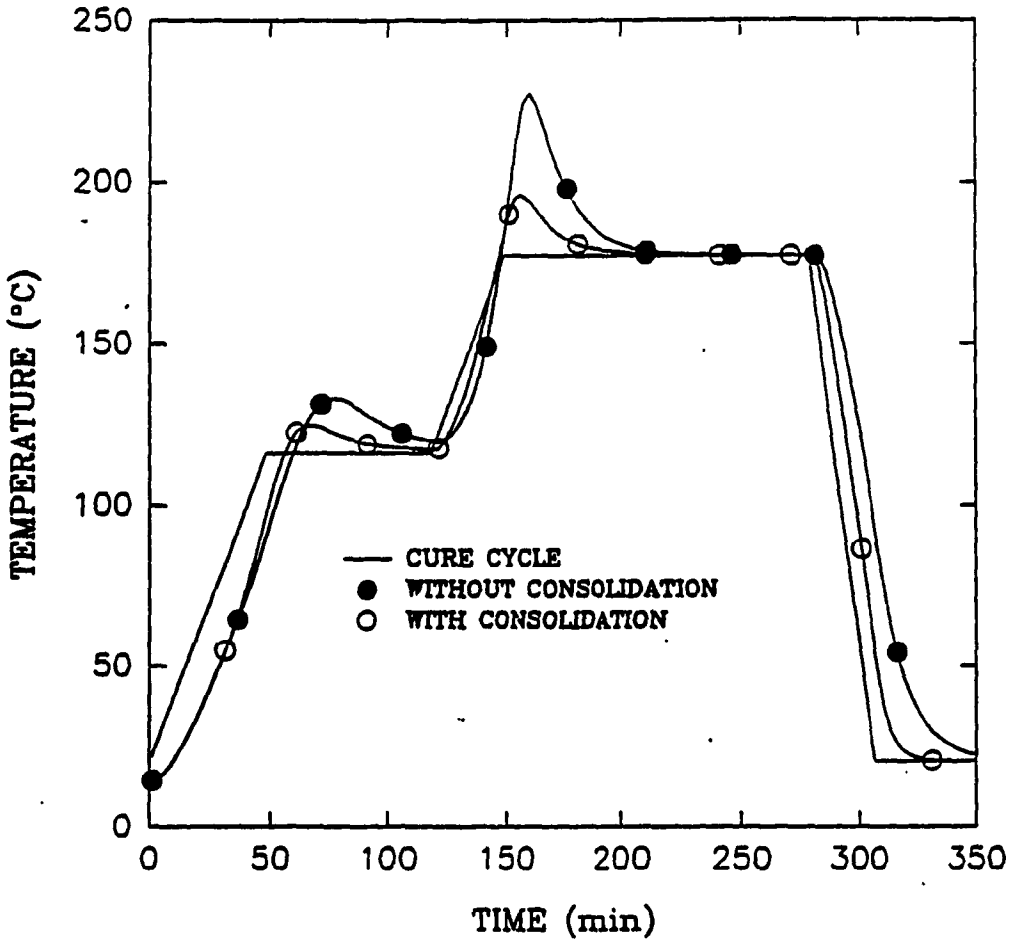

Figure 5.13: Temperature profile at the center of the thick composite (5cm) using cure cycle 1.

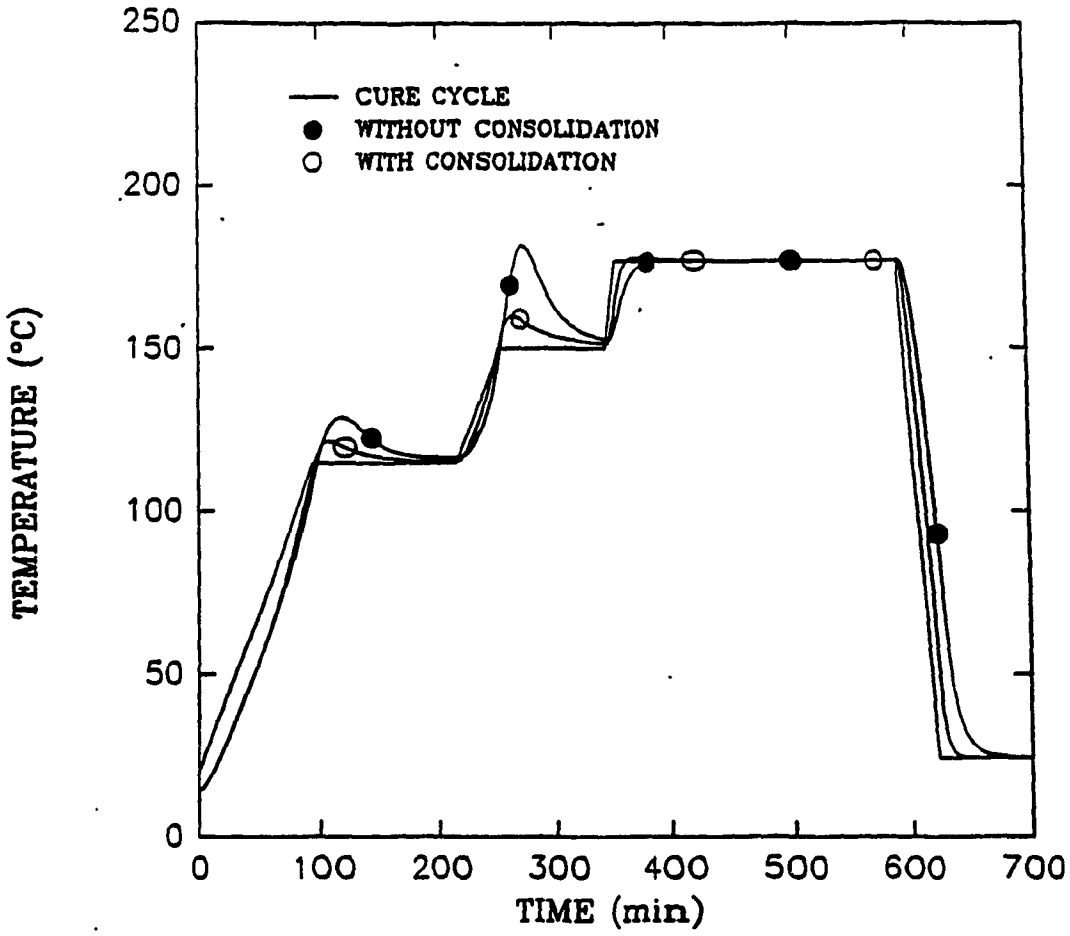

Figure 5.14: Temperature profile at the center of the thick composite (5cm) using cure cycle 2.

simulation shows that this cure cycle can not help the consolidation problem at all (Figure 5.15).

5.4.3 Consolidation mechanism

Little attention has been paid to the composite consolidation during the cure process. There are different parameters involved in the consolidation. Viscosity which is a function of time, temperature, and degree of cure plays a major role in the consolidation process. Figure 5.17 shows the variation of the fiber volume fraction through the thickness at different times for a laminate with $2.5cm$ thickness. Increasing autoclave temperature from room condition causes heat to penetrate into the laminate, from the top and bottom surfaces. Therefore, resin viscosity will drop at the top and bottom. Since the resin is allowed to move out only from the top, consolidation is started from there. At the beginning due to the high viscosity resin at the middle of laminate, low viscosity resin at the bottom can not move up. When the heat reaches to the center and therefore viscosity drops there, the entrapped resin at the bottom of laminate starts to move. Nonuniform consolidation occurs through the thickness at different time steps. Finally the whole excess resin is removed and a laminate with uniform fiber volume fraction through the thickness can be achieved. Uniform fiber volume fraction can not always be achieved.

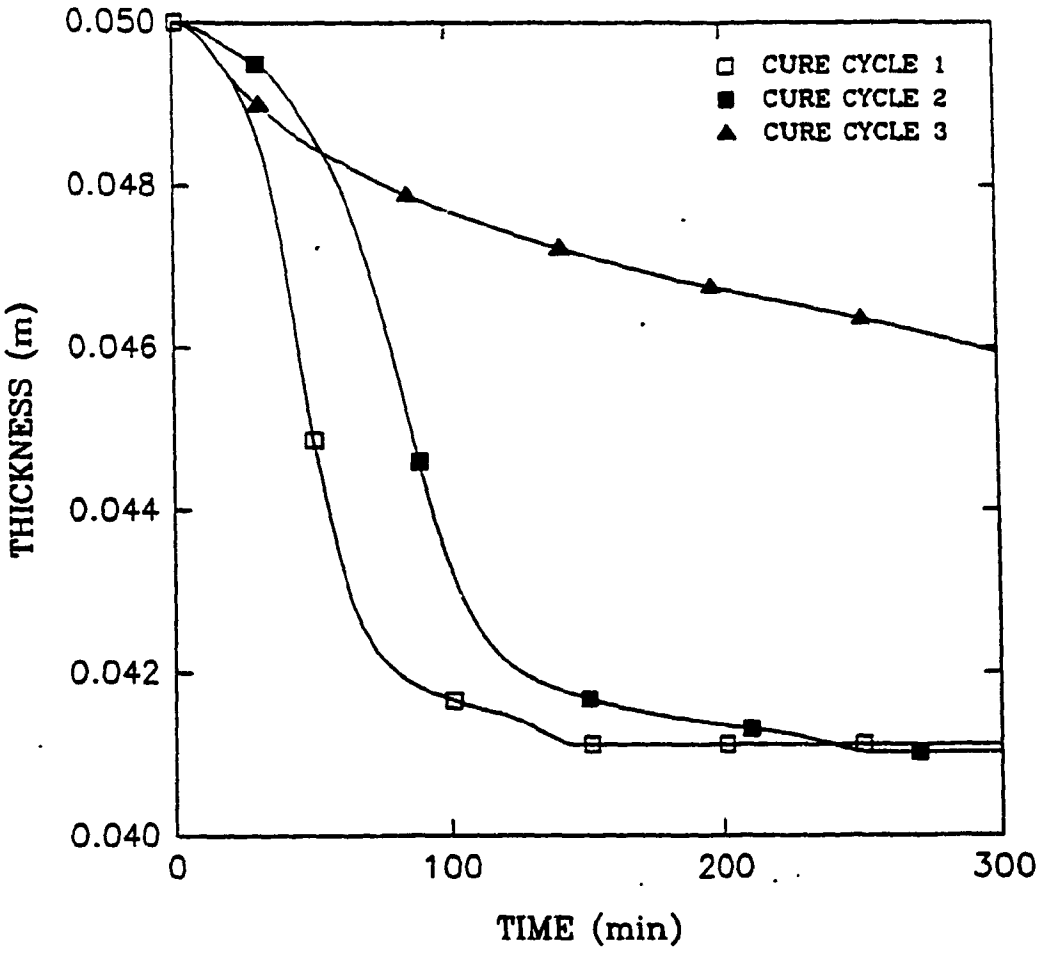

Figure 5.15: Variation of laminate thickness during curing for different cure cycles.

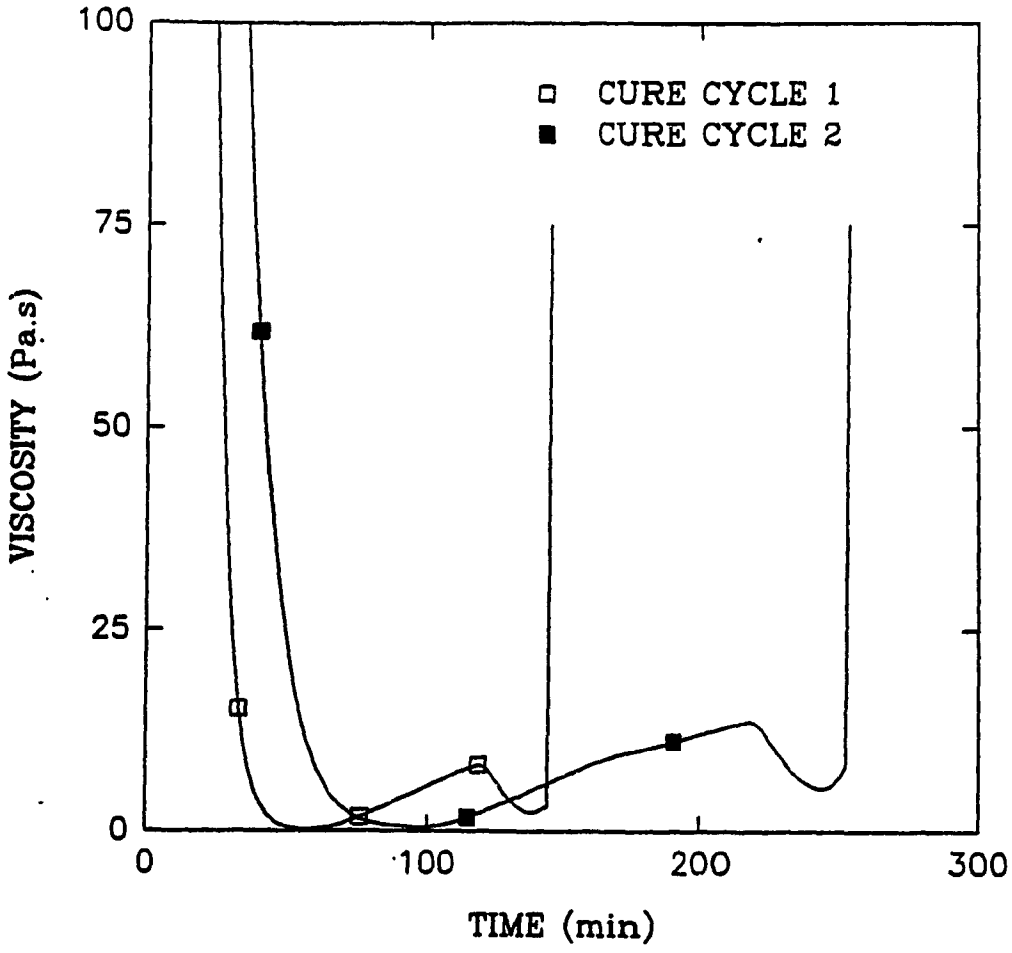

Figure 5.16: Variation of viscosity at the middle of laminate (5*cm*) for different cure cycles.

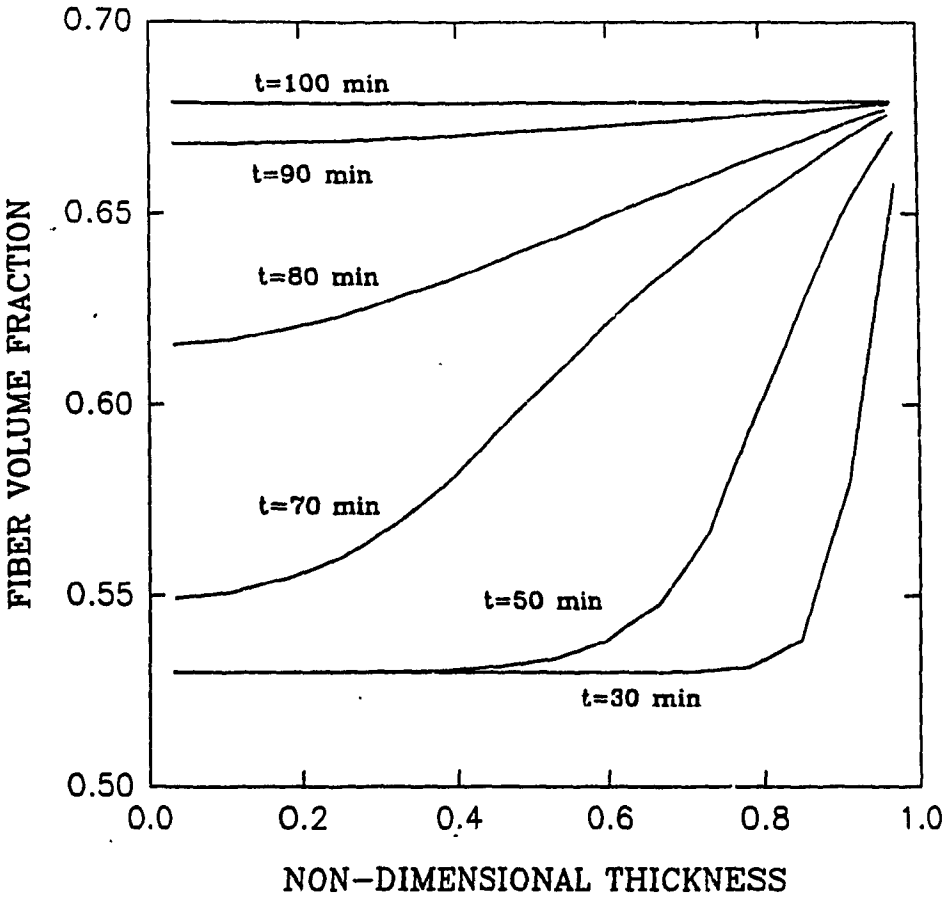

Figure 5.17: Fiber volume fraction distribution through the thickness for 2.5cm thick laminate subjected to the cure cycle 2.

5.4.4 Thickness effects

The thickness of laminate will strongly influence the curing process. During curing, two conditions should be satisfied in order to have a perfect composite. The temperature overshoot should be less than the allowable temperature and also the complete through-the-thickness consolidation should be achieved. Based on these two criteria, using the thick or thin composite terms in processing, in general, are not appropriate. For each cure cycle, the maximum thickness for which these two conditions are completely satisfied should be determined. Therefore, each cure cycle can be employed up to a certain thickness.

The effect of laminate thickness on the temperature and consolidation is examined for laminates between 2.5cm and 5cm thick for cure cycle 1. The results are shown in Figures 5.18 and 5.19. The maximum thickness for which cure cycle 1 can be applied is 2.5cm. Up to 2.5cm thickness the maximum temperature is less than 180°C and complete consolidation is obtained. The complete consolidation can be obtained up to 3cm thickness, however the temperature condition is violated (maximum 180°C). Therefore, the temperature condition puts restriction on the application of this cure cycle for laminates thicker than 2.5cm .

Cure cycle 2 as a candidate for laminates thicker than 2.5cm is examined. The results are shown in Figures 5.20 and 5.21. This cure cycle is recommended by the manufacturer for thick composites[52]. The consolidation condition limits the application of this cure cycle to laminates up to 3cm thick. Temperature condition

is satisfied up to $9cm$ thick laminates. Study of the simulation results indicates that three different situations may happen for the laminate during the cure. The first and the second situations are the complete (up to $3cm$) and partially through the thickness (between $3cm$ and $10cm$) consolidation, respectively. Heat is reached throughout the laminate thickness for these two types of consolidation. Gelation started at the laminate center and then propagated in two directions. The third situation which is the worst one takes place when gelation started from the laminate surfaces and propagated into the laminate (more than $10cm$). All volatile and vapor and air bubbles are entrapped inside the composite. The result will be poor laminate with a large amount of void.

In cure cycle 1, the temperature overshoot is responsible for restriction of application of this cure cycle. Cure cycle 2 is recommended to satisfy the temperature condition. In cure cycle 2, incomplete consolidation makes the laminate imperfect. For this cure cycle, there is no problem encountered in terms of temperature at the middle of laminate with thickness up to $9cm$. Therefore, it was decided to focus on the different ways to solve the partial consolidation inside the laminates. Pressure effect, consolidation from top and bottom, and prebleeding technique are investigated.

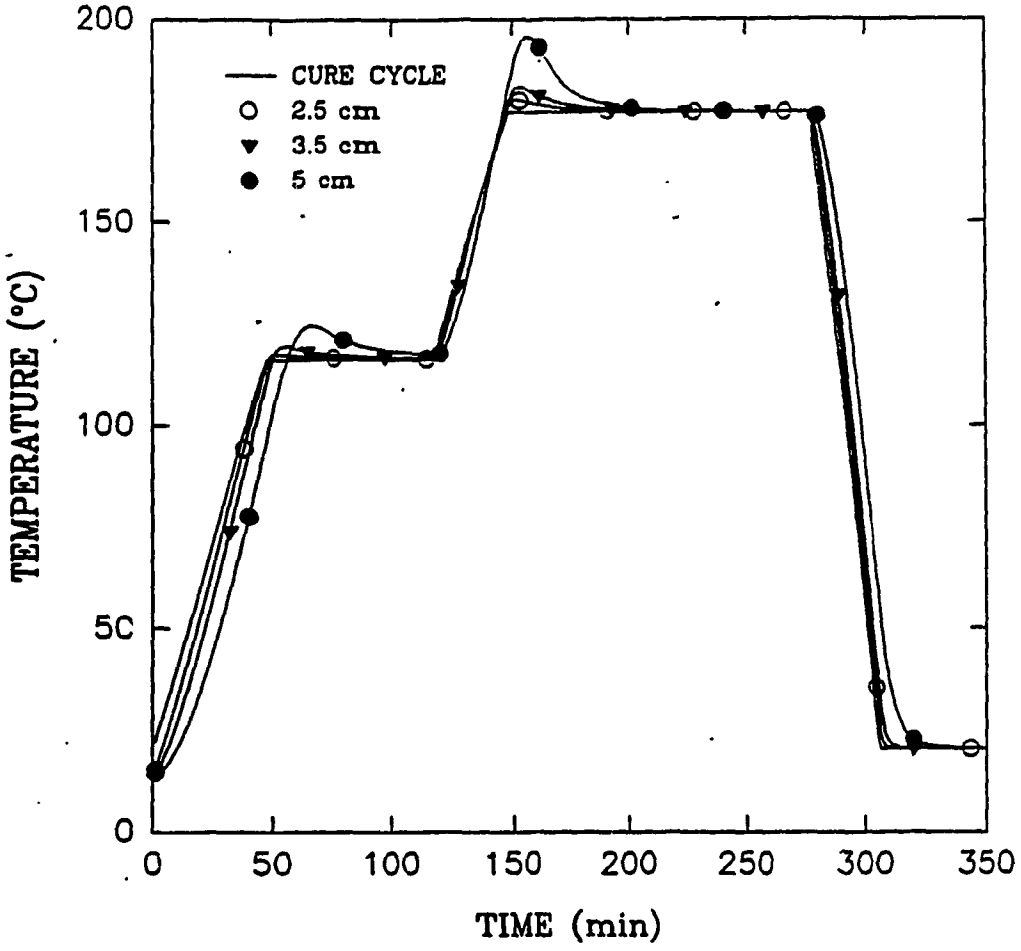

Figure 5.18: Temperature at the composite center for different thicknesses using cure cycle 1.

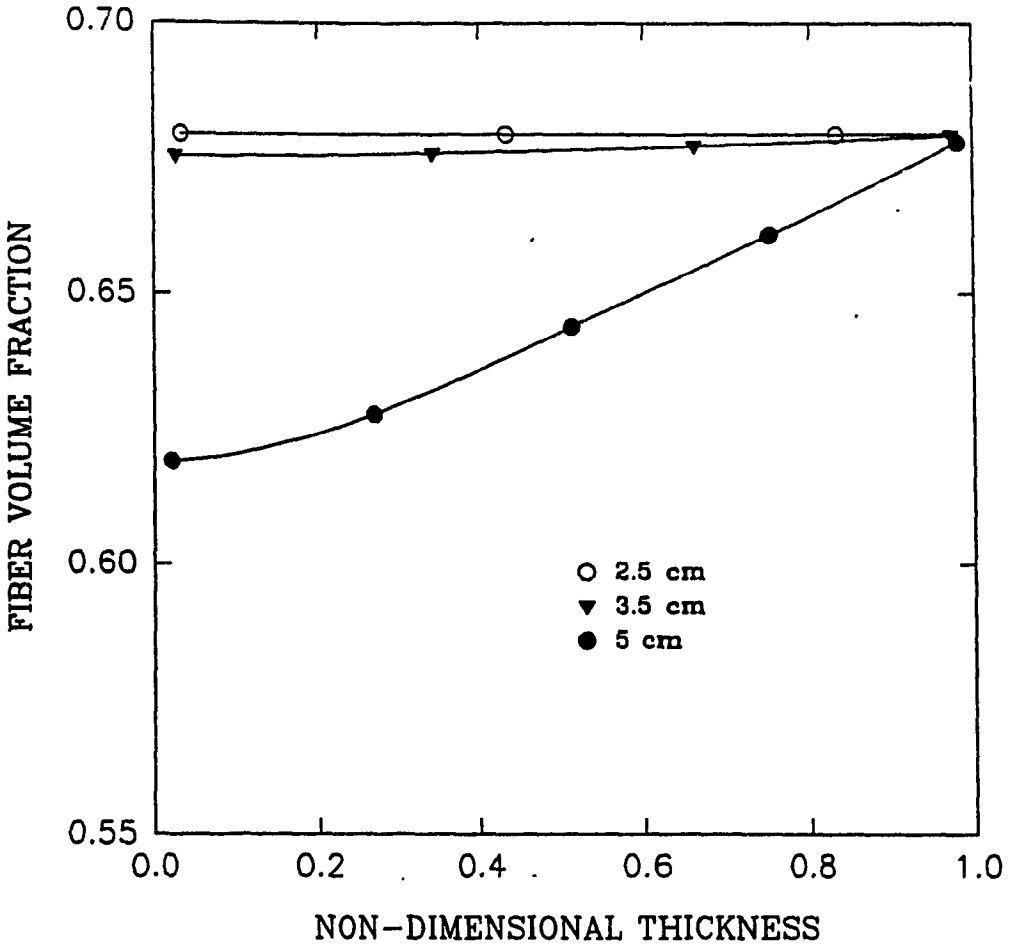

Figure 5.19: Final fiber volume fraction distribution for different thicknesses using cure cycle 1.

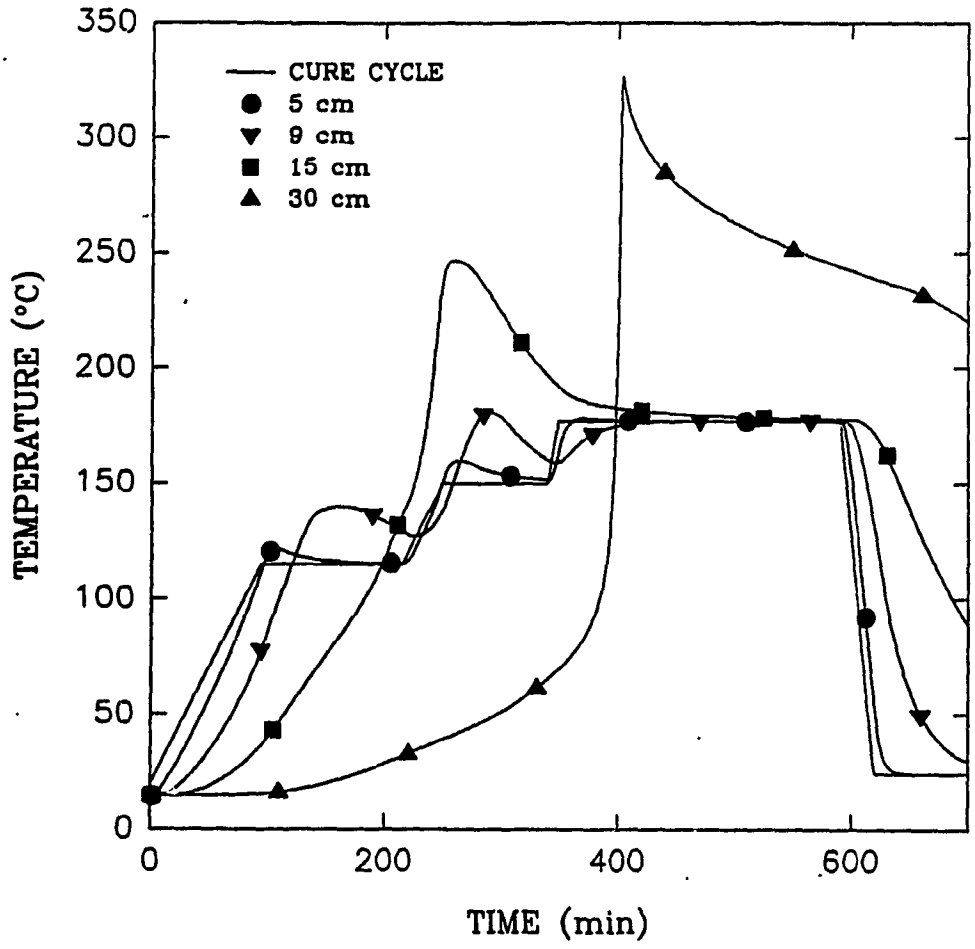

Figure 5.20: Temperature at the composite center for different thicknesses using cure cycle 2.

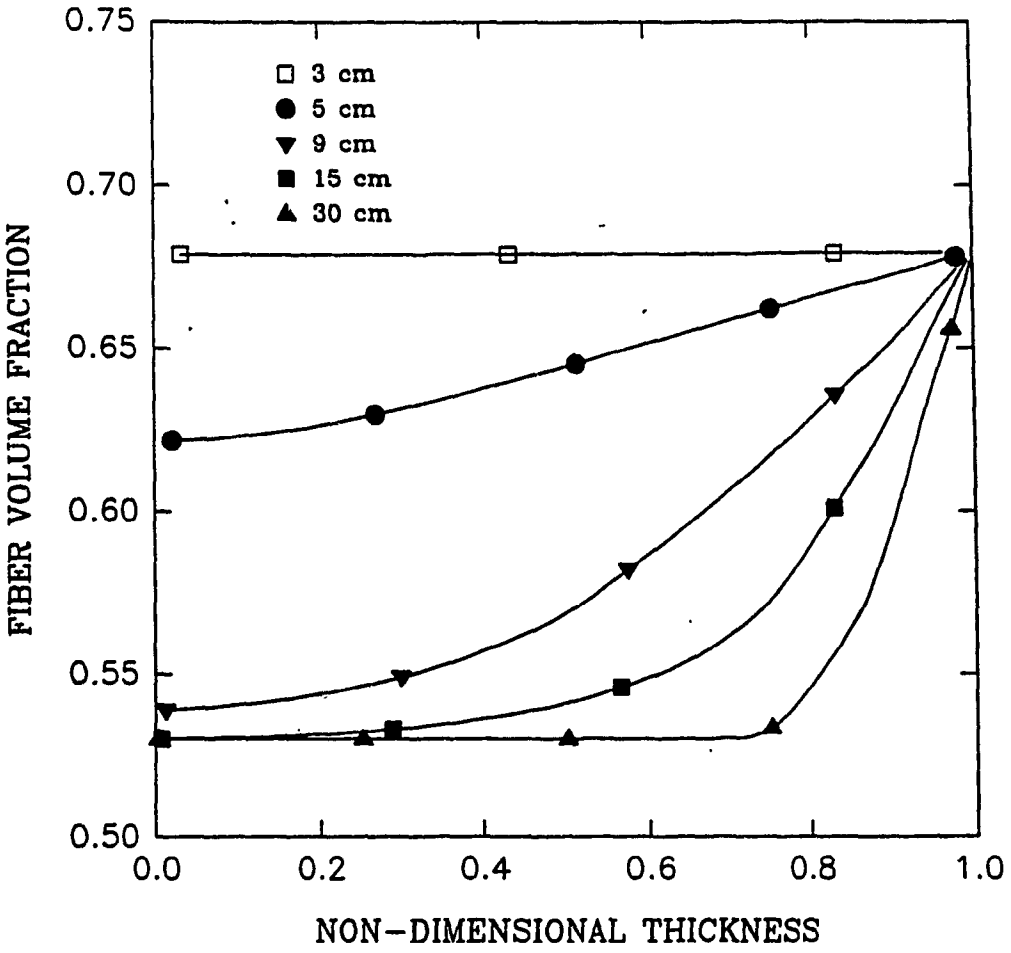

Figure 5.21: Final fiber volume fraction distribution for different thicknesses using cure cycle 2.

5.4.5 Pressure effect

The final fiber volume fraction of the composite is determined by the deformation characteristic of the fiber structure. In the case of complete consolidation ,increasing the autoclave pressure results in higher final fiber volume fraction throughout the laminate. For partially consolidated laminate, by increasing the autoclave pressure, higher fiber volume fraction distribution can be obtained. Figure 5.22 shows the final fiber volume fraction distribution during the cure of a $5cm$ thick composite at different autoclave pressures. Higher autoclave pressure can not solve the nonuniform distribution of the fiber volume fraction. Application of higher pressure pushes more resin out of laminate. Due to the deformation characteristic of the fiber bed, these extra resins are supplied from the different layers of laminate, from top to bottom layers. Therefore laminates still do not have enough time to be fully compacted before gelation.

5.4.6 Consolidation from top and bottom

It is assumed that there are some bleeder plies at the bottom of laminate over the tool plate. Therefore, resin is able to move out from top and bottom of laminate. Consolidation can be improved in this type of arrangement. Complete compaction is achieved up to $6cm$ thick laminates (Figure 5.24) in comparison with $3cm$ thick laminates in the case of consolidation from top (Figure 5.21). Since the temperature condition is satisfied, cure cycle 2 can be used to fabricate high quality

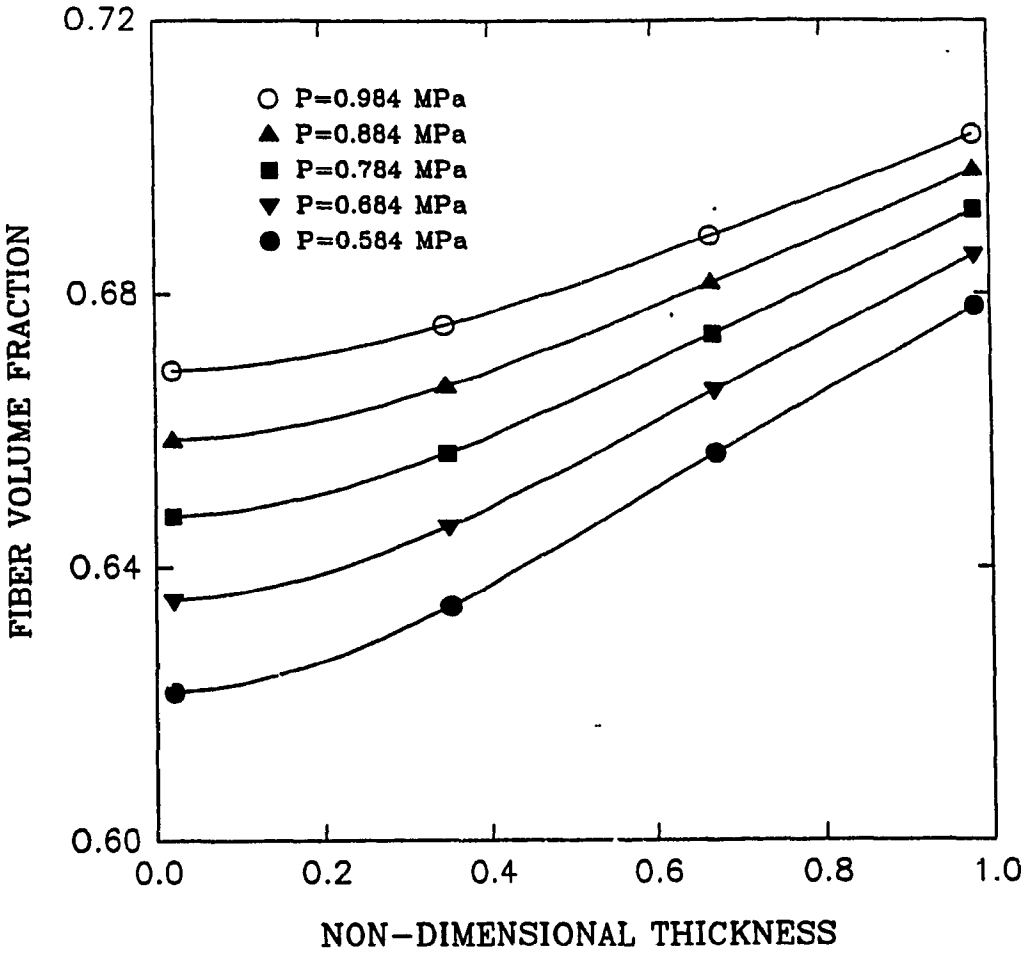

Figure 5.22: Pressure effect on final fiber volume fraction distribution through the thickness for 5cm thick composite.

composites up to $6cm$ thick. For laminates thicker than $6cm$, compaction condition is violated, however, the temperature condition is satisfied up to $10cm$ thick laminates. Comparison between Figure 5.20 and Figure 5.23 indicates the strong dependence of the temperature overshoot on the consolidation process (i.e. maximum temperature for 15 cm thick laminate is 250°C in Figure 5.20 and 225°C in Figure 5.23).

5.4.7 Prebleeding

Incomplete consolidation restricts the application of cure cycle 2. It seems that both conditions, temperature overshoot and complete consolidation, in general can not be satisfied for thick composite parts. Using the prebleeding technique, both conditions are achieved separately. Thick composite is divided into the thin parts (sublaminates). Using manufacturer recommended cure cycle for the consolidation (Figure 5.25), complete compaction is achieved for the sublaminates. This cure cycle allows the resin inside the sublaminates to cure partially. Sublaminates are put together to make a thick part. The thick composite is exposed to the second cure cycle (Figure 5.26) inside the autoclave. At this stage, the temperature overshoot is the only parameter that should be taken care of.

Using recommended cure cycle for the consolidation (Figure 5.25), simulation shows that the complete compaction can be achieved up to $2.5cm$ thick laminate. For these $2.5cm$ thick prebled sublaminates, degree of cure is 0.3 and final

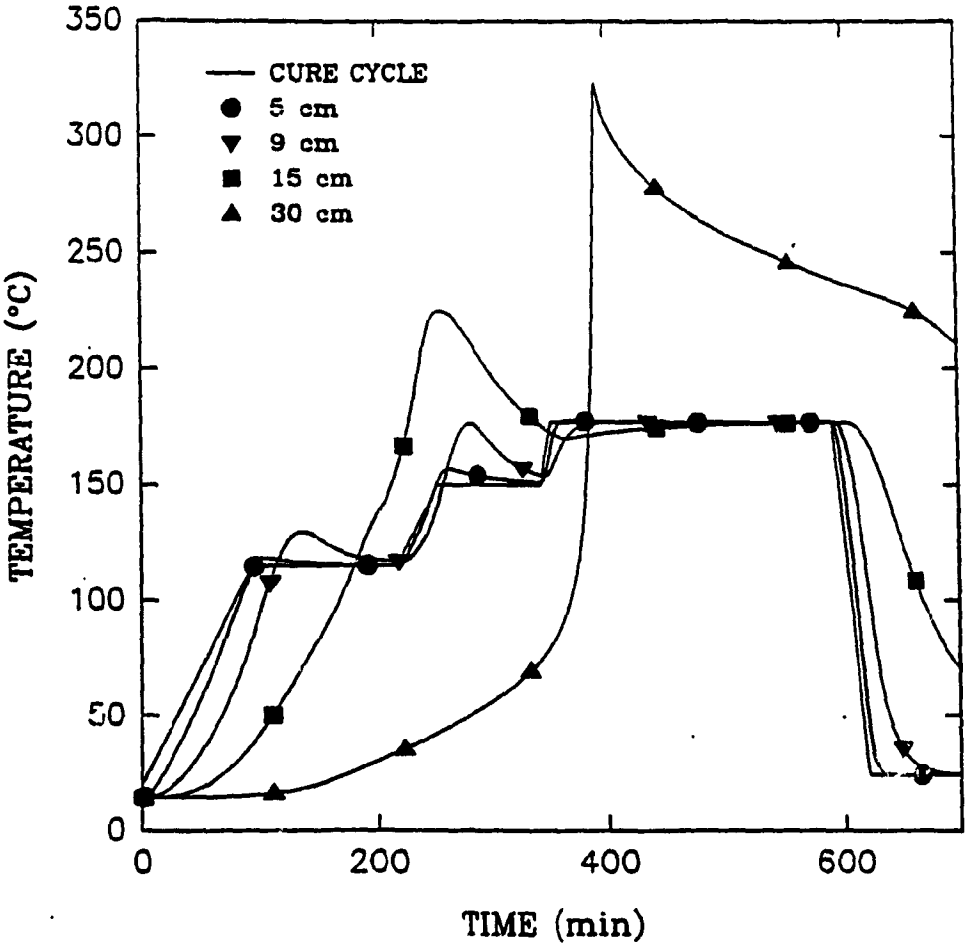

Figure 5.23: Temperature at the composite center for consolidation from top and bottom for different thicknesses.

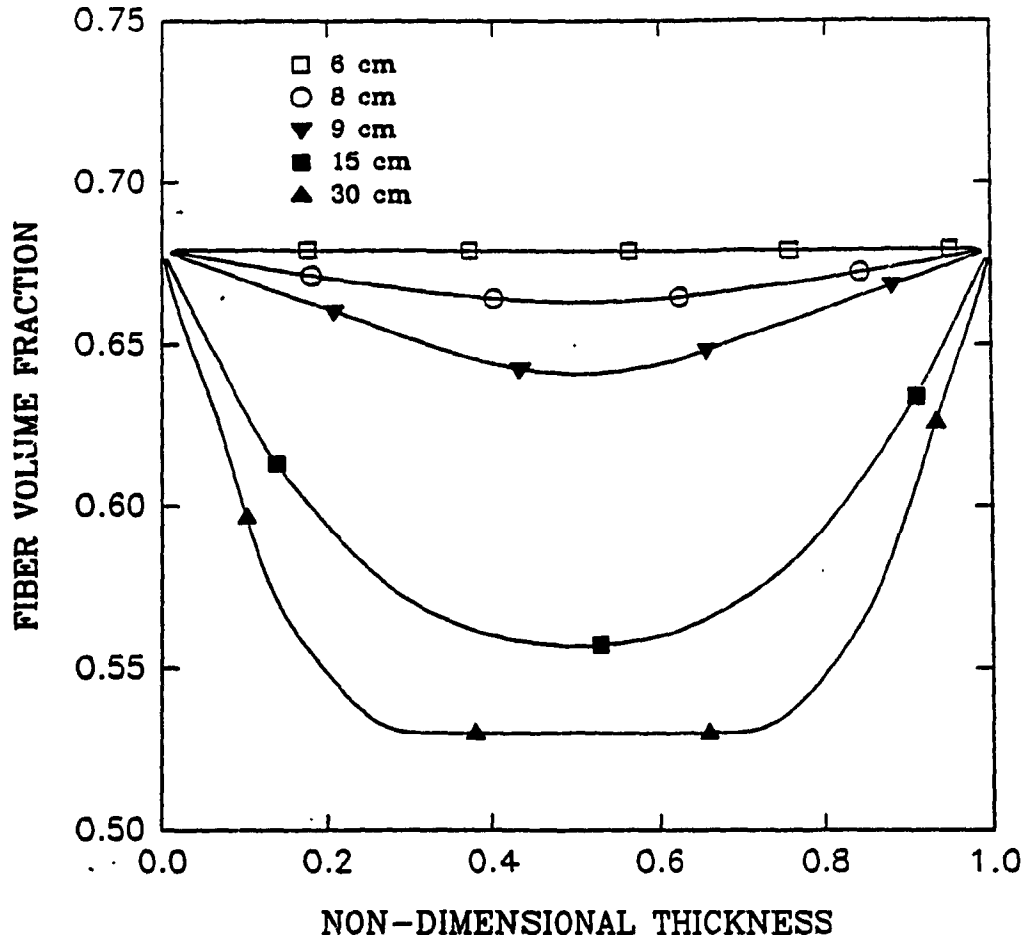

Figure 5.24: Final fiber volume fraction distribution for consolidation from top and bottom for different thicknesses.

fiber volume fraction is 0.68 throughout the laminate. The temperature profile for the thick composite composed of 2.5cm prebled sublaminates is shown in Figure 5.27. Laminates up to 10cm thick using simplified cure cycle (Figure 5.27) can be fabricated with high quality.

Although prebleeding technique takes a large amount of time for the fabrication, simulation indicates that prebleeding is the best way to fabricate high quality and high performance thick composite parts.

5.4.8 Bleeder effect

When consolidation is allowed during curing, bleeder plies are required in the tooling setup to absorb the extra resin. Glass and polyester cloths are two materials commonly used as bleeder [5]. Both glass and polyester have low thermal conductivity which can have significant effect on curing process, particularly for thick composites.

Tooling setup shown in Figure 5.1 is used for simulation. Polyester bleeder has fiber volume fraction equal to 0.3 and its thickness is assumed to be 11.5 mm, just enough bleeder material to absorb 8 mm resin produced by laminate compaction. If ν_f is bleeder fiber volume fraction and L_t is the total laminate thickness reduction after curing , the bleeder thickness for that compaction can be obtained using following expression

$$t_b = \frac{L_t}{1 - \nu_f} \tag{5.2}$$

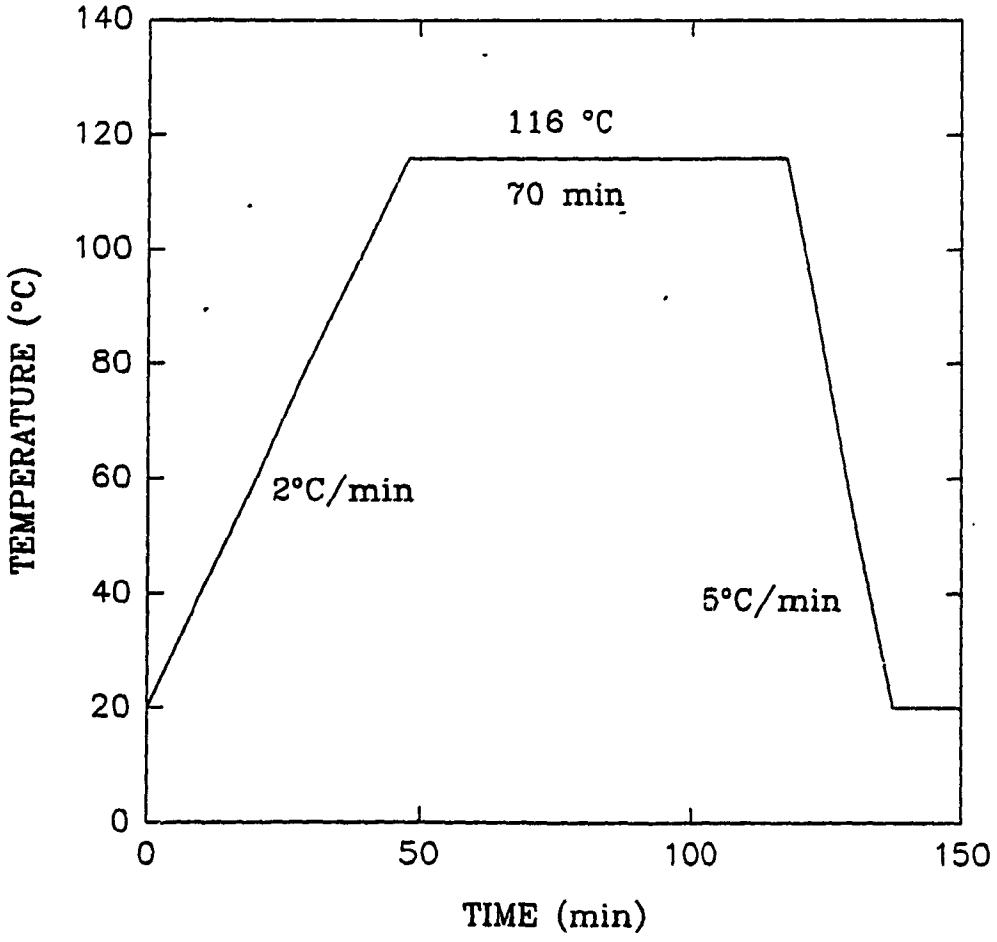

Figure 5.25: Compaction cure cycle for prebleeding technique.

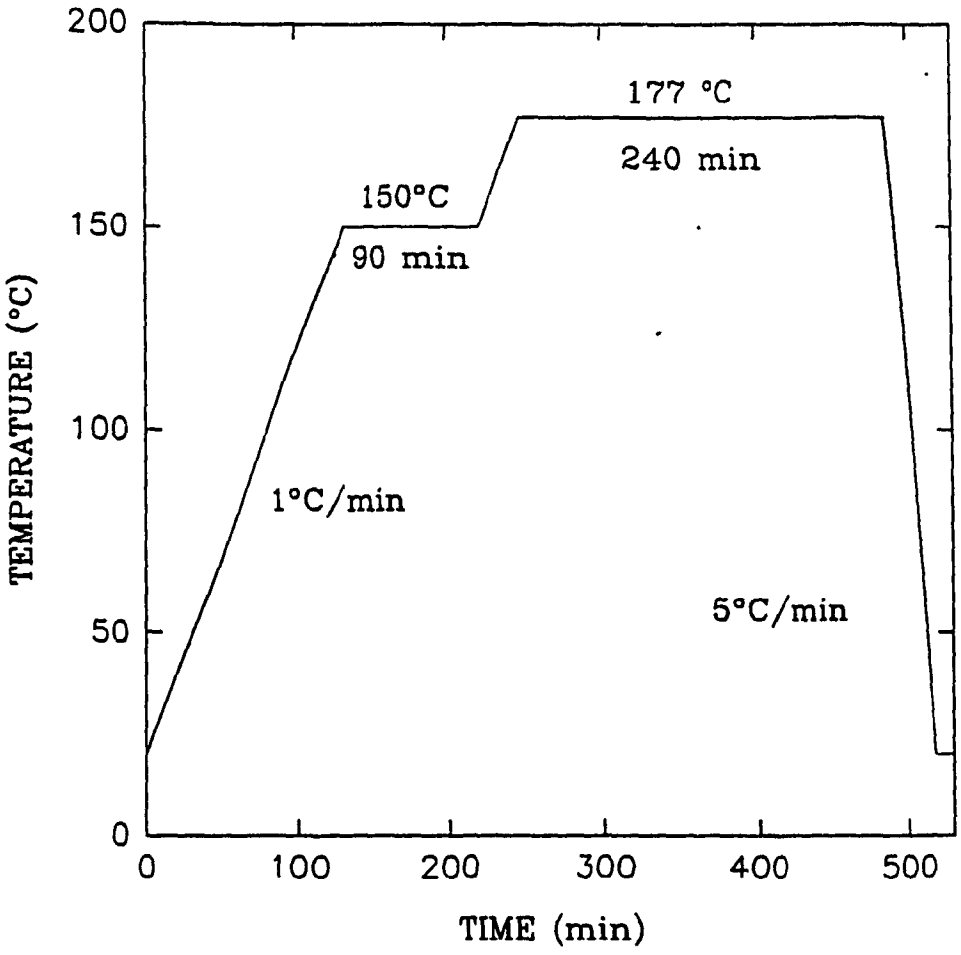

Figure 5.26: Simplified curing cycle for prebleeding technique.

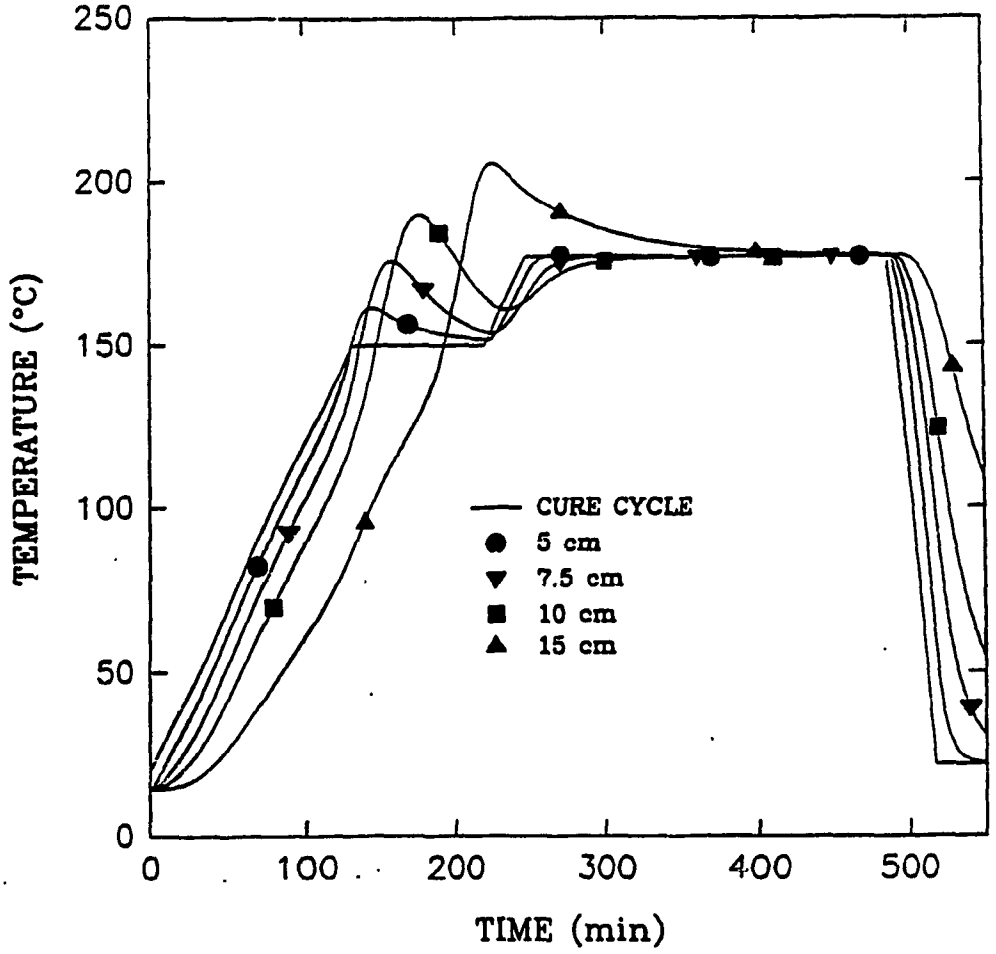

Figure 5.27: Temperature profile at the center of composite made of prebled sub-laminates and subjected to the simplified curing cycle.

Bleeder thermal conductivity is calculated using Equation (5.1).

Temperature history at the top and middle of 5 cm thick laminate considering insulating effect of bleeders are shown in Figures 5.28 and 5.29. Low thermal conductivity of bleeder as well as the bleeder thickness create some problems. At the beginning of the curing, bleeders are empty and their thermal conductivities are very low, delaying heat to reach to the laminate. When maximum reaction happens and heat generates rapidly, again bleeder prevents the heat to dissipate fast, increasing the laminate temperature. Figure 5.30 shows the temperature distribution through-the-thickness which is not symmetric. Maximum temperature happens at the top of laminate, close to the bleeder side. Figure 5.31 represents the laminate compaction. Bleeder prevents heat to penetrate inside laminate rapidly and delays the laminate compaction. However it does not affect very much the final laminate compaction.

5.5 Summary

Experimental results for temperature history and laminate compaction with simulation results were compared. Good agreement was observed. Simulation was employed to study the curing process. Consolidation is shown to be an important processing variable in curing. It is shown that consolidation can be non-uniform through the thickness during the cure process. Having satisfied the temperature overshoot condition and complete compaction, different cure cycles were studied.

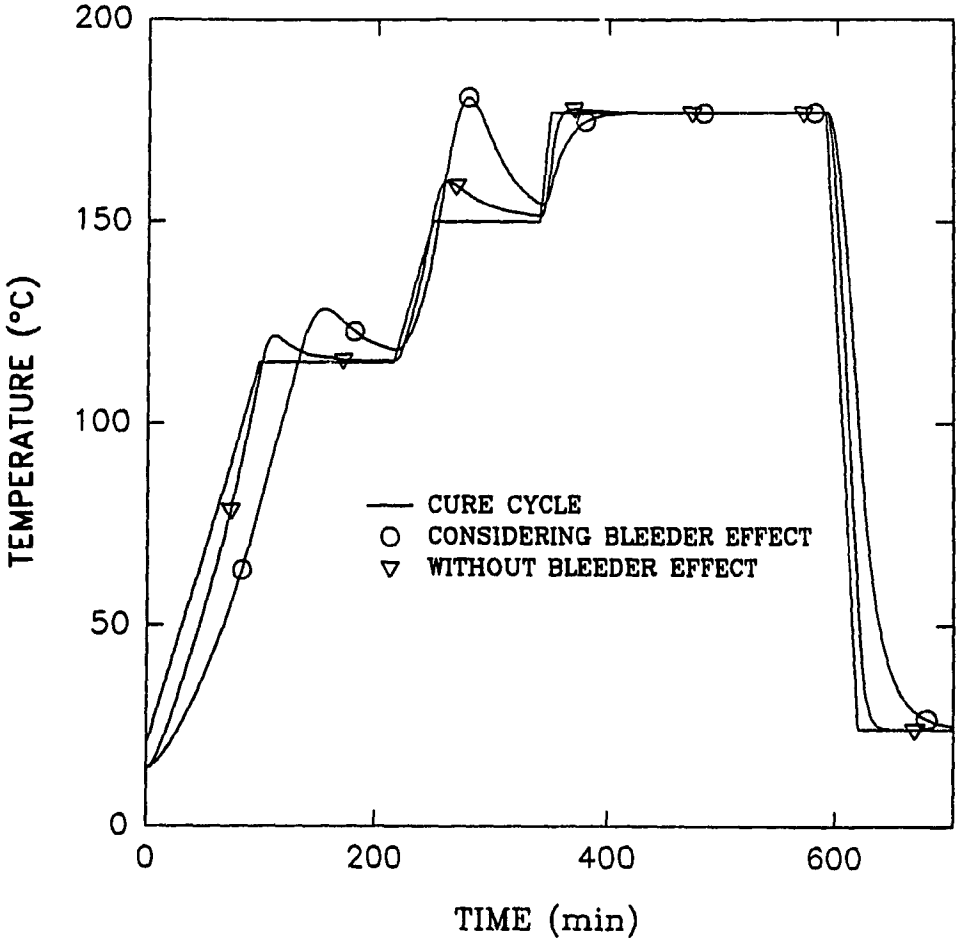

Figure 5.28: Predicted temperature at the middle of 5 *cm* thick laminate (Bleeder effect).

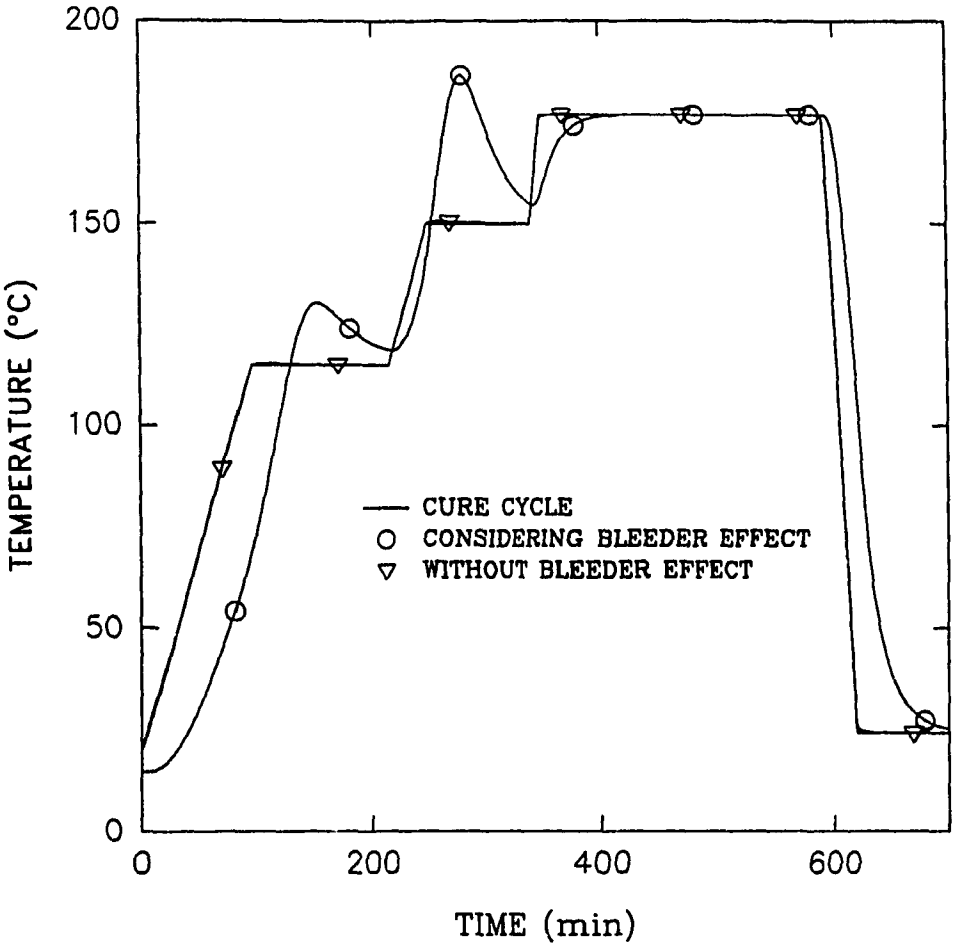

Figure 5.29: Predicted temperature at the top of 5 *cm* thick laminate (Bleeder effect).

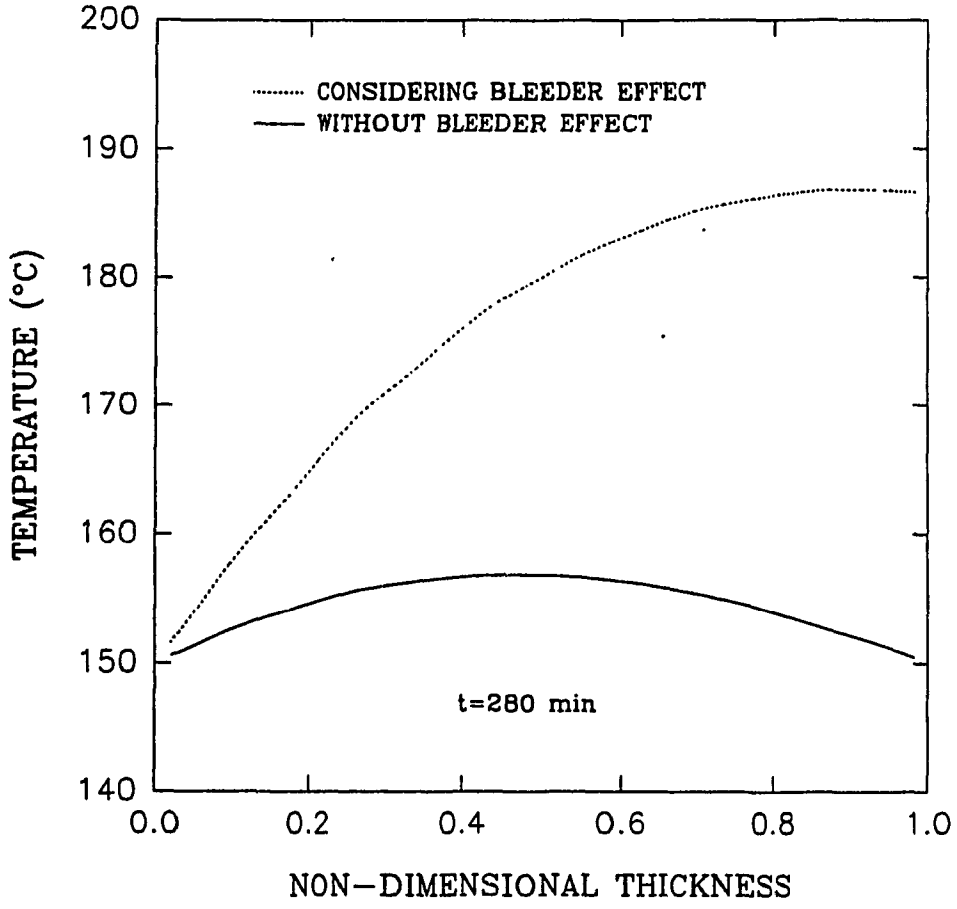

Figure 5.30: Temperature distribution through-the-thickness of 5 cm thick laminate (Bleeder effect).

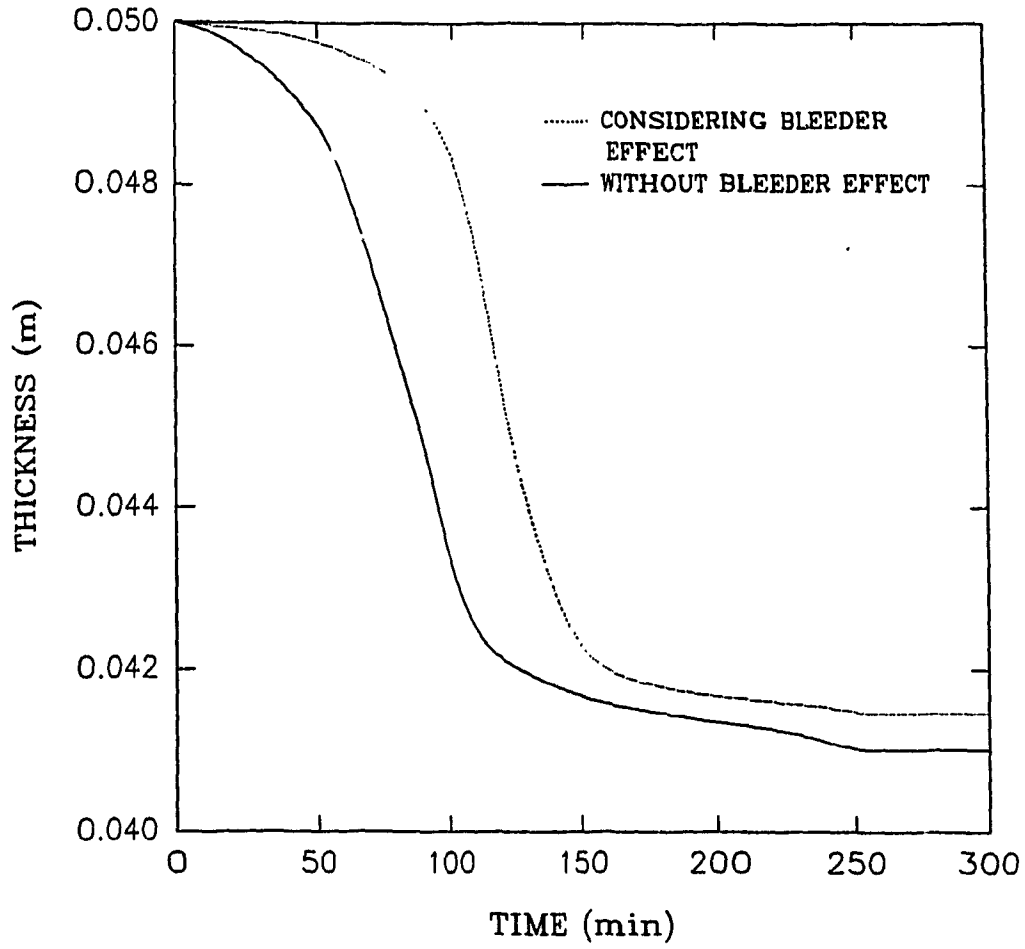

Figure 5.31: Compaction of 5 cm thick laminate (Bleeder effect).

It is shown that either temperature overshoot or incomplete compaction can put restriction on the application of each cure cycle up to a certain thickness.

It is observed that incomplete consolidation is mostly troublesome. Different ways to deal with this problem were investigated. It is shown that increasing the autoclave pressure does not solve the incomplete consolidation. Bleeding from top and bottom of laminate improves consolidation. Prebleeding technique was examined. First the compaction is achieved for the sublaminates and then these sublaminates are put together to fabricate thick parts. The final assembly is placed inside the autoclave to complete the cure process. Using this technique the complete compaction and temperature overshoot limit are achieved separately for thick parts.

Bleeder effect on curing was discussed. It is shown that due to the low thermal conductivity of bleeder, temperature distribution through-the-thickness is not symmetric. It is also shown that maximum temperature overshoot may happen at the top of laminate (not at the middle of laminate). Bleeder delays heat to penetrate inside laminate during the heating time and increases the temperature overshoot at the time of maximum chemical reaction.

Finally, based on all of those mentioned observations, it seems that the prebleeding is the most promising method for fabrication of thick composites.

Chapter 6

Model Laws

Performing experiments to obtain optimum processing parameters for thick composite parts is usually expensive. The cost of materials for large scale evaluation can be very high for most composite materials. The common practice to study the different processing parameters for curing of thick thermosetting composites is to develop a mathematical model and then to do computer simulations[13, 14, 22, 49, 52, 78]. For a few cases (usually the thickness is around $5cm$)[13, 14, 52], the experiment is performed and compared with the simulation results. After verification of the mathematical model and computer simulation, this computer code is used to predict and to study the behavior of thick thermosetting composites under various processing parameters. Kinetic equation is required for computer simulation. For most resins, this equation is not defined. Even the available kinetic equations can not predict the reaction rate accurately (see chapter 5).

A generalized approach to modelling curing of thermosetting composites has

been done in terms of non-dimensional groups based on the process and product parameters[53, 70]. The power of non-dimensional approach is its ability to represent a wide range of different cases in a unified manner, therefore one can use this approach to generalize the process modeling instead of system dependent process modeling. The other application of non-dimensional analysis is to reduce the large number of variables involved in the process to a few physical groups. Then the system solution can be expressed in terms of these dimensionless groups. This type of analysis also requires an accurate description of the kinetic equation.

Another way to study the behavior of thermosetting composites (particularly complex shapes and thick composites) during the curing process is to make a model. In model work, one tries to predict the performance of a final system called the *prototype* from tests on the performance of another actual system called the *model.* For such work to be useful, two conditions must be satisfied : (a) it must be easier and/or less expensive to determine the desired results on the model than on the prototype, and (b) it must be possible to accurately predict the performance of the prototype from that of the model [72]. The first condition is usually satisfied, otherwise there would be no point in using a model. To satisfy the second condition, the similarity rules and model laws should be established.

In general, there is a point-to-point correspondence between a model and its prototype. In geometrical terminology, two points that correspond to each other are *homologous*[71]. The concept of homologous points leads to the concept of

homologous times. Therefore, if a model is built up based on model laws from a prototype, one can say that the response of model and prototype are similar at homologous points and homologous times.

The objective of this chapter is to establish the *model laws* for curing of thermosetting composite parts. One can use the model laws to design a model based on the prototype (i.e. thick composite) in such a way that the performance of the prototype (i.e. temperature and degree of cure distribution inside composite) can be predicted from the performance of the model. The transient heat conduction coupled with kinetic equation and initial and boundary conditions are non-dimensionalized. Dimensionless parameters are extracted from non-dimensional equations and boundary conditions. Any relationship among dimensionless groups of model and prototype can be expressed in the form of a model law. It is shown how one can use these model laws to design a model based on the prototype. Therefore, model and prototype will have the same behavior at homologous points and times. These concepts are used to design a Glass/Epoxy model for a Graphite/Epoxy prototype. Not only the glass fiber is less expensive than graphite fiber (high modulus or high strength), but also the model can have smaller dimensions, and therefore, material can be saved.

For the sake of simplicity, the design of a model for a unidirectional flat plate prototype is considered. . However, it should be emphasized that this type of approach is particularly suitable for complex geometry and configuration for which

any new dimensionless groups might be necessary identified. For those geometries that the one-dimensional through-the-thickness is adequate to predict the material behavior during the cure process (thin composites), this analysis can be used directly by eliminating those terms which represent the other two directions, from governing partial differential equations and boundary conditions.

Consider the manufacture of a flat-plate composite (as prototype) composed of unidirectional fiber reinforced thermosetting resin matrix prepreg materials. As shown in Figure 6.1, the composite has a rectangular cross-section of width M, thickness N and length L. It is assumed that the fiber volume fraction ν_f throughout the composite is the same which means the thermal conductivity in each direction remains the same throughout the composite. This composite is subjected to a specified cure cycle inside autoclave and temperature and degree of cure are monitored inside the composite at different points and times.

The objective here is to develop the model laws and use those laws to design a composite model based on prototype. This model may be constructed from another type of composite with dimensions of length L_m, width M_m, and thickness N_m and fiber volume fraction ν_{fm}. Then this model is subjected to the different cure cycles while temperature and degree of cure are monitored. One can use the model laws and model test results to obtain the cure cycle to which the prototype should be subjected. One can also calculate the temperature and degree of cure inside the real composite (prototype) at different points and different times.

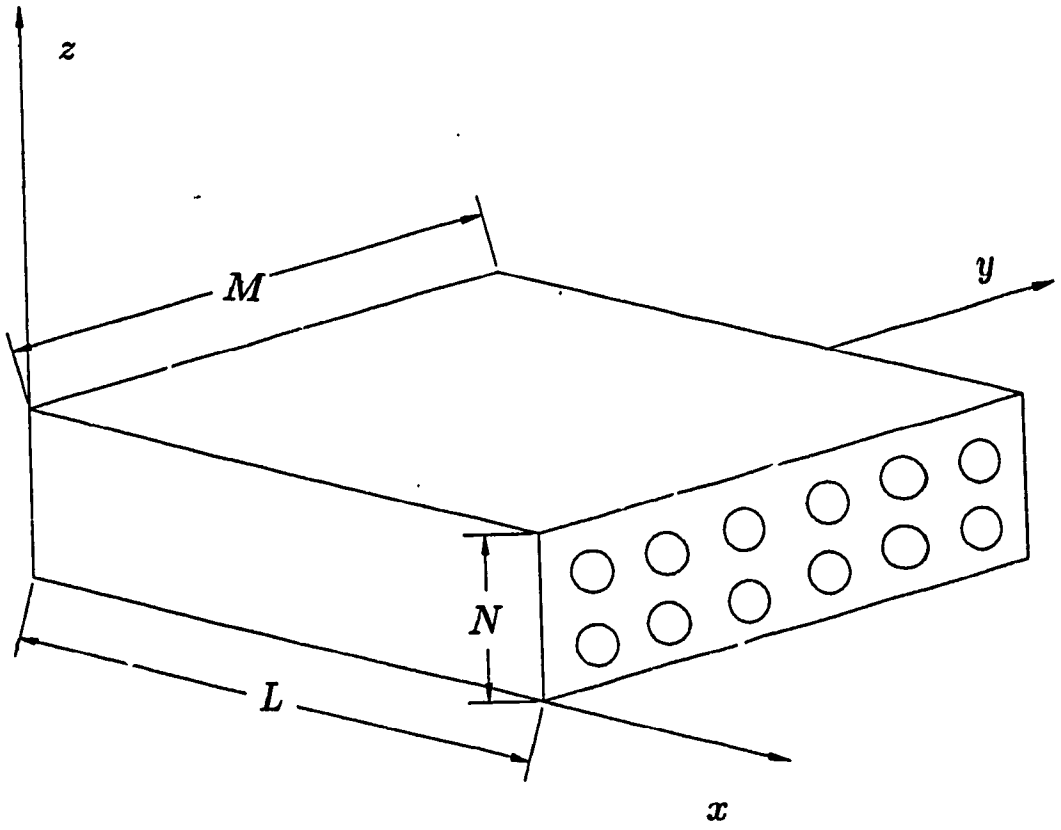

Figure 6.1: Composite Geometry

6.1 Dimensional Governing Equation

The transient heat conduction equation with an internal heat generation source term (Equation (2.8)) considering constant thermal conductivities in different directions can be written as

$$k_x\frac{\partial^2 T}{\partial x^2} + k_y\frac{\partial^2 T}{\partial y^2} + k_z\frac{\partial^2 T}{\partial z^2} + \dot{g} = \rho c_p\frac{\partial T}{\partial t} \tag{6.1}$$

Heat generation term $\dot{g}$ is defined by Equation (2.13). $\frac{d\alpha}{dt}$ is the rate of cure and should be calculated from kinetic equation. The kinetic model chosen for this study is a simplified Arhenius type first order rate equation expressed as [56]

$$\frac{d\alpha}{dt} = A\exp(\frac{-E_o}{RT})(1-\alpha) \tag{6.2}$$

where A is pre-exponential factor and E_o is activation energy. It should be mentioned that the first order kinetic equation is not representative of many of the new resins where the conversion reactions are not well understood. This equation has been chosen only for simplicity. It will be shown later that using the more advanced and complicated kinetic equations does not change the analysis.

Initial conditions are

$$T(x,y,z,0) = T_o \tag{6.3}$$

$$\alpha(x,y,z,0) = 0$$

where T_o is the initial temperature inside the composite. Boundary conditions are

$$T(0,y,z,t) = T_a$$

$$T(L,y,z,t) = T_a$$

$$T(x,0,z,t) = T_a \tag{6.4}$$

$$T(x,M,z,t) = T_a$$

$$T(x,y,0,t) = T_a$$

$$T(x,y,N,t) = T_a$$

T_a is autoclave temperature and can be either a constant or a function of time.

6.2 Non-dimensional Governing Equations

The model laws can be extracted from non-dimensional set of governing equations and initial and boundary conditions[72]. The non-dimensional approach reduces the large number of variables involved in the process to a few groups which each group has a physical meaning. In terms of non-dimensional parameters, the heat conduction equation (Equation (6.1)) and kinetic equation (Equation (6.2)) can be expressed as

$$\frac{k_x}{k_z}(\frac{N}{L})^2\frac{\partial^2 T}{\partial \bar{x}^2} + \frac{k_y}{k_z}(\frac{N}{M})^2\frac{\partial^2 T}{\partial \bar{y}^2} + \frac{\partial^2 T}{\partial \bar{z}^2} + \frac{\rho_r(1-\nu_f)H_R}{\rho c_p T_o}\frac{d\alpha}{d\tau} = \frac{\partial T}{\partial \tau} \tag{6.5}$$

$$\frac{d\alpha}{d\tau} = \frac{\rho c_p N^2 A}{k_z}\exp(-\frac{\frac{E_a}{RT_o}}{T})(1-\alpha) \tag{6.6}$$

The initial and boundary conditions in the new system of coordinates can be written as

$$T(\bar{x},\bar{y},\bar{z},0) = 1 \tag{6.7}$$

$$\alpha(\bar{x},\bar{y},\bar{z},0) = 0$$

and

$$\begin{aligned}
&\bar{T}(0,\bar{y},\bar{z},\tau) = \bar{T}_a \\
&\bar{T}(1,\bar{y},\bar{z},\tau) = \bar{T}_a \\
&\bar{T}(\bar{x},0,\bar{z},\tau) = \bar{T}_a \\
&\bar{T}(\bar{x},1,\bar{z},\tau) = \bar{T}_a \\
&\bar{T}(\bar{x},\bar{y},0,\tau) = \bar{T}_a \\
&\bar{T}(\bar{x},\bar{y},1,\tau) = \bar{T}_a
\end{aligned} \tag{6.8}$$

Equations (6.5)-(6.8) employ the following dimensionless parameters

$$\begin{aligned}
&\bar{T} = \frac{T}{T_o}, \quad \bar{T}_a = \frac{T_a}{T_o}, \quad \tau = \frac{k_z t}{\rho c_p N^2} \\
&\bar{x} = \frac{x}{L}, \quad \bar{y} = \frac{y}{M}, \quad \bar{z} = \frac{z}{N}
\end{aligned} \tag{6.9}$$

$\bar{x}$,$\bar{y}$ and $\bar{z}$ are dimensionless independent variables in the new system of coordinates. $\bar{T}$ and τ are dimensionless temperature and time, respectively.

For establishment of model laws, the initial and boundary conditions are very important. From mathematical point of view , since partial differential equations are involved, a change in boundary conditions means a change in the form of the solution and may involve a change in the solution magnitudes [72]. Therefore, these conditions should be carefully considered during the analysis.

6.3 Model Laws

It is sufficient to extract the dimensionless parameters from non-dimensional governing equations and boundary conditions. These parameters are necessary and sufficient for modeling procedure[72]. Each dimensionless parameters is called as a π. Therefore, it can be written

$$\begin{aligned}
\pi_1 &= \overline{E}_o = \frac{E_o}{RT_o} \\
\pi_2 &= \overline{T}_a = \frac{T_a}{T_o} \\
\pi_3 &= B_o = \frac{\rho_r(1-\nu_f)H_R}{\rho c_p T_o} \\
\pi_4 &= \overline{k}_o = \frac{\rho c_p N^2 A}{k_z} \\
\pi_5 &= \frac{k_x}{k_z}(\frac{N}{L})^2 \\
\pi_6 &= \frac{k_y}{k_z}(\frac{N}{M})^2
\end{aligned} \tag{6.10}$$

Each dimensionless group which is obtained from non-dimensional governing equations has a physical meaning. π_1 is called *Dimensionless Activation Energy* [70]. The higher the value of π_1, the smaller is the reaction rate. π_2 which is obtained from boundary conditions represents the effect of two important processing parameters, the composite initial temperature and autoclave temperature. π_3 is called *Dimensionless Adiabatic Temperature* [70] which represents the temperature rise potential due to the heat of reaction H_R. π_4 is called *Damköhler number* [53] which represents the ratio of the conduction time scale (here in the z-direction) $\frac{\rho c_p N^2}{k_z}$ to the reaction time scale $\frac{1}{A}$. The higher the value of the Damköhler num-

ber, the faster is the cure reaction relative to heat conduction. π_5 and π_6 are the ratios of heat conduction in the x and y directions with respect to the heat conduction in the z direction, respectively. These two numbers can be used to compare the effect of heat conduction in different directions in the whole process of heat transfer.

Equations (6.5) and (6.6) can be written as

$$\pi_5 \frac{\partial^2 T}{\partial \bar{x}^2} + \pi_6 \frac{\partial^2 T}{\partial \bar{y}^2} + \frac{\partial^2 T}{\partial \bar{z}^2} + \pi_3 \frac{d\alpha}{d\tau} = \frac{\partial T}{\partial \tau} \tag{6.11}$$

$$\frac{d\alpha}{d\tau} = \pi_4 \exp(-\frac{\pi_1}{T})(1-\alpha) \tag{6.12}$$

Boundary conditions (Equation (6.8)) can be written as

$$\begin{aligned} T(0,\bar{y},\bar{z},\tau) &= \pi_2 \\ T(1,\bar{y},\bar{z},\tau) &= \pi_2 \\ T(\bar{x},0,\bar{z},\tau) &= \pi_2 \\ T(\bar{x},1,\bar{z},\tau) &= \pi_2 \\ T(\bar{x},\bar{y},0,\tau) &= \pi_2 \\ T(\bar{x},\bar{y},1,\tau) &= \pi_2 \end{aligned} \tag{6.13}$$

Any two composite systems which have the same value of the π's will have the same behavior in the non-dimensional system of coordinates. This does not mean the same value of each quantity found in any π, but only equality of each of the overall π's [72]. Therefore, the similarity rules and model laws for curing of

thermosetting composite can be expressed as

$$\pi_{im} = \pi_{ip} \qquad i = 1, \cdots, 6 \tag{6.14}$$

Subscripts m and p refer to model and prototype, respectively. Such model laws are not restricted to geometrically similar systems or other requirement of this type[72]. If one composite system(model) has the same non-dimensional equations and boundary conditions with the same value of the π's which appear in these equations with another composite system(prototype), then similarity of behavior between two systems is completely achieved.

There is another way to express the model laws[71]. Equation(6.14) can be written as

$$\begin{aligned} K_{T_o} &= K_{T_a} = K_{E_o} \\ \frac{K_{(1-\nu_f)}}{K_\rho K_{c_p}} &= \frac{K_{E_o}}{K_{\rho_r} K_{H_R}} \\ K_L^2 &= \frac{K_{k_x}}{K_\rho K_{c_p} K_A} \\ K_M^2 &= \frac{K_{k_y}}{K_\rho K_{c_p} K_A} \\ K_N^2 &= \frac{K_{k_z}}{K_\rho K_{c_p} K_A} \end{aligned} \tag{6.15}$$

where $K_{T_o} = \frac{T_{om}}{T_{op}}, K_{T_a} = \frac{T_{am}}{T_{aP}}$ and in general $K_i = \frac{i_m}{i_p}$. The K's are called *scale factors.*

It is important to keep in mind that due to the transient type of equations, simultaneous states of the two systems may not be considered. Having two composite systems with the same π's, the solution is the same at homologous points

($\overline{x}_{im} = \overline{x}_{ip}, \overline{y}_{im} = \overline{y}_{ip}$, and $\overline{z}_{im} = \overline{z}_{ip}$) and at homologous time ($\tau_m = \tau_p$). In terms of scale factors, the equivalence at homologous times can be written as (see Equation (6.9))

$$(\frac{k_z t}{\rho c_p N^2})_m = (\frac{k_z t}{\rho c_p N^2})_p \tag{6.16}$$

and therefore

$$K_t = \frac{K_\rho K_{c_p} K_N^2}{K_{k_z}} \tag{6.17}$$

Combination of Equation (6.17) and the last equation of Equations (6.15) results

$$K_t = \frac{1}{K_A} \tag{6.18}$$

or

$$t_m = \frac{t_p}{K_A} \tag{6.19}$$

where t_m and t_p are real time scale of model and prototype respectively.

Considering the homologous points between model and prototype, the relation between the model and prototype independent variables can be expressed as

$$\begin{aligned} x_p &= \frac{x_m}{K_L} \\ y_p &= \frac{y_m}{K_M} \\ z_p &= \frac{z_m}{K_N} \end{aligned} \tag{6.20}$$

Dimensionless temperature and degree of cure are the same for model and prototype at homologous points and homologous times ($\overline{T} = \overline{T}_m = \overline{T}_p$ and $\alpha = \alpha_m = \alpha_p$). Therefore, it can be written

$$(\frac{T_i(x,y,z,t)}{T_o})_p = (\frac{T_i(x,y,z,t)}{T_o})_m \tag{6.21}$$

$$(\alpha_i(x,y,z,t))_p = (\alpha_i(x,y,z,t))_m$$

and therefore

$$T_{ip}(x_p,y_p,z_p,t_p) = \frac{T_{im}(x_m,y_m,z_m,t_m)}{K_{T_o}} \tag{6.22}$$

$$\alpha_{ip}(x_p,y_p,z_p,t_p) = \alpha_{im}(x_m,y_m,z_m,t_m)$$

where $T_{ip}, \alpha_{ip}, T_{im}$, and α_{im} are temperature and degree of cure at homologous point i inside prototype and model, respectively. Combination of the first equation of Equations (6.15) and Equations (6.19), (6.20), (6.22) results

$$T_{ip}(\frac{x_m}{K_L},\frac{y_m}{K_M},\frac{z_m}{K_N},K_A t_m) = \frac{T_{im}(x_m,y_m,z_m,t_m)}{K_{E_o}} \tag{6.23}$$

$$\alpha_{ip}(\frac{x_m}{K_L},\frac{y_m}{K_M},\frac{z_m}{K_N},K_A t_m) = \alpha_{im}(x_m,y_m,z_m,t_m)$$

Equations (6.23) should be used to transfer the model experimental results to the prototype one.

6.4 Kinetic Equation

The simplified Arhenius type first order rate equation is employed in this analysis. In general, it is impossible to express the kinetic equations for all resin systems in a single functional form. There is a type of expression usually used to obtain kinetic equation. For both epoxy and unsaturated polyester systems, the kinetic equations in dimensional form can be expressed by Equation (2.16). In non-

dimensional form, kinetic equation (2.16) can be written as

$$\frac{d\alpha}{d\tau} = \frac{\rho c_p N^2 A_2}{k_z}\left(\frac{A_1}{A_2}\exp\left(\frac{\frac{-E_1}{RT_o}}{T}\right) + \exp\left(\frac{\frac{-E_2}{RT_o}}{T}\right)\alpha^a\right)(B-\alpha^b)(1-\alpha^d)^c \qquad (6.24)$$

Looking at this equation, a few new non-dimensional groups are extracted. These new π's are

$$\begin{aligned}
\pi_7 &= \frac{\rho c_p N^2 A_2}{k_z} \\
\pi_8 &= \frac{A_1}{A_2} \\
\pi_9 &= \frac{-E_1}{RT_o} \\
\pi_{10} &= \frac{-E_2}{RT_o} \\
\pi_{11} &= B \qquad (6.25) \\
\pi_{12} &= a \\
\pi_{13} &= b \\
\pi_{14} &= c \\
\pi_{15} &= d
\end{aligned}$$

π_7 is equivalent to π_4. π_9 and π_{10} are equivalent to π_1. In order to have similar behavior between composite model and composite prototype which are constructed from different resin systems, Equations(6.25) should be the same for the model resin and prototype resin. It is too difficult to find such a similarity between two different resin systems (almost impossible). However, it does not mean that one can not design a model for the composite.

6.5 Convective Boundary condition

In some cases the boundary condition is given based on the heat convection at the composite surface. In dimensional form, it is expressed as (in the z-direction)

$$-k_z\frac{\partial T}{\partial z} = h(T_s - T_a) \tag{6.26}$$

where T_s is the surface temperature and h is the convective heat transfer coefficient. In non-dimensional form, it can be written as

$$-\frac{\partial T}{\partial z} = Bi(T_s - T_a) \tag{6.27}$$

where $Bi = \frac{hN}{k_z}$ is called *Biot Number.* The Biot number physically denotes the ratio of the conductive thermal resistance within the composite $\frac{N}{k_z}$ to the convective thermal resistance of the fluid $\frac{1}{h}$ used to cool the composite. A large value of Biot number indicates rapid cooling of the composite surface. $Bi = \infty$ corresponds to the instantaneous equilibration of the composite surface temperature with the surrounding temperature. Conversely, $Bi = 0$ corresponds to an insulated boundary condition [53].

This boundary condition introduces a new non-dimensional parameter (Bi) which should be the same during the curing of both model and prototype. This model law can be expressed as

$$K_h = \frac{K_{k_z}}{K_N} \tag{6.28}$$

6.6 Model Design Procedure

So far the non-dimensional parameters and model laws (Equations (6.10),(6.15)) for curing of thermosetting composites have been obtained. One should know how to use model laws to determine the composite model specifications from composite prototype specifications. Consider a composite flat-plate (as prototype) with dimensions L_p, M_p, N_p, and fiber volume fraction ν_{fp} which is subjected to a specified cure cycle. The physical properties of model constituent as well as resin kinetic equation are given for both model and prototype. The task here is to determine the model dimensions L_m, M_m, N_m and fiber volume fraction ν_m and the new cure cycle during which model should be subjected to. The model design procedure is as follows :

1. Calculate the initial temperature for model as

$$T_{om} = K_{E_o} T_{op} \tag{6.29}$$

2. Calculate the autoclave temperature (model cure cycle) as

$$T_{am} = K_{E_o} T_{ap} \tag{6.30}$$

   It should be mentioned that if T_{ap} is a function of time (t_p), the real time (t_m) for T_{am} should be calculated using Equation (6.19). Therefore, the cure cycle for model may be different from that for the prototype.

3. The next and most important step in obtaining the model specifications is to calculate model fiber volume fraction ν_{fm}. To do this, consider the second

equation of Equations(6.15). Right hand side of this equation is given. This equation combined with the rule of mixture equations which are used to calculate composite density and specific heat are employed to calculate model fiber volume fraction. Density ρ_p and specific heat c_{pp} of prototype are also calculated using the role of mixture, using the fiber volume fraction in the prototype ν_{fp} which is given. Therefore, this equation can be written as

$$\frac{1-\nu_{fm}}{[\rho_{fm}\nu_{fm}+\rho_{rm}(1-\nu_{fm})][c_{pfm}\nu_{fm}+c_{prm}(1-\nu_{fm})]}=\frac{(1-\nu_{fp})K_{E_0}}{\rho_p c_{pp}K_{\rho_r}K_{H_R}} \tag{6.31}$$

Rearranging this equation results in

$$(\rho_{fm}-\rho_{rm})(c_{pfm}-c_{prm})\nu_{fm}^2+[\rho_{rm}(c_{pfm}-c_{prm})+c_{prm}(\rho_{fm}-\rho_{rm})+\frac{1}{C_0}]\nu_{fm}$$

$$+(\rho_{rm}c_{prm}-\frac{1}{C_0})=0 \tag{6.32}$$

where

$$C_0=\frac{(1-\nu_{fp})K_{E_0}}{\rho_p c_{pp}K_{\rho_r}K_{H_R}} \tag{6.33}$$

C_0 is determined by given properties. Subscript f and r refer to fiber and resin respectively. All parameters involved in Equation (6.32) are specified except ν_{fm}. Any real root of this quadratic equation which lies between 0 and 0.907 (The maximum fiber volume fraction possible in a unidirectional composite assuming contact between fibers) [37] can be a solution. Otherwise, there would be no solution and a new system of materials should be selected for the model.

4. Having determined ν_{fm}, the physical properties of the model can be calculated. The relation proposed by Tsai and Springer[64] and corrected by Walker [52] is used to calculate thermal conductivities in the y and z directions. The model thermal conductivity in the x direction,density, and specific heat are obtained by applying the rule of mixture.

5. The last step is to calculate the model dimensions L_m, M_m,and N_m. The last three equations of Equations(6.15) are used to obtain the length,width, and thickness of model.

A model with a new system of fiber and resin and dimensions L_m, M_m, and N_m and fiber volume fraction ν_m is designed. This model may be subjected to the model cure cycle and then temperature and degree of cure are monitored at different times and locations. The behavior of composite model and composite prototype are similar at homologous points and homologous times. Therefore, the prototype temperature and degree of cure at different times and locations can be obtained by using Equation (6.23).

Four cases can be considered to design a composite model based on composite prototype :

Case (a) To design a model using a completely different system of fiber and resin.

Case (b) To design a model using the same system of fiber and resin.

Case (c) To design a model using the same fiber, but different resin.

Case (d) To design a model using the same resin, but different fiber.

Refer to Equations (6.24) and (6.25), it is very difficult (almost impossible) to find two different resin systems which satisfy the similarity conditions and model laws. Therefore, cases (a) and (c) usually can not be used for model design. However, if the model laws are satisfied for two different resin systems, the model design procedure can be followed as explained before.

In cases (b) and (d) the same resin is used. Application of same resin means

$$K_{E_a} = K_{\rho_r} = K_{H_R} = K_A = 1 \tag{6.34}$$

Combination of Equations (6.29),(6.30),(6.34) shows that the initial temperature of model should be the same as prototype. It also shows that the model should be subjected to the same cure cycle as the prototype. Since $t_m = t_p$ (see equation (6.19)), Equation (6.23) can be written as

$$T_{ip}(\frac{x_m}{K_L}, \frac{y_m}{K_M}, \frac{z_m}{K_N}, t_m) = T_{im}(x_m, y_m, z_m, t_m) \tag{6.35}$$
$$\alpha_{ip}(\frac{x_m}{K_L}, \frac{y_m}{K_M}, \frac{z_m}{K_N}, t_m) = \alpha_{im}(x_m, y_m, z_m, t_m)$$

Therefore, application of the same resin for both model and prototype produces the same temperature and degree of cure at homologous points inside the model and prototype.

Consider case (b). Application of equation (6.32) shows that the only acceptable solution is

$$\nu_{fm} = \nu_{fp} \tag{6.36}$$

Fiber density	ρ_{fm}	$2.60 \times 10^3 \frac{kg}{m^3}$
Specific heat of fiber	$c_{p_{fm}}$	$9.50 \times 10^2 \frac{J}{kg \circ K}$
Thermal conductivity of fiber	k_{fm}	$1 \frac{W}{m \circ K}$

Table 6.1: Typical physical properties of glass fiber (model)

Therefore, the model and prototype should be completely the same. In other words, there is no benefit in designing a model using the same system of materials.

Case (d) is the last case and the only applicable case. As an illustration of applying the model design procedure for this case, consider the manufacture of the Hercules graphite epoxy prepreg tape, commercially called as AS4/3501-6. This is a representative epoxy system used widely in aerospace applications. The prepreg specification as well as the kinetic parameters are shown in Table 3.1. The kinetic equation for this resin is given by Equation (2.18). The objective here is to replace the graphite fiber with glass fiber and design and fabricate a model using Glass/3501-6 material for doing experiments and monitoring temperature and degree of cure. The typical physical properties of glass fiber are given in Table 6.1.

Since the same resin is used for both model and prototype, the cure cycle is the same for both model and prototype. Equation (6.32) is used to obtain the glass fiber volume fraction inside the model. For each graphite fiber volume fraction, there are two solutions for glass fiber volume fraction. One of the solutions is always greater than unity which is unacceptable. The variation of glass fiber

volume fraction (model) with respect to graphite fiber volume fraction (prototype) is shown in Figure 6.2. Due to the higher density and specific heat of glass fiber in comparison with graphite fiber, ν_{fm} is less than ν_{fp} as shown in Figure 6.2. Therefore, the more heat per unit volume is generated inside the glass fiber model during the chemical reaction. However, the glass fiber higher density and specific heat compensate for this effect and keep the same temperature rise potential due to heat of reaction for both model and prototype.

The physical properties of composite model are calculated based on physical properties of its constituents and fiber volume fraction ν_{fm}. Then the model dimensions L_m, M_m, N_m are obtained. Figures 6.3 and 6.4 show the variation of K_L and K_N with respect to graphite fiber volume fraction. It should be mentioned that in this specific example K_M is equal to K_N. With increasing the fiber volume fraction, K_L and K_N decrease. At higher fiber volume fraction, the fibers play a more dominant role on the composite properties. Therefore, higher specific heat and density and lower thermal conductivity of glass in comparison with graphite are main reasons for decrease of K_L and K_N at higher fiber volume fractions. K_L is much lower than K_N. K_L should be small enough to compensate for the effect of high thermal conductivity of graphite composite in the x-direction with respect to low thermal conductivity of glass composite in the same direction.

It should be emphasized that K_L and K_N are smaller than unity which means the model dimensions are smaller than the prototype dimensions. Physical prop-

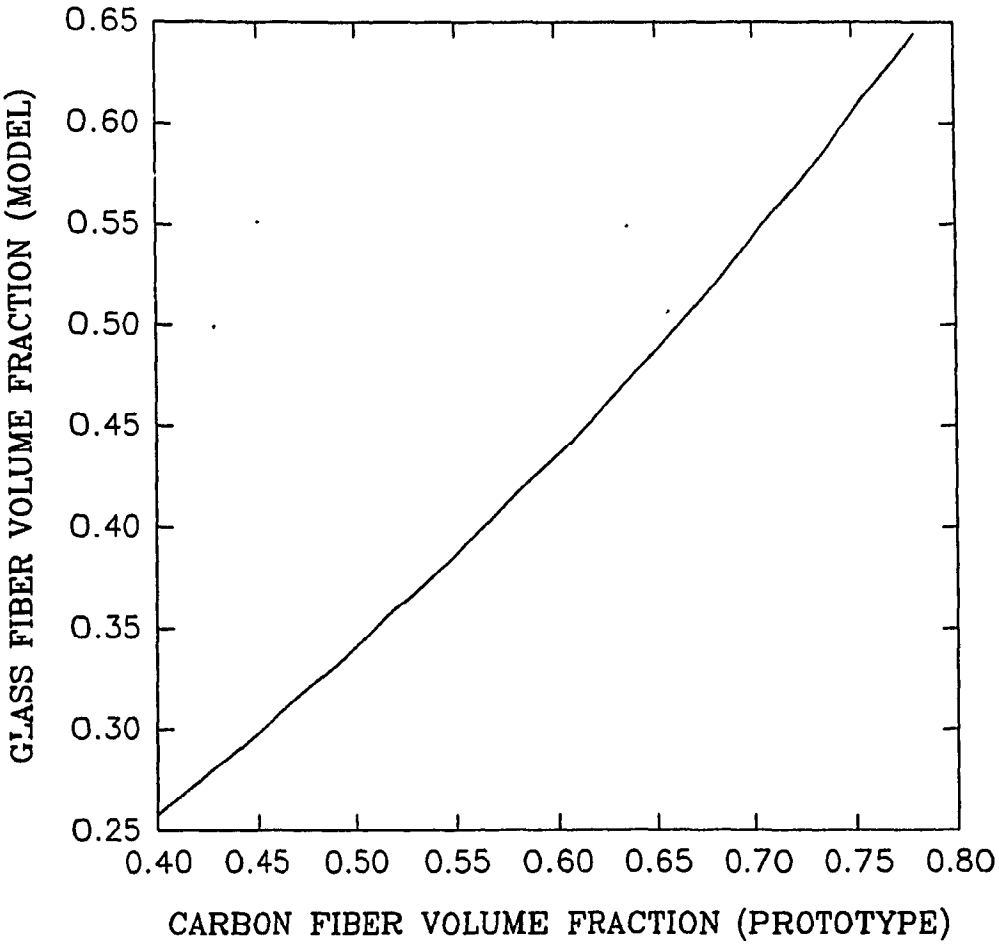

Figure 6.2: Glass fiber volume fraction (model) versus Graphite fiber volume fraction (prototype)

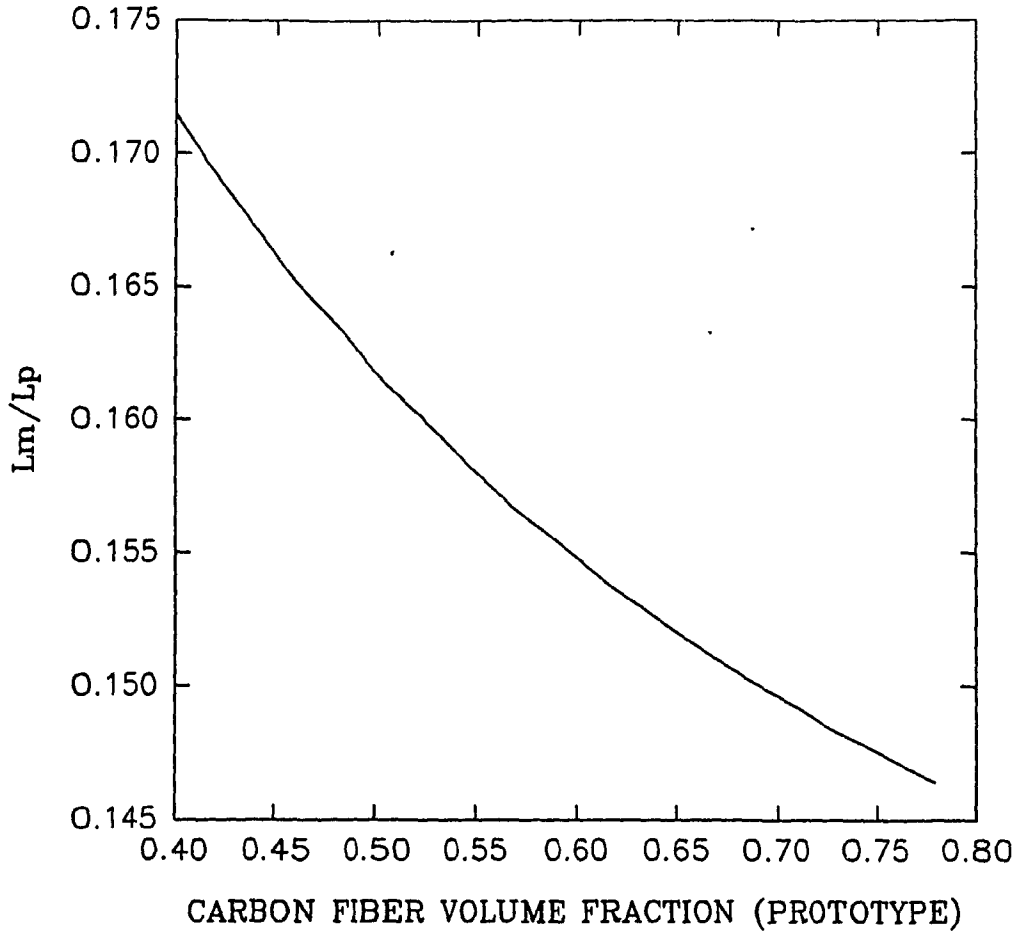

Figure 6.3: Length scale factor (K_L) versus Graphite fiber volume fraction (prototype)

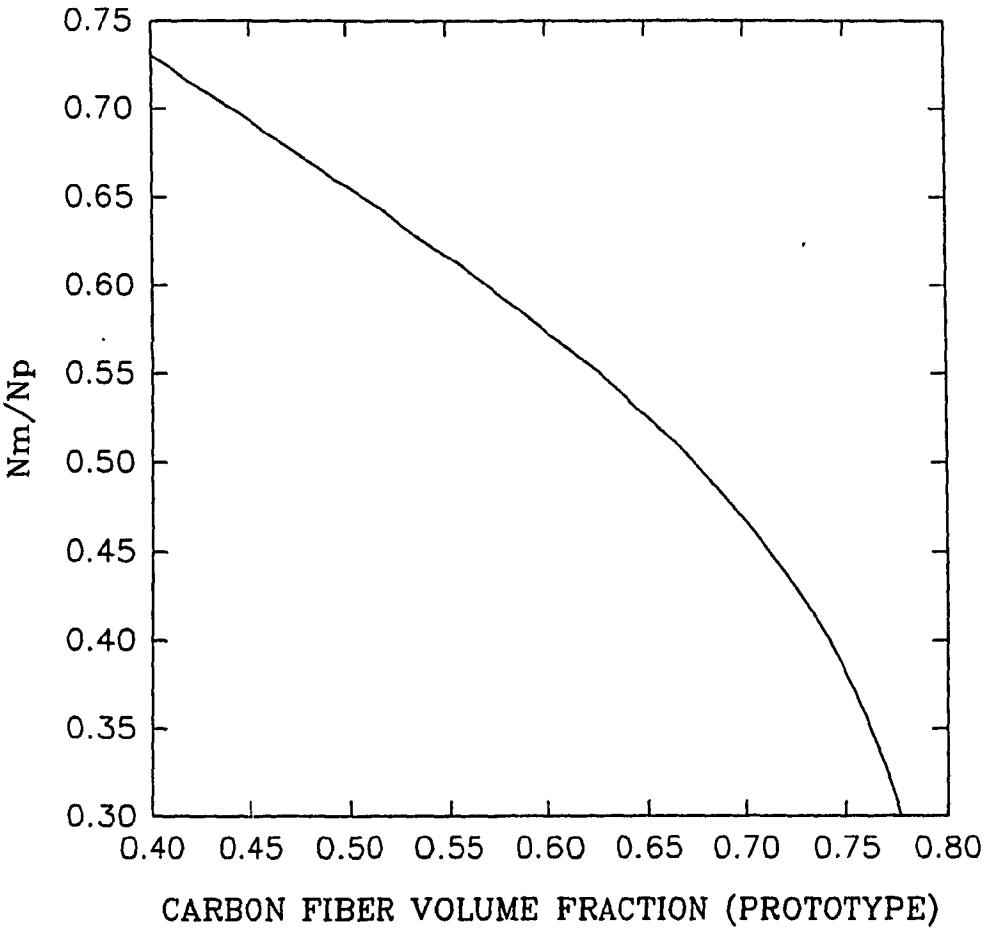

Figure 6.4: Thickness scale factor (K_N) versus Graphite fiber volume fraction (prototype)

erties of composites are involved in determination of K_L and K_N. Physically one can say that due to the low thermal conductivities of model, the heat should travel less distance between the different points inside the model and the boundaries. Therefore, the model sizes should be less than the prototype one. If K_L or K_N becomes greater than unity, the cost of constituent materials (resin and fiber) determines the efficiency of the model. However, owing to the cost of bagging and labor work, it is preferred to replace model materials with a new materials in order to have K_L and K_N smaller than unity.

Those stated goals have been achieved. First, since the model laws are satisfied, the behavior of model and prototype are similar. Secondly, not only the more expensive graphite fiber is replaced with less expensive glass fiber but also the model dimensions are reduced a lot which means material is saved. Resin weight ratio (the ratio of the resin amount inside model to resin amount inside the prototype) and fiber weight ratio (the ratio of the fiber weight inside the model to the fiber weight inside the prototype) can be calculated as

$$Resin\ Weight\ Ratio = K_{(1-\nu_f)} K_L K_M K_N \tag{6.37}$$

$$Fiber\ Weight\ Ratio = K_{\rho_f} K_{\nu_f} K_L K_M K_N$$

Figure 6.5 shows the resin weight ratio for three different cases. For one-dimensional through-the-thickness (z–direction) analysis, K_L and K_M are removed from Equations (6.37). For two-dimensional ($y - z$ directions) analysis, K_L is removed from Equations (6.37). Figure 6.6 also shows the fiber weight ratio can be achieved for

three different cases.

Convective boundary condition may be considered in some application. Figure 6.7 shows the variation of $K_h = \frac{h_m}{h_p}$ with respect to graphite fiber volume fraction (prototype) for one-dimensional through-the-thickness analysis (Equation (6.28)). h_m and h_p are the convective heat transfer coefficients at the model and prototype boundaries, respectively. Lower thermal conductivities of model cause the rates of heat transfer at the boundaries to decrease. Less heat per unit time should be removed by convection at the surface of model. Therefore, the convective heat transfer coefficient at the model boundaries should be less than the prototype one. At higher fiber volume fraction, the difference between the model and prototype thermal conductivities become larger which cause the K_h to decrease with increasing fiber volume fraction.

Dielectrometry is usually used to monitor the cure of resin inside the composites during the cure process. For both conventional dielectrometry and microdielectrometry, the direct contact between the highly conductive fibers (carbon and boron) and the electrodes can short out the sensors, making the measurement inoperative[74, 75, 76, 77]. This difficulty can be solved by using the glass fiber model. This is another advantage of using glass model for performing experiments.

This analysis also shows that in order to design a model, using the same resin as prototype, it is not necessary to know the resin kinetic equation (as long as the kinetic equation can be expressed typically as in Equation (2.16)). One can design

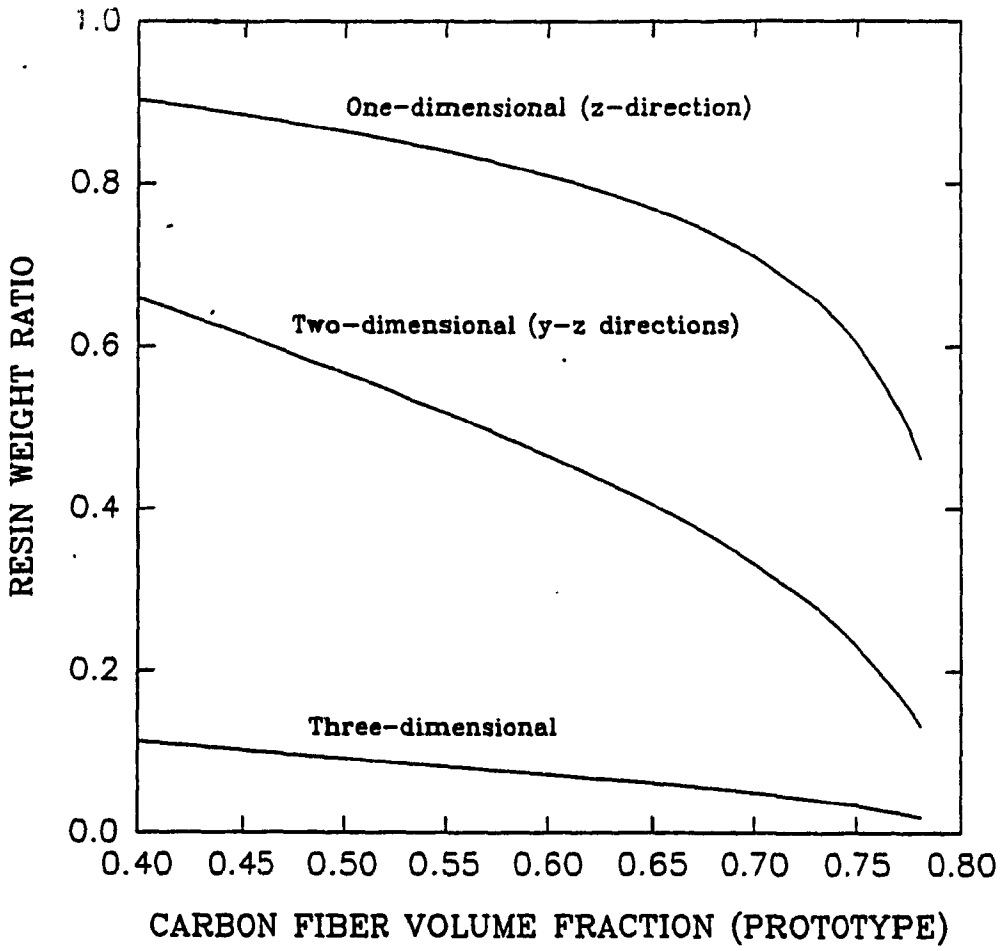

Figure 6.5: Resin weight ratio

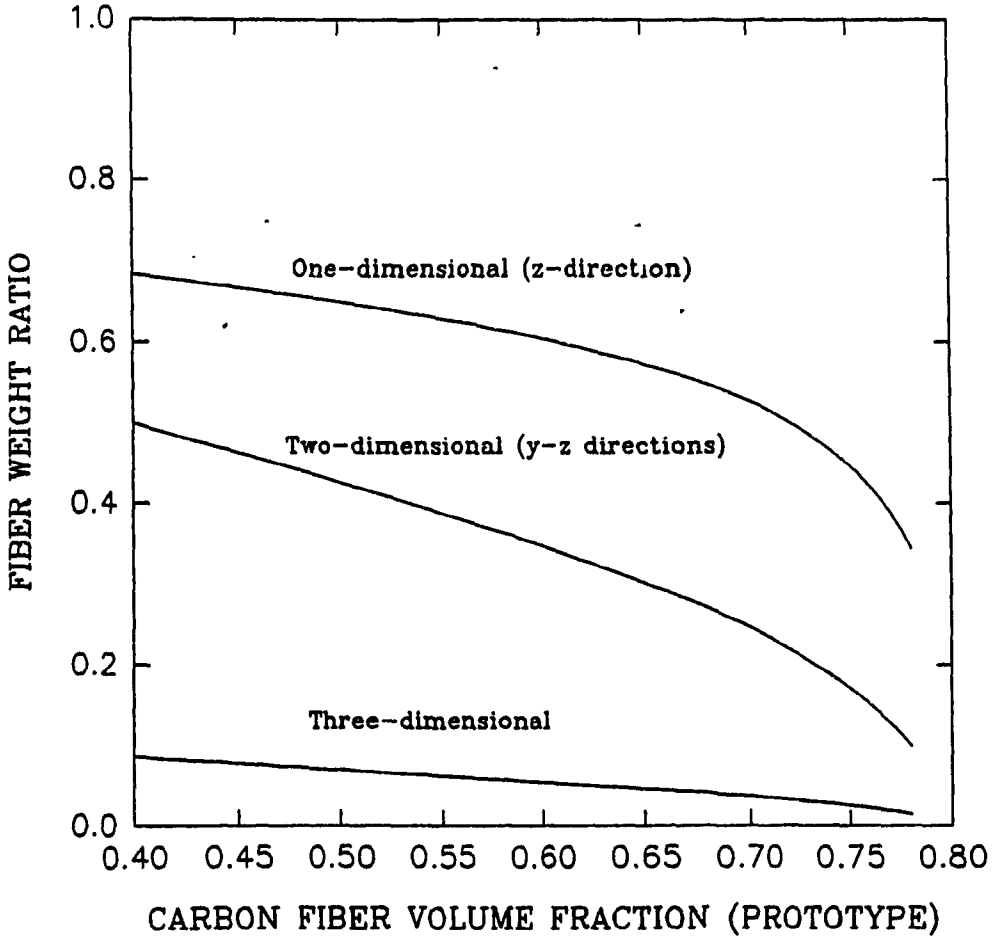

Figure 6.6: Fiber weight ratio

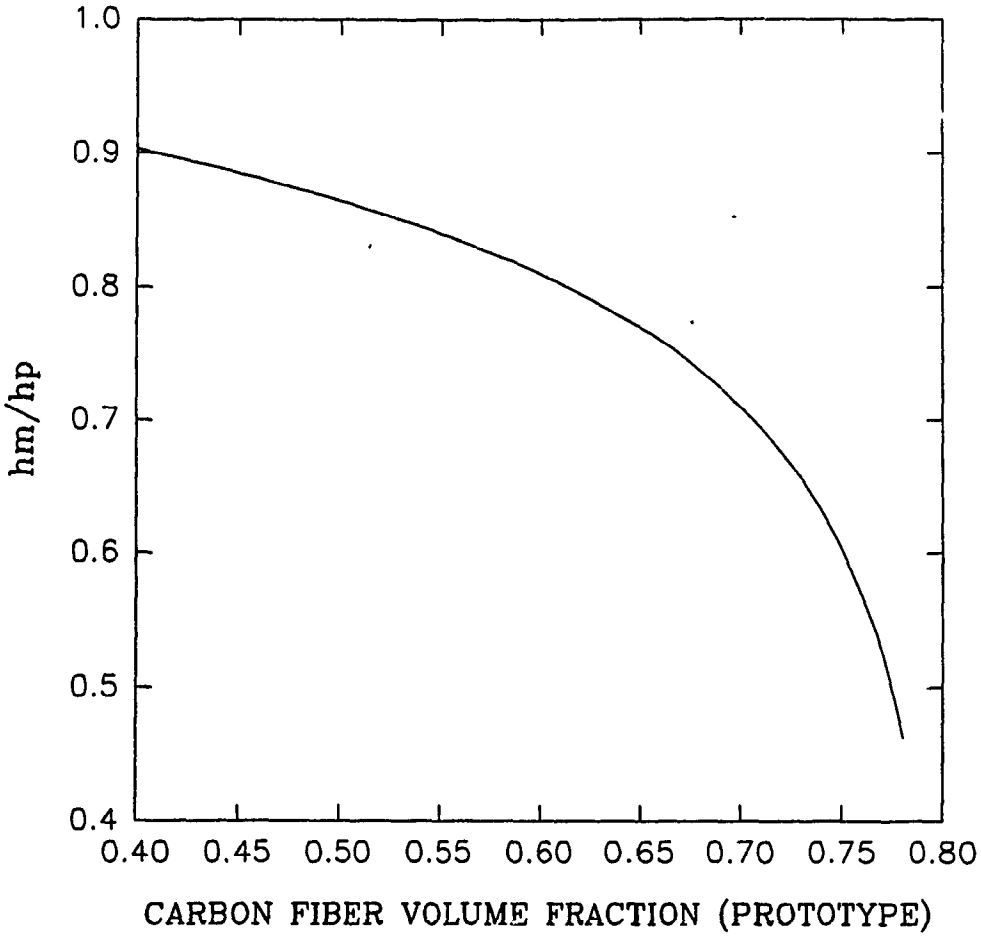

Figure 6.7: Convective heat transfer coefficient scale factor K_h versus graphite fiber volume fraction

a model and perform experiment to get specifications for a cure cycle. Then these results can be extended to the prototype using the model laws without having the resin kinetic equation.

Curing of thermosetting composite parts consists of heat transfer and fluid flow. In this chapter, heat transfer was studied. In general, however, the flow problem should also be considered. The resin flow for autoclave curing can be modeled using the consolidation theory and Darcy's law [30, 27]. These equations combined with initial and boundary conditions should be non-dimensionalized, and from which, dimensionless parameters should be extracted. The relationship between the new dimensionless parameters and those obtained from thermochemical model should be identified. Then these dimensionless groups can be used to design the model.

6.7 Numerical Results

Suppose that one wants to perform experiment and measure the temperature and degree of cure distribution inside a unidirectional thick composite made of AS4/3501-6 . The thickness is $10cm$ and fiber volume fraction is 0.7 and it should be subjected to a specified cure cycle (Figure 6.8). The experiment is designed for one-dimensional through-the-thickness situation.

Using Figures 6.2 and 6.4, the glass fiber model should have fiber volume fraction of 0.544 and model thickness should be $4.67cm$. As mentioned before,

since the same resin is used, the initial temperature and cure cycle for both model and prototype should be the same.

The governing equations, Equations (6.5) and (6.6), and the associated initial and boundary conditions, Equations (6.7) and (6.8), were solved using a Fully Implicit Finite Difference Method[62]. Since the dimensionless parameters in the governing equations and boundary conditions are the same for both model and prototype, both systems have the same solution in the new system of coordinates. Using the same resin for both model and prototype produces the same temperature and degree of cure variation with respect to real time. Temperature and degree of cure variation at the composite center with respect to time for both model and prototype are shown in Figures 6.8 and 6.9. Temperature and degree of cure variation through-the-thickness at different times are shown in Figures 6.10 and 6.11.

The other independent code which has been already developed in previous chapters based on discretization of dimensional governing equations and boundary conditions using Control-Volume formulation and Alternating Direction Explicit method is used to simulate the curing process for one-dimensional through-the-thickness analysis for both model and prototype. As expected, exactly the same results as shown in Figures 6.8,6.9,6.10,6.11 are obtained for both model and prototype. Therefore, the model can be used to obtain directly the optimum cure cycle for fabrication of prototype.

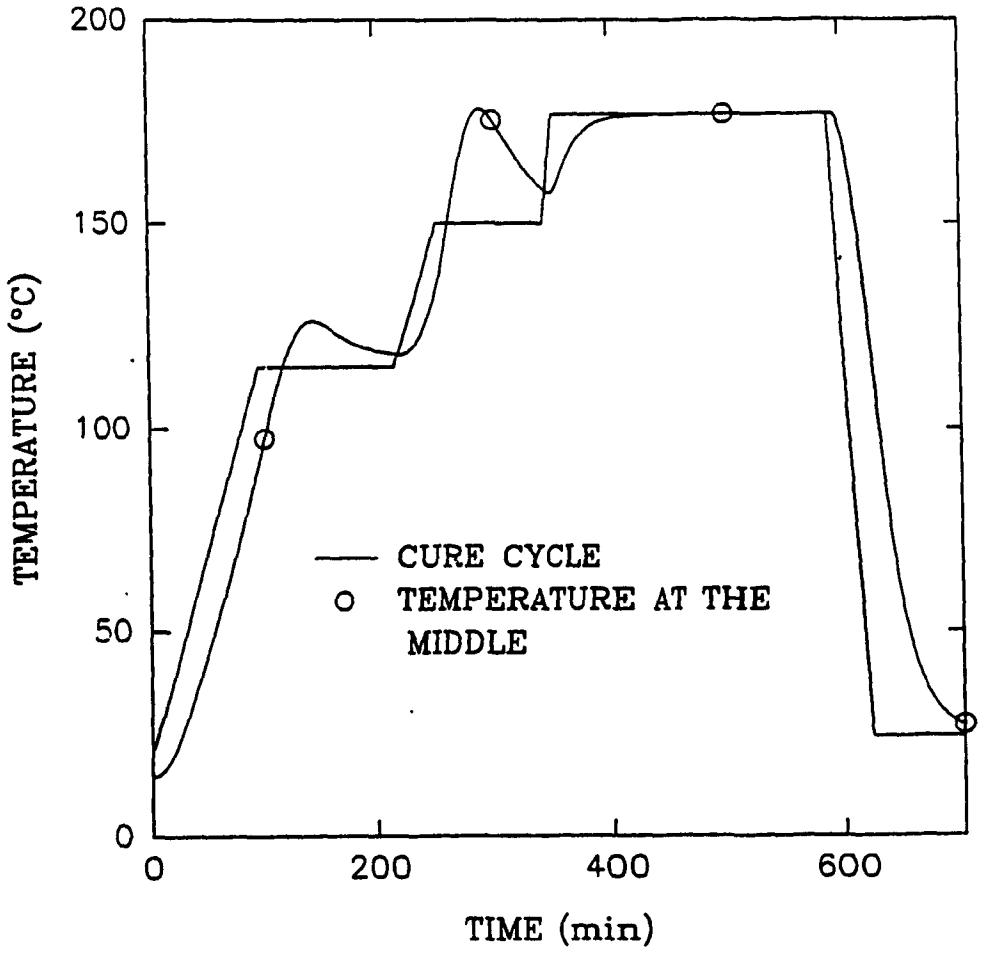

Figure 6.8: Temperature variation at the center of composite (AS4/3501-6 with thickness 10cm and ν_f = .7 or Glass/3501-6 with thickness 4.67cm and ν_f = .544)

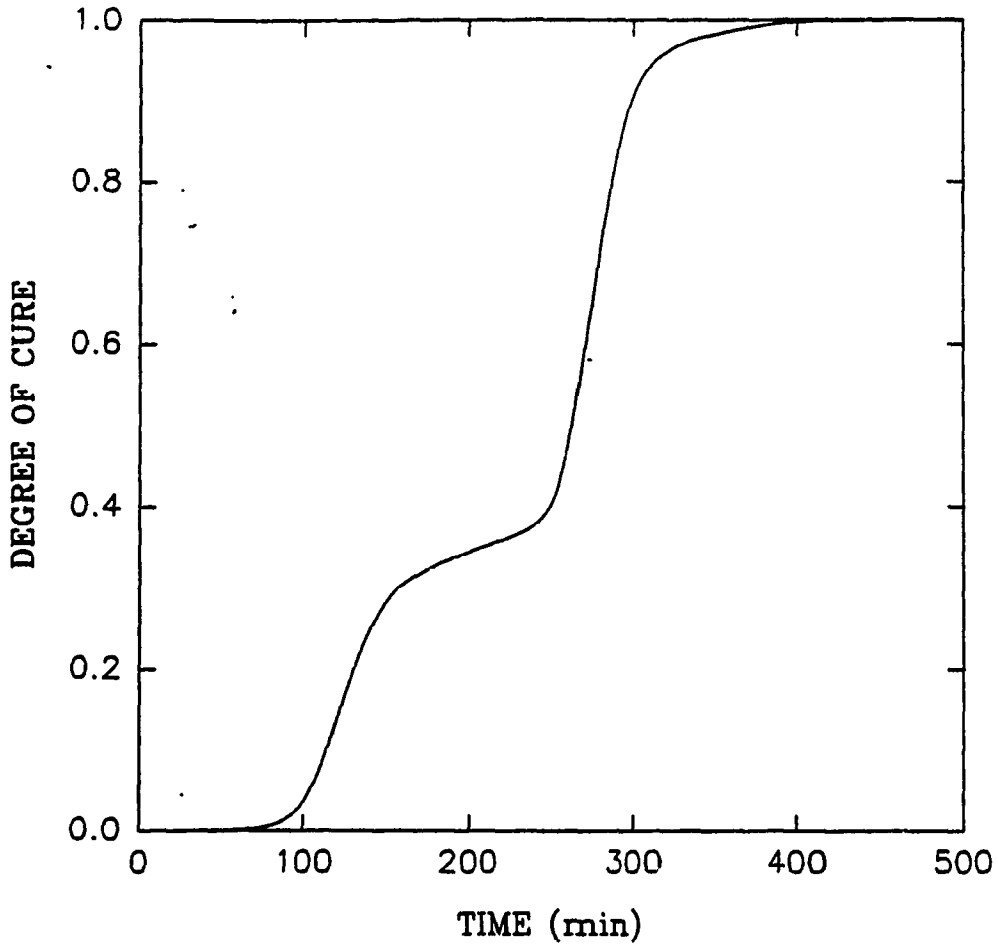

Figure 6.9: Degree of cure variation at the center of composite (AS4/3501-6 with thickness 10cm and ν_f = .7 or Glass/3501-6 with thickness 4.67cm and ν_f = .544)

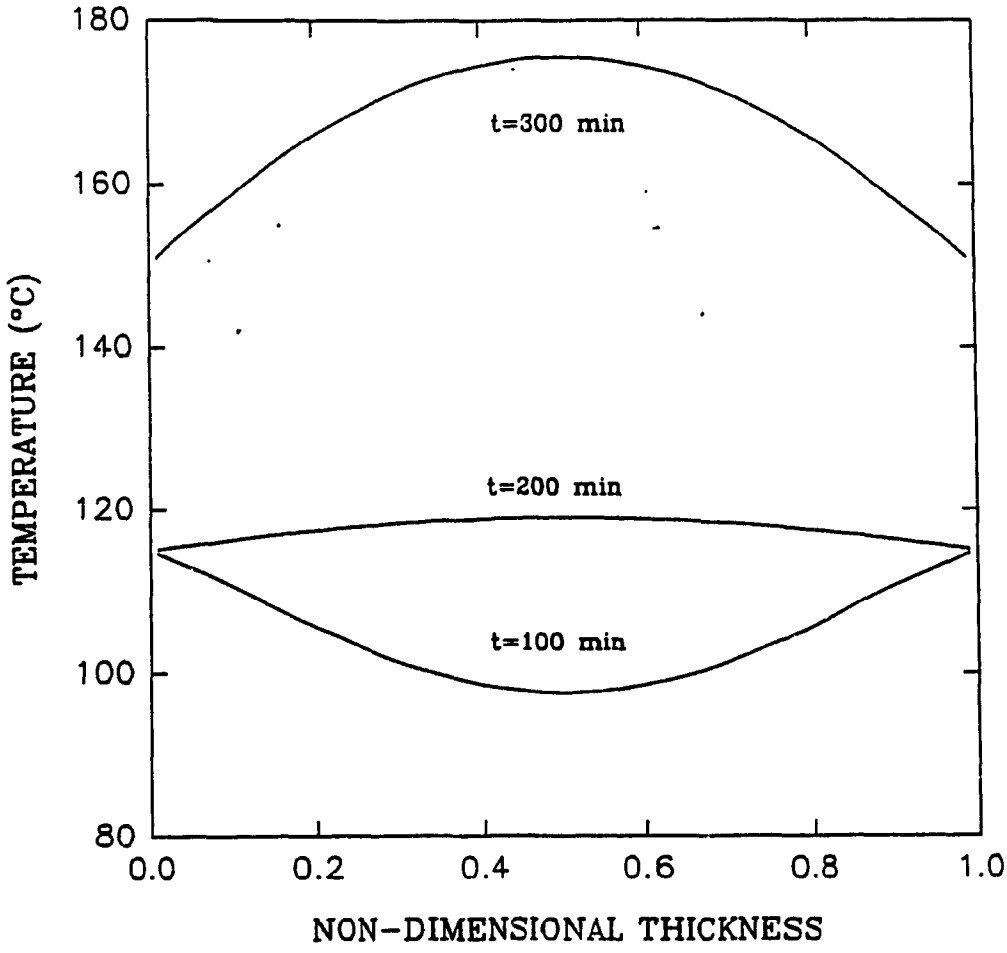

Figure 6.10: Temperature distribution through-the-thickness (AS4/3501-6 with thickness 10cm and ν_f = .7 or Glass/3501-6 with thickness 4.67cm and ν_f = .544)

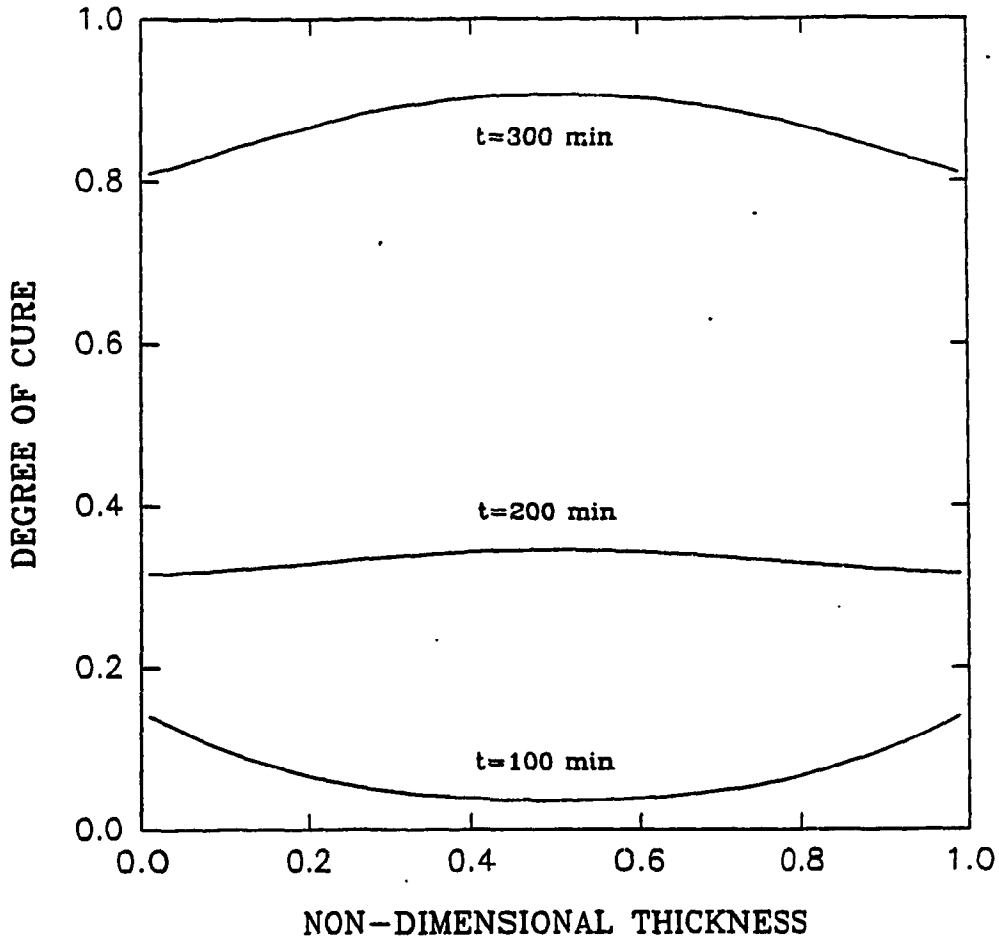

Figure 6.11: Degree of cure distribution through-the-thickness (AS4/3501-6 with thickness 10cm and ν_f = .7 or Glass/3501-6 with thickness 4.67cm and ν_f = .544)

6.8 Summary

For curing of thermosetting composites, the model laws were developed. The model laws were constructed based on dimensionless parameters which were obtained from non-dimensional heat conduction equation, non-dimensional kinetic equation , and non-dimensional initial and boundary conditions. Application of model laws to design a model was shown. Generally a composite model made of less expensive materials can be used to determine the optimum processing parameters for a composite prototype made of more expensive materials. The relations between different variables and processing parameters for model and prototype are determined through the model laws.

Four different possible systems of materials were considered to design a model. Different kinetic equations exist for different resin systems. Therefore, the same resin should be used for the model design. It was shown that using the same resin but different fibers is the only feasible case to design a model. For this case, the initial temperature and cure cycle are the same for both model and prototype. Once the optimum cure cycle is determined for the model, it can be used directly for the prototype. Application of the same resin has another advantage. As shown before, to transfer the model experimental results to prototype, one does not need to know the resin kinetic equation.

These concepts were used to design a model made of Glass/3501-6 for a AS4/3501-6 prototype. Not only the less expensive glass fiber is used inside the

model, but also it was shown that the model has smaller dimensions, and therefore, materials are saved. It was also discussed that using the glass fiber creates less problem during the measurement of degree of cure inside the composite. The glass fiber model also needs less bagging materials and less labor work.

Chapter 7

Conclusions and Contributions

7.1 Conclusions

Curing of thick thermosetting composites was studied by three different methods: experiment, simulation, and scaling (modeling). One-dimensional through-the-thickness experiment was performed. Bleed setup was used. Two problems, temperature overshoot and incomplete through-the-thickness consolidation, were observed. It was also found that the temperature distribution through-the-thickness was not symmetric and maximum temperature happened at the top of laminate. Two-dimensional experiment was performed to reduce the temperature overshoot. Experimental results showed improvement in temperature overshoot reduction as well as decrease of cure cycle time. To obtain complete through-the-thickness compaction, prebleeding method was used. Different sublaminates first were pre-

bled and then were put together and cured. Good quality thick composite was fabricated by this method.

A one-dimensional through-the-thickness simulation was developed. Heat conduction, kinetic, viscosity, and flow (squeezed sponge model) equations were solved as a coupled system of equations. Heat capacity, density, thermal conductivity, and permeability of composite were considered as functions of fiber volume fraction. Simulation results were compared to experimental results . Good agreement was obtained. The simulation was used to study the laminate behavior under different processing parameters. The following results are obtained by simulation:

- Either temperature overshoot or incomplete through-the-thickness consolidation can put restriction on the application of each cure cycle up to a certain thickness.

- Although the recommended cure cycle by manufacturer for thick composite can satisfy the temperature condition, mostly the complete through-the-thickness consolidation can not be achieved.

- Due to the deformation characteristic of the fiber structure, increasing autoclave pressure does not solve the incomplete consolidation.

- Bleeding from top and bottom improves the consolidation.

- Low thermal conductivity of bleeder as well as bleeder thickness delay heat to reach to laminate and therefore increase the cure cycle time. It also prevents

heat to dissipate fast during the maximum chemical reaction, increases the temperature overshoot.

- Due to the bleeder plies, maximum temperature may not occur at the center of laminate.

- Due to the bleeder plies, temperature distribution through-the-thickness is not symmetric.

- Considering the temperature overshoot, incomplete through-the-thickness consolidation, and bleeder effect , it can be concluded that the prebleeding technique is the most promising method for fabrication of thick thermosetting composite parts.

Performing experiment to obtain optimum processing parameters for curing of thick composites requires the expensive prepreg materials and labor work. Using simulation to obtain optimum processing parameters is economical. However, to do simulation, an accurate expression for kinetic equation is required. Kinetic equation is not available for most resins. Even the available kinetic equations do not predict the rate of reaction accurately. Scaling (modeling) has been proposed as an alternative to study the curing process. For curing of thermosetting composites, the model laws were established The model laws were constructed based on dimensionless parameters which were obtained from non-dimensional heat conduction equation, non-dimensional kinetic equation, and non-dimensional

initial and boundary conditions. Application of model laws to design a model was shown. It was also shown that the only feasible way to design a model is to use the same resin but different fibers. To transfer the model experimental results to prototype, one does not need to know the resin kinetic equation if the same resin is used.

7.2 Contributions

- The development of a reasonable simulation model for the curing of thick thermosetting composites in which the heat, cure kinetics, viscosity, and flow (squeezed sponge model) equations considered as a coupled system of equations was done. Heat conduction equation combined with cure kinetic equation were used to obtain the temperature and degree of cure distribution through-the-thickness during the cure cycle. The squeezed sponge model was considered to simulate the resin flow. Control-volume method combined with Alternating Direction Explicit method (ADE) were employed in the solution. Composite physical properties were considered as functions of fiber volume fraction. After performing experiment and simulation verification, simulation were used to study the different parameters and mechanisms involved in the curing.

- Model laws for curing of thermosetting composite parts were established.

The transient heat conduction coupled with kinetic equation and initial and boundary conditions were non-dimensionalized. Dimensionless parameters were extracted from non-dimensional equations and boundary conditions. Model laws were constructed based on those dimensionless parameters. It was shown how one can use these model laws to design a composite model based on the prototype one. Therefore, one can use a less expensive model to determine the optimum cure cycle and processing parameters by performing experiments and then the results can be interpreted for the more expensive prototype.

7.3 Recommendations for future work

The kinetic equation currently available and used in this thesis overestimates the rate of reaction and has to be improved. Resin flow is assumed to be Newtonian flow. However, due to the small gap between fibers and resin high viscosity during chemical reaction, non-Newtonian flow and viscoelastic behavior has to be studied.

Model laws for laminates consisting of laminae with different fiber orientations and complicated shape have to be derived.

Bibliography

[1] Hahn,H.T. and N.J. Pagano,"Curing Stresses in Composite Laminates" *Journal of Composite Materials* 9:91-105 (1975).

[2] Hahn,H.T.,"Residual Stresses in Polymer Matrix Composite Laminates" *Journal of Composite Materials* 10:266-277 (1976).

[3] Griffin,O.H.,"Three-Dimensional Curing Stresses in Symmetric Cross-ply Laminates with Temperature-Dependent Properties" *Journal of Composite Materials* 17:449-463 (1983).

[4] Stango,R.J. and S.S. Wang,"Process-Induced Residual Thermal Stresses in Advanced Fiber-Reinforced Composite Laminates" *Journal of Engineering for Industry* 106:48-54 (1984).

[5] McGann,T.W. and E.R. Crilly,"Preparation for Cure" *Engineering Materials Handbook Volume 1-Composites* ASM International (1987).

[6] Boll,D.J. and J.C. Weidner,"Curing Epoxy Resins" *Engineering Materials Handbook Volume 1-Composites* ASM International (1987).

[7] Kau,H.T.,"Dimensional Stability and Property Gradients in Thick SMC Section" *Proceeding of the 34th International SAMPE symposium and exhibition, Reno, Nevada* Vol 34, Book 1 pp 436-447 (1989).

[8] White,S.R. and H.T. Hahn,"Process Modeling of Composite Materials :Residual Stress Development During Cure.Part I.Model Formulation" *Journal of Composite Materials* 26(16):2402-2422 (1992).

[9] Tang,J. and G.S. Springer"Effects of Cure and Moisture on the properties of Fiberite 976 Resin" *Journal of Composite Materials* 22:2-14 (1988).

[10] Lee,S.Y. and G.S. Springer,"Effects of Cure on the Mechanical properties of Composites " *Journal of Composite Materials* 22:15-29 (1988).

[11] Bogetti,T.A. and J.W. Gillespie,"Process-Induced Stress and Deformation in Thick Section Thermosetting Composite Laminates " in *21st SAMPE Technical Conference ,N.J.*,September (1989).

[12] McGee,S.H.,"Curing of Particulate Filled Composites" *Polymer Engineering and Science* 22(8):484-491 (1982).

[13] Bogetti,T.A. and J.W.Gillespie,"Two-Dimensional Cure Simulation of Thick Thermosetting Composites," *Journal of Composite Materials* 25:239-273 (1991).

[14] Loos,A.C. and G.S. Springer,"Curing of Epoxy Matrix Composites," *Journal of Composite Materials* 17:135-169 (1983).

[15] Meade,L.E.,"Fabrication of Thick Graphite/Epoxy Wing Surface Structure" *Proceeding of the 24th national SAMPE symposium and exhibition,San Francisco, CA.* Vol 24, Book 1 pp 252-259 (1979).

[16] Kim,T.W.,E.J. Jun and W.I. Lee,"Compaction Behavior of Thick Composites Laminates During Cure" *Proceeding of the 34th International SAMPE symposium and exhibition, Reno, Nevada* Vol 34, Book 1 pp 15-19 (1989).

[17] Walsh,S.M.,"Curing Thick Laminates Using Internal Heat Sources" *Proceeding of the 34th International SAMPE symposium and exhibition, Reno, Nevada* Vol 34, Book 1 pp 20-31 (1989).

[18] Springer,G.S.,"Selection and Control of Manufacturing Process Variables for Thermoset and Thermoplastic Composites " in*ICCM-VII ,Proceedings of the 7th International Conference on Composite Materials,* pp. 7-26, (1989).

[19] Lee,S.Y. and G.S. Springer,"Filament Winding Cylinders: I.Process Model" *Journal of Composite Materials* 24:1270-1298 (1990).

[20] Lee,S.Y. and G.S. Springer,"Filament Winding Cylinders: II. Validation of the Process Model" *Journal of Composite Materials* 24:1299-1343 (1990).

[21] Calius,E.P. and G.S. Springer,"A Model of Filament-Wound Thin Cylinders " *International Journal of Solid Structures* 26(3):271-297 (1990).

[22] Mallow, A.R.,F.R. Muncaster and F.C. Campbell,"Science Based Cure Model For Composites" *in Proceeding of the American Society for Composites First Technical Conference, Dayton, OH,* pp.171-186 (1986).

[23] Kemblowski,Z. and M. Dziubinski. "Resistance of Flow of Molten Polymers Through Granular Beds," *Rheol.Acta* 17:176-187 (1978).

[24] Durst,F.,R. Hass and B.U. Kaczmzr. "Flows of dilute hydrolyzed polyacrylamide solutions in porous media under various solvent conditions," *Journal of Applied Polymer Science* 26:3117-3124 (1981).

[25] Springer,G.S.,"Resin Flow During the Cure of Fiber Reinforced Composites" *Journal of Composite Materials* 16:400-410 (1982).

[26] Gutowski,T.G., "A Resin Flow/Fiber Deformation Model For Composites," *SAMPE Quarterly* 16(4):58-64 (1985).

[27] Gutowski,T.G.,T. Morigaki and Z. Cai,"The Consolidation of Laminate Composites," *Journal of Composite Materials* 21:172-188 (1987).

[28] Gutowski,T.G.,Z. Cai,S. Bauer,S. Boucher,S. Kingery and S. Wineman, "Consolidation Experiments for Laminate Composites ," *Journal of Composite Materials* 21:650-669 (1987).

[29] Dave,R.,J.L. Kardos and M.P. Dudukovic,"Process Modeling of Thermosetting Matrix Composites: A Guide for Autoclave Cure Cycle Selection" *in Pro-*

ceedings of the American Society for Composites First Technical Conference, Dayton, OH, pp.137-153 (1986).

[30] Dave,R.,J.L. Kardos and M.P. Dudukovic,"A Model For Resin Flow During Composite Processing:Part 1.General Mathematical Development" *Polymer Composites* 8(1):29-38 (1987).

[31] Dave,R.,J.L. Kardos and M.P. Dudukovic,"A Model For Resin Flow During Composite Processing:Part 2.Numerical Analysis for Unidirectional Graphite-Epoxy Laminates." *Polymer Composites* 8(2):123-132 (1987).

[32] Dave,R.,"A Unified Approach to Modeling Resin Flow During Composite Processing" *Journal of Composite Materials* 24:22-41 (1990).

[33] Poursartip,A., G. Riahi, L. Frederick and X. lin ," A Method to Determine Resin Flow During Curing of Composite Laminates" *Polymer Composites* 13(1):58-65 (1992).

[34] Smith,G.D. and A. Poursartip,"A Comparison of Two Resin Flow Models For Laminate Processing " *Journal of Composite Materials* 27(17):1695-1711 (1993).

[35] Lindt,J.T., "Consolidation of Circular Cylinders in a Newtonian Fluid I-Simple Cubic Configuration," *Journal of Rheology* 30(2):251-269 (1986).

[36] Chmielewski,C.,C.A. Petty and K. Jayaraman. "Crossflow of Elastic Liquids Through Arrays of Cylinders," *Journal of Non-Newtonian Fluid Mechanics* 35:309-325 (1990).

[37] Astrom,B.T.,R.B. Pipes and S.G. Advani. "On Flow Through Aligned Fiber Beds And Its Application To Composite Processing," *Journal of Composite Materials* 26(9):1351-1373 (1992).

[38] Gebart,B.R., "Permeability of Unidirectional Reinforcements for RTM," *Journal of Composite Materials* 26(8):1100-1134 (1992).

[39] Skartsis,L.,J.L. Kardos and B. Khomami,"Resin Flow Through Fiber Beds During Composite Manufacturing Processes. Part I: Review of Newtonian Flow Through Fiber Beds" *Polymer Engineering And Science* 32(4):221-230 (1992).

[40] Skartsis,L.,B. Khomami and J.L. Kardos,"Resin Flow Through Fiber Beds During Composite Manufacturing Processes. Part II: Numerical and Experimental Studies of Newtonian Flow Through Ideal and Actual Fiber Beds " *Polymer Engineering And Science* 32(4):231-239 (1992).

[41] Bafna,S.S. and D.G. Baird. " An Impregnation Model For the Preparation of Thermoplastic Prepregs," *Journal of Composite Materials* 26(5):683-707 (1992).

[42] Cai,Z. ,"A generalized Model for Flow of Polymer Fluids Through Fibrous Media" *Journal of Advanced Materials* 25(1):58-63 (1993).

[43] Skartsis,L.,B. Khomami and J.L. Kardos ,"A Semi-Analytical One-Dimensional Model for Viscoelastic Impregnation of Fibrous Media"*Journal of Advanced Materials* 25(3):38-44 (1994).

[44] Young,W.B. ,"A Simplified Flow Model for Resin Transfer Molding of Polymer Composites" *Journal of Advanced Materials* 25(3):60-64 (1994).

[45] Kays,A.O.,"Exploratory development on processing science of thick section composites" Technical report AFWAL-TR-85-4090, Air Force Wright Aeronautical Laboratories, Wright Patterson AFB,OH (1985).

[46] Woo,I.L.,and G.S. Springer,"Microwave Curing of Composites" *Journal of Composite Materials* 18:387-409 (1984).

[47] Han,C.D. and H.B. chin,"Development of a Mathematical Model For the Pultrusion Process" *Polymer Engineering and Science* 26(6):393-404 (1986).

[48] Han,C.D. and H.B. chin,"Development of a Mathematical Model For the Pultrusion of Unsaturated Polyester Resin" *Polymer Engineering and Science* 28(5):321-332 (1988).

[49] Hjellming,L.N. and J.S. Walker,"Thermal Curing Cycles for Composite Cylinder with Thick Walls and Thermoset Resins" *Journal of Composite Materials* 23:1048-1064 (1989).

[50] Bezier,D. and B. Capdepuy,"Electron Beam Curing of Composites" *Proceeding of the 35th International SAMPE symposium and exhibition, Anaheim, CA.* Vol 35, Book 2 pp 1220-1232 (1990).

[51] Martinez,G.M.,"Fast Cures For Thick Laminated Organic Matrix Composites"*Chemical Engineering Science* 46(2):439-450 (1991).

[52] Twardowski,T.E.,S.E. Lin and P.H. Geil,"Curing in Thick Composite Laminates: Experiment and Simulation"*Journal of Composite Materials* 27(3):216-250 (1993).

[53] Pitchumani,R. and S.C. Yao ,"Non-dimensional Analysis of an Idealized Thermoset Composites Manufacture " *Journal of Composite Materials* 27(6):613-636 (1993).

[54] Ozisik,M.N.,"*Heat Conduction* " John Wiley and Sons (1980).

[55] Kamal,M.R.,"Thermoset Characterization for Moldability Analysis" *Polymer Engineering And Science* 14(3):231-239 (1974).

[56] Lee,Woo II,A.C. Loos and G.S. Springer,"Heat of Reaction, Degree of Cure, and Viscosity of Hercules 3501-6 Resin" *Journal of Composite Materials* 16:510-520 (1982).

[57] Dusi,M.R.,W.I. Lee,P.R. Ciriscioli and G.S. Springer,"Cure Kinetics and viscosity of Fiberite 976 Resin" *Journal of Composite Materials* 21:243-261 (1987).

[58] Adams,D.C.,"Cure Behavior of Unsaturated Polyester Resin Composite" Technical Report CCM-88-16 Center for composite Materials, University of Delaware, Newark, DE., (1988).

[59] Chiao, L. and R.E.Lyon ,"A Fundamental Approach to Resin Cure Kinetics" *Journal of Composite Materials* 24:739-752 (1990).

[60] Mantell,S.C. and P.R. Ciriscioli ,"Cure Model for ICI Fiberite 977-2 and 977-3 Resins"*38th International SAMPE symposium* (1993).

[61] Scott, C.R.,"*Soil Mechanics and Foundations* " Applied Science Publisher, (1980).

[62] Patankar,S.V.,"*Numerical Heat Transfer and Fluid Flow*' Hemisphere Publishing Corporation (1980).

[63] Barakat,H.Z. and J.A. Clark,"On the Solution of the Diffusion Equations by Numerical Methods" *Journal of Heat Transfer* pp. 421-427 (1966)

[64] Springer,G.S. and S.W. Tsai,"Thermal Conductivities of Unidirectional Materials"*Journal of Composite Materials* 1:166-173 (1967).

[65] Han,S.L. and A.A. Cosner ,"Effective Thermal Conductivities of Fibrous Composites" *Journal of Heat Transfer* 103:387-392 (1981).

[66] Pitchumani,R. and S.C. Yao,"Correlation of Thermal Conductivities of Unidirectional Fibrous Composites Using Local Fractal Techniques" *Journal of Heat Transfer* 113:788-796 (1991).

[67] Carlsson, L.A. and R. Byron Pipes ,"*Experimental Characterization Of Advanced Composite Materials*" Prentice-Hall, N.J. (1987).

[68] Rosen, B.W. and N.F. Dow ,"Overview of Composite Materials Analysis and Design" *Engineering Materials Handbook Volume 1- Composites* ASM International (1987).

[69] Anonymous ,"Low-temperature Thermoset Matrix Composites " *Engineering Materials Handbook Volume 1- Composites* ASM International (1987).

[70] Broyer,E. and C.W. Macosko ,"Heat Transfer and Curing in Polymer Reaction Molding " *AIChE Journal* 22(2):268-275 (1976).

[71] Langhaar,H.L.,"*Dimensional Analysis and Theory of Models* " John Wiely and Sons, (1954).

[72] Kline,S.J. ,"*Similitude and Approximation Theory*" McGraw-Hill Book Company, (1965).

[73] Sedov, L.I. ,"*Similarity and Dimensional Methods in Mechanics*" Mir Publisher (1982).

[74] Bidstrup W.W., N.F. Sheppard and S.D. Senturia ,"Monitoring of Laminate Cure with Microdielectrometry" *Polymer Engineering and Science* 26(5):358-361 (1986).

[75] Day,D.R. ,"Effects of Stoichiometric Mixing Ratio On Epoxy Cure-a Dielectric Analysis" *Polymer Engineering and Science* 26(5):362-366 (1986).

[76] Sanjana Z.N. ,"The Use of Microdielectrometry in Monitoring the Cure of Resins and Composites " *Polymer Engineering and Science* 26(5):373-379 (1986).

[77] Day,D.R. ,"Cure Monitoring: Microdielectric Technique" in Coatings Technology Handbooks Edited by D. Satas, Marcel Dekker, Inc. (1991).

[78] Hojjati, M. and S.V. Hoa ,"Curing Simulation of Thick Thermosetting Composites" *Composites Manufacturing*, in press.